BIOMECHANICAL EVALUATION OF THE ROLES OF DECORIN AND BIGLYCAN DURING NEONATAL TENDON DEVELOPMENT AND HEALING

Zakary Michael Beach

A DISSERTATION

In

Bioengineering

Presented to the Faculties of the University of Pennsylvania

in

Partial Fulfillment of the Requirements for the

Degree of Doctor of Philosophy

2023

Supervisor of Dissertation

_____

Louis J. Soslowsky, PhD

Fairhill Professor of Orthopaedic Surgery

Graduate Group Chairperson

_____

Yale Cohen, PhD

Professor of Bioengineering

Dissertation Committee

Robert L. Mauck, PhD (Committee Chair)
Professor for Education and Research in Orthopaedic Surgery

Nathaniel A. Dyment, PhD
Assistant Professor of Orthopaedic Surgery

Lin Han, PhD
Associate Professor of Bioengineering, Drexel University

David E. Birk, PhD
Professor of Molecular Pharmacology and Physiology, University of South Florida

BIOMECHANICAL EVALUATION OF THE ROLES OF DECORIN AND BIGLYCAN DURING NEONATAL TENDON DEVELOPMENT AND HEALING

ABSTRACT

BIOMECHANICAL EVALUATION OF THE ROLES OF DECORIN AND BIGLYCAN DURING NEONATAL TENDON DEVELOPMENT AND HEALING

Zakary Michael Beach

Louis J. Soslowsky

Tendons are a soft tissue composed primarily of type I collagen, which is organized into a hierarchical structure to transmit large forces between muscle and bone. Tendon injuries are common and costly, with treatments remaining ineffective. To develop effective treatments more work must be done to understand the processes underlying tendon health. Besides collagens, proteoglycans are a class of proteins that compose the tendon extracellular matrix (ECM). Decorin and biglycan are abundant in the ECM, two class I small leucine-rich proteoglycans that are capable of binding to collagen I fibrils and regulating fibrillogenesis, the primary process responsible for growth and maturity of the tendon ECM. While previous studies have demonstrated the importance of decorin and biglycan in the formation and maintenance of tendon biomechanical properties, inducible knockdown models have been developed that allow for precise temporal control over expression at the desired experimental timepoint. Using these models this work aims to define the regulatory roles of decorin and biglycan throughout multiple stages of life: during neonatal development, in skeletally mature adult, and throughout the aging process. Additionally, the roles of these proteins in the neonatal healing model will also be determined. A sophisticated viscoelastic biomechanical testing protocol will be used alongside structural analyses to determine the properties of tendon throughout these studies. First, we demonstrated in mature animals that biglycan plays a major role in maintaining tendon properties, a previously unknown role for this protein. Next, we determined that knockdown of decorin in mature animals was beneficial for the aging process, producing tendons with higher mechanical properties that resisted the age-related decline in tendon mechanics. Finally, decorin and biglycan expression was reduced during neonatal development and after injury of the neonate. In

both cases, the tendons had a large population of small diameter collagen fibrils with reduced mechanical properties due to the tendon collagen microstructure. In conclusion, this work demonstrated the importance of decorin and biglycan in the regulation and maintenance of tendon mechanical properties and health throughout our lifetimes.

TABLE OF CONTENTS

LIST OF TABLES

LIST OF ILLUSTRATIONS

CHAPTER 1: INTRODUCTION AND BACKGROUND

1.1 Significance

1.1.1 Significance of Clinical Problem

Musculoskeletal injuries are the most reported medical condition, with 126.6 million incidences in the United States alone.[1] These injuries represent a significant economic burden and limitations in daily activities, with as many as 60-77% of all injuries being musculoskeletal in nature. Soft tissue injuries make up a significant portion of these injuries, with tendinous or ligamentous injury resulting in medical treatment of 106.2/100,000 people per year.[2] Unfortunately, current therapeutics for tendon injuries remain controversial, with weak or inconclusive evidence for improving outcomes after injury.[3]

Figure 1. Anatomy of the Achilles tendon and surrounding musculature. The Achilles connects the gastrocnemius and soleus to the calcaneus bone to facilitate force transmission from the calf muscles. (Bardof, 2014)

1.1.2 Importance of Evaluating Tendon Composition, Structure, and Mechanics

Tendons are a highly organized soft connective tissue that provide joint stability and transmit tensile forces between muscle and bone (Figure 1). Forces are transferred through the parallel collagen fiber bundles that are surrounded by extracellular matrix (ECM) and tendon fibroblasts. Tendons are composed primarily of

water and collagen.[4,5] Proteoglycans, specifically small leucine-rich proteoglycans (SLRPs), such as decorin and biglycan, are approximately 1-5% of the dry weight, with decorin being the most highly expressed, making up 63-80% of SLRP expression in tendon.[6–8] Due to the native properties of collagen, combined with the proteoglycan and water content, tendons possess time- and history-dependent viscoelastic properties. The viscoelastic properties can be measured via stress-relaxation tests and dynamic loading via frequency sweeps at varying magnitudes and rates of loading. From these tests, we can derive the percent relaxation, dynamic modulus, and phase angle delta to observe the viscoelastic response across a variety of loading conditions. The material and viscoelastic properties of tendon will vary according to age, genotype, and overall health of the tendon, including time after injury.[9–12]

1.1.3 Differences in Outcome Between Tendon Healing and Regeneration

Following tendon injury, composition and structure are altered, resulting in compromised mechanics and function. While composition and structure will improve over time, the fibrotic nature of the adult wound healing response will not allow for complete recovery of these parameters. One potential solution to improve fibrotic healing is to recreate the developmental processes that produce the native structure of tendon. Studies in skin, articular cartilage, bone, and tendon have demonstrated that fetal injuries recover via regeneration.[13–17] Fetal healing occurs quickly and without inflammation or scar formation and appears to be an intrinsic property of the tissue, not the environment.[16,18] It has been hypothesized that an immature immune system and lack of inflammation play a role in the ability of these models to regenerate after injury.[19] However, increased inflammation has also been exhibited alongside a reduced

fibrotic response after injury, indicating a need for additional study of these complicated processes.

It has been hypothesized that the healing response occurs along a gradient from the fetal stage, throughout neonatal development, and into adulthood, thus prompting the exploration of neonatal injury models to help improve our knowledge of tendon development, regeneration, and healing. The neonatal injury model has demonstrated an improved healing phenotype compared to adult in a variety of tissues, including the heart, hair, skin, tendon, and the human digit tip.[20–26] In the neonatal tendon, injuries at P7 returned to baseline cross-sectional area (CSA) and modulus at 10 days post-injury.[25] The same injury induced at P21 more closely resembled that of the adult, with increased CSA and decreased modulus 10 days post-injury. The differences in healing response between P7 and P21 were further highlighted by the expression profiles of decorin and biglycan, with P21 having higher expression of both proteins and 10 days post-injury. However, the collagen fibril diameter of P7 and P21 were both altered vs baseline at 10 days post-injury, indicating an inability to recover the native structural properties at these ages. This was the first study to show an improved tendon healing response during early neonatal development, but little work has been done to examine the mechanisms behind the improved response.

1.2 Background

1.2.1 Tendon Composition and Structure

Tendon is a highly organized soft connective tissue that primarily functions by providing joint stability and transmitting force from muscle to bone. Tendons are relatively hypocellular compared to other tissues throughout the body and relies on interactions between molecules within the ECM for proper regulation and function. Tendon is composed of 55-70% water, while the remaining 30-45% is dry mass that mainly consists of ECM. The tendon ECM is primarily composed of collagens, which comprise 60-85% of the dry mass. Most of the tendon ECM is made up of collagen I, a stiff structural protein that provides the tissue with the ability to transmit tensile forces. The remaining 15-40% of tendon dry mass is composed of less abundant collagens and non-collagenous ECM proteins, where elastin, cartilage oligomeric matrix protein, and proteoglycans are the most abundant of the non-collagenous ECM proteins.[27] Proteoglycans, such as decorin and biglycan, account for approximately 1-5% of the

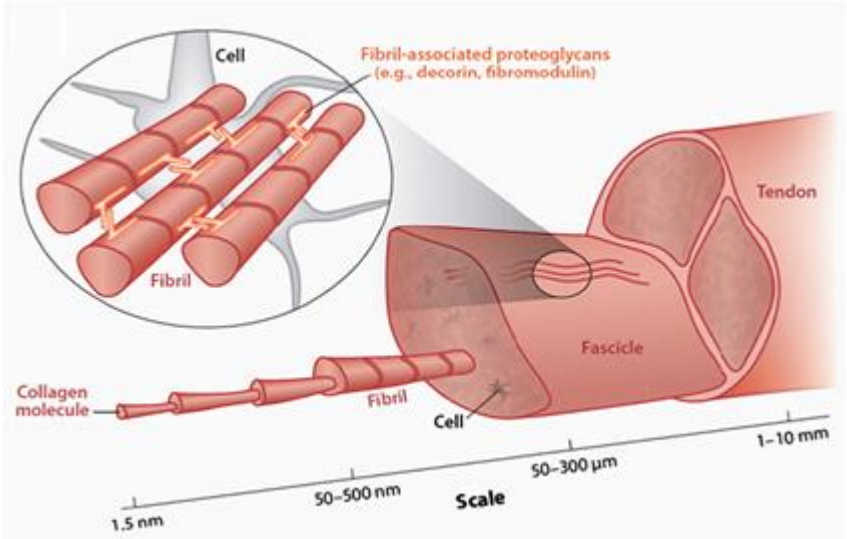

Figure 2. **The tendon is organized in a hierarchical structure.** Starting at the smallest unit as a collagen molecule the structure forms collagen fibrils, which are organized into fascicles, then the fascicles combined to form the tendon. (Thomopoulos, 2002)

tendon dry weight and are of particular interest within the ECM because of the variance in expression throughout development, aging, and healing.

The highly organized hierarchical structure of tendon (Figure 2) is developed through fibrillogenesis, which consists of multiple distinct phases [28–30]. Initially, immature collagen molecules are assembled extracellularly and form collagen fibril intermediates. Next, linear fibril growth occurs, where the fibril intermediates assemble to form longer fibrils that begin to resemble mature collagen fibrils. Finally, lateral fibril growth occurs for the creating of larger diameter fibrils. This process occurs during tendon development and healing to create a population of collagen fibrils with a broad distribution of diameters. The hierarchical structure of tendon is organized with the assembly of collagen fibrils along the longitudinal axis of the tendon to form collagen fibers. These collagen fibers are organized into fascicles, then bound by endotenon sheaths and further surrounded by the epitenon to create the tendon. This highly regulated process gives tendon the mechanical integrity that facilitates proper function.

1.2.2 Tendon Mechanics

The longitudinal and fibrillar structure of tendon results in anisotropic and nonlinear mechanical properties. The anisotropic properties of tendon allow for the transfer of loads that are 1,000 times larger during tensile testing along the longitudinal axis compared to the transverse axis. The nonlinear characteristics of tendon results in an initial increase in stiffness as force is applied and the tissue is lengthened, a phenomenon known as strain stiffening. This nonlinear mechanical response results in two distinct regions in the load-elongation curve in response to tension along the longitudinal axis, called the toe (low strain) and linear (high strain) regions. The toe region of the load-elongation curve describes the behavior of tendon at low levels of

deformation where the collagens fibrils are undergoing loading and the fibril crimp is straightened due to increased load. As load is increased and deformation of the tendon continues, the crimp disappears, and the collagen fibers begin to stretch, creating the linear region of the curve. If further load is applied, the tendon will accumulate irreversible damage, resulting in plastic deformation, and eventually rupture.

Throughout loading tendons display viscoelastic behavior, exhibiting both viscous and elastic behavior in response to loading. Once load is applied to the tissue, it simultaneously results in an instantaneous elastic response followed by a viscous time-dependent response, which arises because of the composition of the tendon ECM. The viscoelastic mechanical response of tendon during loading is complex and must be measured using a variety of mechanical tests. A ramp to failure mechanical test is the most common method to evaluate tendon mechanics by loading the tissue at a constant strain rate. This yields useful data that includes the elastic modulus, failure stress, and failure strain. While this data is useful, it does not assess the full viscoelastic behavior in response to dynamic loading that tendon experiences *in vivo*. To address this, time-dependent tests can be run that measures the response of the tendon to an applied load over time. This includes sinusoidal frequency sweeps, which applies an oscillatory stress at various rates and tissue strain levels, to determine the dynamic tensile modulus and the phase angle (the delay between an applied stress and resulting strain response in the tissue). Additionally, stress-relaxation tests can be performed by applying a variable load that keeps the tissue at a constant strain to determine how the load in the tendon decreases over time. These time-dependent measures are highly sensitive and evaluate how tendon responds within a physiologically relevant loading environment.

1.2.3 Tendon Development

Tendon development begins during fetal development and continues throughout neonatal development until skeletal maturity. Tendon collagen fibrillogenesis begins with the assembly of collagen fibrils, which progresses steadily to form a fully functional tendon. Collagen fibril assembly to form the tendon mostly occurs *in utero*, while collagen fibril growth and maturation is established at neonatal stages, which is accompanied by dramatic changes to tendon fibril organization and mechanical properties.[30] Tendon collagen fibrillogenesis begins with the production of collagen molecules that are assembled to create a fibril intermediate.[30] Next, linear growth of the fibril intermediates occur via end-to-end growth to produce longer fibrils.[30] Finally, lateral growth occurs with lateral association of the developing collagen fibrils to create large diameter fibrils.[30] The lateral growth step, combined with linear growth, creates the array of collagen fibrils that are characteristic of mature tendon.

In tendon, the fibrils are assembled with multiple fibril-forming collagens that also interact with fibril-associated collagen and fibril-associated proteoglycans that assist with regulation of fibrillogenesis. These collagens include type I collagen, which is the major component of the tendon ECM, and minor amounts of collagen III and V that assist with fibril formation.[31] Collagens XII and XIV are fibril associated collagens that are also expressed during development that are involved in the regulation of collagen fibril formation and in modulating the interactions between fibrils during assembly of the ECM.[32–34] In addition to collagens, small leucine-rich proteoglycans such as decorin and biglycan are involved in fibrillogenesis and tendon development. During early tendon development, biglycan and collagen XIV are highly expressed while decorin expression is relatively low.[35–38] As tendon development ends and tendon growth progresses, then

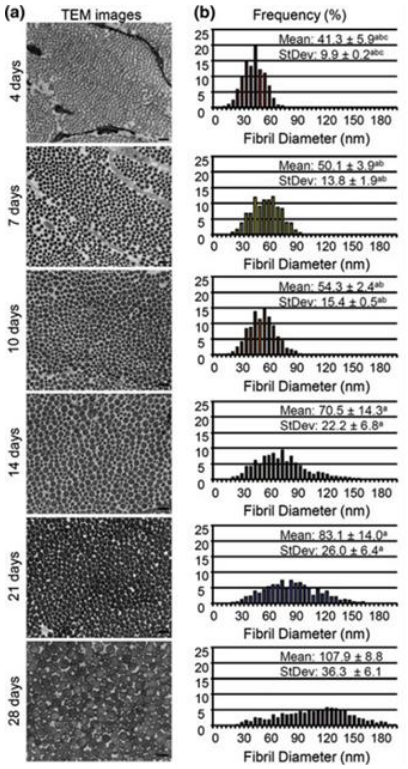

Figure 3. Collagen fibril diameter distribution throughout neonatal development. Neonatal tendon development begins with a narrow distribution of small diameter collagen fibrils. As the tendon matures and ambulation begins the distribution broadens to create more large diameter fibrils through coalescence of smaller fibrils. (Ansorge, 2011)

biglycan and collagen XIV expression is down regulated while decorin expression is upregulated.[35–38] *In vivo* decorin- and biglycan-null mice have also revealed altered tendon fibrillogenesis and tendon mechanics,[9,11] further supporting the idea that these minor collagens, decorin, and biglycan play crucial roles in the development and maturation of tendon structure, mechanics, and ultimately function.

As development of the tendon progresses the fibril diameter distribution rises in complexity, allowing for the tendon to transmit larger loads as it matures (Figure 3). Initially, the collagen fibril diameter distribution of tendon is narrow, with most of the collagen fibril diameters falling within a range from 0-40 nm in rat tail and extensor digitorum longus tendons at birth.[39] After 6 weeks of neonatal development collagen fibril growth results in an expansion of the distribution of the diameter of the fibrils, with approximately 70% of the fibrils measuring between 40-200 nm in diameter.[39] During this shift in collagen fibril diameter distribution the tendon cross-sectional area and failure load increases significantly, while transitional stress does not appear to change, suggesting that the quality of tissue initially present during neonatal development is sufficient for the loads experienced at low levels of tissue strain.[40] These structural, mechanical, and compositional changes that tendon undergoes during neonatal development allow the tissue to grow and endure loads that are necessary for

function at maturity. Interestingly, these changes parallel the changes that the tendon undergoes after injury, and fully understanding the mechanisms that govern tendon development may provide insights to improve tendon healing in fully developed tissue.

1.2.4 Reparative Tendon Healing

After injury tendons initiate a reparative healing process that produces a biomechanically inferior tissue with reduced function and a higher likelihood of reinjury compared to native tendon tissue. The healing process can generally be categorized into three overlapping phases: inflammation, proliferation, and remodeling (Figure 4).[41,42]

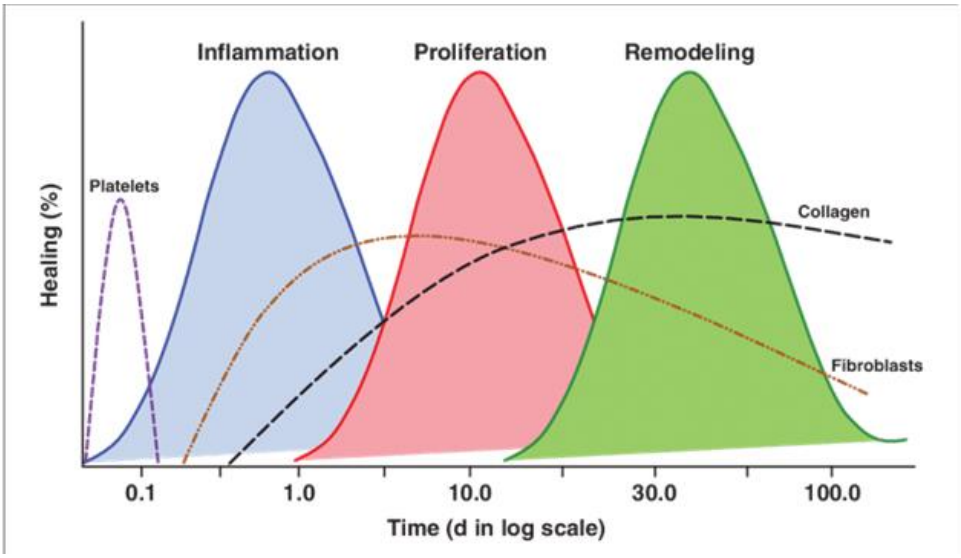

Figure 4. Wound healing occurs through a series of overlapping phases. Inflammation begins at the time of injury, which is followed by proliferation in the days following the injury, then remodeling occurs for months to years after injury. (Lee, 2011)

The inflammatory phase occurs at the time of injury and typically resolves over a few days. The site of injury is infiltrated by platelets, red blood cells, and leukocytes, which produce important cytokines to initiate angiogenesis, stimulate tenocyte proliferation, and recruit additional inflammatory cells.[43,44] Macrophages dominate the latter stages of

the inflammatory phase as they digest necrotic tissue via phagocytosis and recruit tenocytes to the wound as the proliferation phase begins.[45]

Approximately two days after injury the proliferation phase is initiated, which is characterized by the upregulation of extracellular matrix production. Macrophages shift from phagocytic to reparative as they direct the healing process by releasing growth factors and direct cell recruitment.[46] Tenocytes begin to alter the composition of the wound by depositing a mechanically inferior matrix primarily composed of collagen III and increasing water and glycosaminoglycan content, primarily decorin and biglycan.[47,48] Throughout this phase the structure of the tendon is also altered. The collagen fibril diameter distribution is narrowed and consists primarily of small diameter fibrils, and the newly produced matrix is disorganized, deviating from the highly aligned collagen fibers normally associated with a healthy tendon ECM.[49–52]

The final stage, remodeling, begins 1-2 months after injury and can last more than a year. This phase is dominated by collagen I production, and the ECM becomes more aligned. The tendon collagen fibril diameter distribution broadens as the smaller diameter fibrils increase and reorganize longitudinally along the tendon. Additionally, cell density and ECM production gradually decreases. Ultimately, this long series of complex events after injury produces a tissue that is mechanically and structurally inferior to native tendon.[46]

1.2.5 Regenerative Tendon Healing

Models capable of regenerative tendon healing respond in a fundamentally different way than models that undergo repair via the typical reparative healing process. The regenerative response is typically characterized by faster healing, lack of an inflammatory response, and an absence of scar tissue. Two models that display this

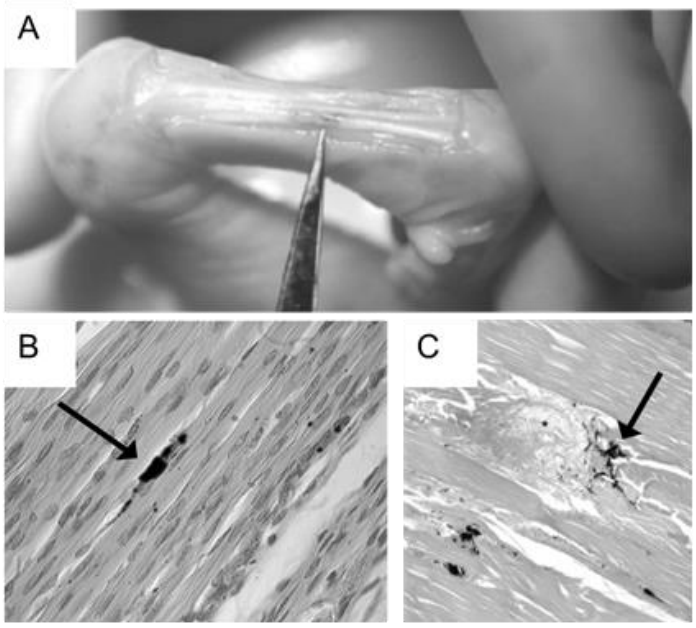

Figure 5. Fetal tendon regenerative healing restores native tendon structure. (A) No gross evidence of enjoy can be observed in the tendon, only the India ink left at the injury site can be seen. (B) The fetal tendon microstructure is fully regenerated with no signs of abnormalities or collagen fibril disruption. (C) The wounded adult tendon shows a disruption of collagen fibers and disorganized granulation tissue at the site of injury. (Beredjiklian, 2003)

healing response in tendon are amphibian and early-gestation fetal mammals. Amphibians display the ability to fully regenerate damaged or lost tissue and organs back to the original state both structurally and functionally. This ability is not seen in mammals, although various mammalian tissues, such as skin, liver, and bone marrow, are able to fully regenerate due to resident stem cell populations.[19]

Generally, mammalian fetal tissue healing occurs at a faster rate than in adults and in the absence of scar formation. Fetal regenerative healing was first observed in tendon using a lamb extensor tendon injury model (Figure 5).[16] One week after injury no abnormalities were noted in the wound, with full reconstitution of the collagen architecture, no presence of inflammatory cells, and no changes to the tendon cross-sectional area.[16] Interestingly, when the fetal tendon was injured and transplanted into an adult environment during healing, the fetal tendon retained its ability to heal scarlessly, indicating that this ability is intrinsic to the tissue itself and not dependent upon the environment.[18] These results ultimately indicate a need to obtain a deeper understanding of the intrinsic properties that allow the fetal tendon to maintain the

scarless healing response that differentiates it from the reparative healing response observed in adults. However, while fetal regenerative healing models have great potential for learning about how to improve the reparative healing process in adults there are major differences, such as the static loading environment and lack of inflammatory response, that are challenging to recreate in the adult. Thus, a different model for improved tendon healing that more closely resembles the adult is required.

1.2.6 Neonatal Tendon Healing

The neonatal injury model offers an alternative to the fetal regenerative model for studying an improved tendon healing response. The neonatal model may even be preferred when attempting to improve healing outcomes in adults due to the similarities in the neonatal and adult injury response. The neonatal injury response resembles the reparative process seen in adult tendon, as it heals through scar formation, however tendon mechanics and structural properties are recovered more quickly after injury (Figure 6).[25] Another advantage of the neonatal tendon injury model is the similarities to the adult mechanical loading environment, since it is able to be applied to mice as young as 5 and 7 days old, which is old enough for weight bearing and approximately when ambulation begins, but young enough for tendon development and growth to still be

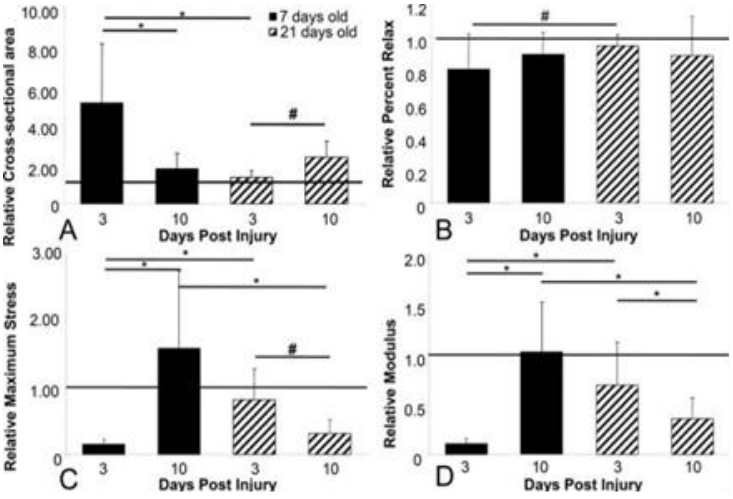

***F*igure 6. Early neonatal tendon injuries show an improved healing response compared to late neonatal injuries at 10-days post injury.** (A) Injury during early neonatal development shows a return to normal cross-sectional area. (B) Few changes were observed in percent relaxation. (C, D) Max stress and modulus returned to normal in the early neonatal injury.

occurring.[25,26] Additionally, there is an upregulation in pro-inflammatory markers after injury that is vital for the neonatal healing process, which is a notable difference from the fetal regenerative healing response.[53] While the neonatal tendon injury model has the potential to improve injury outcomes in adults, the mechanisms that facilitate the improved healing outcomes in neonates are largely unknown.

1.3 Specific Aims and Hypothesis

The overall objective of this study is to evaluate the effects of decorin and biglycan expression on tendon mechanics and structure during homeostasis, aging, neonatal tendon development, and neonatal tendon healing. Tamoxifen-inducible models will be utilized for precise temporal control over when knockdown of decorin and biglycan occur to avoid confounding effects that accumulate in conventional knockout models. The neonatal mouse model is also explored to discover the roles of decorin and biglycan in the early establishment of tendon mechanical and structural properties and to elucidate the roles of these proteins during the neonatal healing process.

Specific Aim 1: Evaluate the effects of tamoxifen and corn oil vehicle on tendon mechanics after injury.

Hypothesis 1: The use of tamoxifen, but not the corn oil delivery vehicle, will disrupt the tendon healing process and produce a mechanically inferior tendon with alterations to cellularity and cellular nuclear aspect ratio.

Specific Aim 2: Investigate the roles of decorin and biglycan in the maintenance of tendon structure and mechanics during homeostasis.

Hypothesis 2a: Knockdown of decorin will result in reduced tendon mechanics and reduced collagen alignment during homeostasis, while knockdown of biglycan will have little to no effect on tendon mechanics or collagen alignment.

Hypothesis 2b: Decorin knockdown will result in an abnormal collagen fibril phenotype, while knockdown of biglycan will have little effect on collagen fibril organization during homeostasis.

Specific Aim 3: Define the mechanisms whereby decorin and biglycan influence tendon aging.

Hypothesis 3a: Decorin knockdown and compound decorin/biglycan knockdown will reduce the negative impact of aging on mechanics relative to WT and biglycan knockdown due to the detrimental role of decorin during aging. Collagen alignment will decrease with age in all genotypes except for the decorin and decorin/biglycan knockdown groups, suggesting a structural mechanism for the mechanical differences with age.

Hypothesis 3b: Knockdown of decorin during aging will maintain the mature fibril structural phenotype, knockdown of biglycan will have little or no effect on fibril structure during aging, and the compound decorin/biglycan knockdown will have a fibril phenotype that resembles the decorin knockdown group.

Specific Aim 4: Determine the differential roles of decorin and biglycan in establishing tendon structure and mechanics during neonatal development.

Hypothesis 4a: Compound knockdown of decorin/biglycan will during neonatal tendon development will disrupt the developmental process and result in decreased tendon mechanics and reduced collagen alignment.

Hypothesis 4b: Knockdown of decorin and biglycan in the developing neonatal tendon will disrupt the collagen fibril organization and result in alteration to fibril diameter and reduced fibril density.

Hypothesis 4c: Decorin/biglycan knockdown will result in alterations to the expression of class II SLRPs to compensate for the lack of decorin and biglycan expression during neonatal development, while no changes will occur in minor collagens that are involved in the regulation of matrix assembly.

Specific Aim 5: Define the effects of decorin and biglycan knockdown during tendon healing in the neonate.

Hypothesis 5a: Compound knockdown of decorin/biglycan after tendon injury in the neonate will result in an impaired ability for the neonatal tendon to recover baseline mechanics and will reduce collagen alignment during loading.

Hypothesis 5b: Decorin/biglycan knockdown will impede recovery of baseline collagen fibril structural parameters to produce alterations in fibril diameter distribution and reduced fibril density after injury.

Hypothesis 5c: Knockdown of decorin/biglycan after injury in the neonate will result in upregulation of class II SLRPs to compensate for reduce decorin and biglycan expression, and alterations in the expression patterns of minor collagens involved in the regulation of matrix assembly will also be present. A reduction in immune cell localization to the site of injury and reduction in MMP expression will also occur after decorin/biglycan knockdown.

1.4 Chapter Overviews

This thesis contains 6 chapters in addition to an Appendix. Chapter 1 is an introduction to the topic and contains the necessary background and framework to understand the rationale for the studies that will be described in the subsequent chapters. The background topics include tendon composition and structure, mechanics, development, healing, regeneration, and animal models utilized in the field. These topics will provide the reader with the background knowledge necessary to understand the concepts and motivation behind the thesis.

Chapter 2 **(Aim 1)** explores the effects of tamoxifen and a corn oil delivery vehicle on tendon healing. These are both used throughout the following studies in a tamoxifen-inducible mouse knockout model. Due to the rising popularity of tamoxifen-inducible models, tamoxifen is increasingly used while studying tendon healing. However, there are concerns that tamoxifen may interfere with tendon healing due to its role as an estrogen agonist and antagonist. Mice were given injections of tamoxifen and corn oil or only corn oil, then a patellar tendon injury was induced. The patellar tendons were evaluated by examining tendon mechanics and the cellular response 3 weeks after injury.

Decorin and biglycan are major regulators of collagen fibrillogenesis and play roles in the maintenance of tendon structure and mechanics during homeostasis. Previous studies have explored effects of decorin and biglycan during tendon homeostasis, but conventional knockout models were utilized, confounding the study results due to the extensive roles of decorin and biglycan in establishing tendon structure and mechanics throughout development. Chapter 3 **(Aim 2)** evaluates the roles of decorin and biglycan during tendon homeostasis using tamoxifen (TM)-inducible

knockdown models (I-*Dcn*$^{-/-}$ and I-*Bgn*$^{-/-}$, respectively) to avoid the confounding effects associated with conventional knockout models. Mice were sacrificed at 150d, 30-days after induction of Cre activity, and tendon mechanics, structure, and composition were analyzed.

Chapter 4 **(Aim 3)** examines the roles of decorin and biglycan in the maintenance of tendon structure and mechanics during aging. While it is known that tendon is more susceptible to injury with age, the mechanisms responsible for this phenomenon are unknown. It has been demonstrated that decorin plays a critical role in tendon during aging, but conventional knockout models were utilized, leading to cumulative effects due to altered development, growth, and maturation. To avoid the confounding effects of conventional knockout models, tamoxifen-inducible decorin (I-*Dcn*$^{-/-}$), biglycan (I-*Bgn*$^{-/-}$), and compound decorin/biglycan (I-*Dcn*$^{-/-}$*Bgn*$^{-/-}$) mouse knockdown models were utilized to isolate the roles of these proteins throughout tendon aging. Mice were treated with tamoxifen at 120d, then the effects of decorin and biglycan knockdown on tendon mechanics and structure were evaluated at 300d and 570d.

Tendon development is a highly coordinated process that produces a hierarchically organized tissue capable of transmitting high loads. Tendon development begins in the fetus but continues after birth in the neonate when the structural mechanical properties are largely established. However, how tendon development progresses during neonatal ages to produce a structurally sound tissue has not been elucidated. Chapter 5 **(Aim 4)** explores the roles of decorin and biglycan during neonatal tendon development using a compound decorin and biglycan tamoxifen inducible mouse knockout model to allow for normal fetal development to occur. Pups are given

tamoxifen at birth at postnatal day 0 (P0), then tendon mechanical and structural properties were analyzed at P7.

Adult tendon healing produces mechanically inferior tissue that is susceptible to reinjury, while injured neonatal tendon is capable of fully recovering mechanical properties in as little as 10-days post-injury. However, the mechanisms that facilitated improved tendon healing in the neonate are unknown. Chapter 5 **(Aim 5) also** examines the roles of decorin and biglycan in neonatal tendon healing due to their roles in collagen fibrillogenesis, tendon development, tendon healing, and cellular regulation. To isolate the roles of decorin and biglycan during neonatal tendon healing without disrupting tendon development and growth, a tamoxifen-inducible compound decorin and biglycan mouse knockdown model (I-*Dcn*$^{-/-}$*Bgn*$^{-/-}$) was utilized. The neonates were treated with tamoxifen at (P7), also coinciding with the time of injury, then tendon mechanics and structure were analyzed 10-days post-injury at P17. Finally, Chapter 6 concludes the document by drawing overall conclusions from the studies in Chapters 2-5 and provides future directions for studies that may build off this body of work.

1.5 References

1. BMUS. United States Bone and Joint Initiative: The Burden of Musculoskeletal Diseases in the United States. Third Edit. Rosemont, IL; 2014.

2. Clayton RAE, Court-Brown CM. The epidemiology of musculoskeletal tendinous and ligamentous injuries. Injury. 2008;39(12):1338–1344. doi:10.1016/j.injury.2008.06.021

3. AAOS. The Diagnosis and Treatment of Achilles Tendon Rupture: Guideline and evidence report. 2009. doi:10.1016/j.injury.2014.06.022

4. Beach ZM, Gittings DJ, Soslowsky LJ. Tendon Biomechanics. In: Canata GL, D'Hooghe P, Hunt KJ, editors. Muscle and Tendon Injuries: Evaluation and Management. Berlin, Heidelberg: Springer Berlin Heidelberg; 2017. p. 15–22. http://dx.doi.org/10.1007/978-3-662-54184-5_2. doi:10.1007/978-3-662-54184-5_2

5. Voleti PB, Buckley MR, Soslowsky LJ. Tendon Healing: Repair and Regeneration. Annual Review of Biomedical Engineering. 2012 [accessed 2016 Nov 21];14(1):47–71. http://www.annualreviews.org/doi/10.1146/annurev-bioeng-071811-150122. doi:10.1146/annurev-bioeng-071811-150122

6. Samiric T, Ilic MZ, Handley CJ. Characterisation of proteoglycans and their catabolic products in tendon and explant cultures of tendon. Matrix Biology. 2004;23(2):127–140. doi:10.1016/j.matbio.2004.03.004

7. Derwin KA, Soslowsky LJ, Kimura JH, Plaas AH. Proteoglycans and glycosaminoglycan fine structure in the mouse tail tendon fascicle. Journal of Orthopaedic Research. 2001;19(2):269–277. doi:10.1016/S0736-0266(00)00032-2

8. Vogel KG, Meyers AB. Proteins in the tensile region of adult bovine deep flexor tendon. Clinical orthopaedics and related research. 1999 [accessed 2018 Nov 27];(367 Suppl):S344-55. http://www.ncbi.nlm.nih.gov/pubmed/10546658

9. Robinson KA, Sun M, Barnum CE, Weiss SN, Huegel J, Shetye SS, Lin L, Saez D, Adams SM, Iozzo R V., et al. Decorin and biglycan are necessary for maintaining collagen fibril structure, fiber realignment, and mechanical properties of mature tendons. Matrix Biology. 2017 Sep 5 [accessed 2017 Sep 25]. http://www.sciencedirect.com/science/article/pii/S0945053X17301063?via%3Dihub. doi:10.1016/j.matbio.2017.08.004

10. Dunkman AA, Buckley MR, Mienaltowski MJ, Adams SM, Thomas SJ, Satchell L, Kumar A, Pathmanathan L, Beason DP, Iozzo R V, et al. Decorin expression is important for age-related changes in tendon structure and mechanical properties. Matrix Biology. 2013 [accessed 2016 Aug 26];32(1):3–13. http://www.ncbi.nlm.nih.gov/pubmed/23178232. doi:10.1016/j.matbio.2012.11.005

11. Robinson PS, Huang T-F, Kazam E, Iozzo R V., Birk DE, Soslowsky LJ. Influence of Decorin and Biglycan on Mechanical Properties of Multiple Tendons in Knockout Mice. Journal of Biomechanical Engineering. 2005;127(1):181. http://biomechanical.asmedigitalcollection.asme.org/article.aspx?articleid=1413750. doi:10.1115/1.1835363

12. Connizzo BK, Sarver JJ, Birk DE, Soslowsky LJ, Iozzo R V. Effect of age and proteoglycan deficiency on collagen fiber re-alignment and mechanical properties in mouse supraspinatus tendon. Journal of biomechanical engineering. 2013 [accessed

2016 Aug 26];135(2):021019. http://www.ncbi.nlm.nih.gov/pubmed/23445064. doi:10.1115/1.4023234

13. Longaker MT, Moelleken BR, Cheng JC, Jennings RW, Adzick NS, Mintorovich J, Levinsohn DG, Gordon L, Harrison MR, Simmons DJ. Fetal fracture healing in a lamb model. Plastic and reconstructive surgery. 1992 [accessed 2018 Nov 29];90(2):161–71; discussion 172-3. http://www.ncbi.nlm.nih.gov/pubmed/1631210

14. Namba RS, Meuli M, Sullivan KM, Le AX, Adzick NS. Spontaneous repair of superficial defects in articular cartilage in a fetal lamb model. Journal of Bone and Joint Surgery - Series A. 1998 [accessed 2018 Nov 29];80(1):4–10. http://www.ncbi.nlm.nih.gov/pubmed/9469302. doi:10.2106/00004623-199801000-00003

15. Longaker MT, Whitby DJ, Adzick NS, Crombleholme TM, Langer JC, Duncan BW, Bradley SM, Stern R, Ferguson MW, Harrison MR. Studies in fetal wound healing, VI. Second and early third trimester fetal wounds demonstrate rapid collagen deposition without scar formation. Journal of pediatric surgery. 1990 [accessed 2018 Nov 29];25(1):63–8; discussion 68-9. http://www.ncbi.nlm.nih.gov/pubmed/2299547

16. Beredjiklian PK, Favata M, Cartmell JS, Flanagan CL, Crombleholme TM, Soslowsky LJ. Regenerative versus reparative healing in tendon: A study of biomechanical and histological properties in fetal sheep. Annals of Biomedical Engineering. 2003;31(10):1143–1152. doi:10.1114/1.1616931

17. Ricchetti ET, Reddy SC, Ansorge HL, Zgonis MH, Van Kleunen JP, Liechty KW, Soslowsky LJ, Beredjiklian PK. Effect of Interleukin-10 Overexpression on the Properties of Healing Tendon in a Murine Patellar Tendon Model. Journal of Hand Surgery.

2008;33(10):1843–1852. http://dx.doi.org/10.1016/j.jhsa.2008.07.020. doi:10.1016/j.jhsa.2008.07.020

18. Favata M, Beredjiklian PK, Zgonis MH, Beason DP, Crombleholme TM, Jawad AF, Soslowsky LJ. Regenerative properties of fetal sheep tendon are not adversely affected by transplantation into an adult environment. Journal of Orthopaedic Research. 2006 [accessed 2016 May 17];24(11):2124–2132. http://doi.wiley.com/10.1002/jor.20271. doi:10.1002/jor.20271

19. Galatz LM, Gerstenfeld L, Heber-Katz E, Rodeo SA. Tendon regeneration and scar formation: The concept of scarless healing. Journal of Orthopaedic Research. 2015;33(6):823–831. doi:10.1002/jor.22853

20. DOUGLAS BS. CONSERVATIVE MANAGEMENT OF GUILLOTINE AMPUTATION OF THE FINGER IN CHILDREN. Journal of Paediatrics and Child Health. 1972 [accessed 2018 Nov 29];8(2):86–89. http://doi.wiley.com/10.1111/j.1440-1754.1972.tb01793.x. doi:10.1111/j.1440-1754.1972.tb01793.x

21. Illingworth CM. Trapped fingers and amputated finger tips in children. Journal of Pediatric Surgery. 1974 [accessed 2018 Nov 29];9(6):853–858. https://www.sciencedirect.com/science/article/pii/S0022346874802204?via%3Dihub. doi:10.1016/S0022-3468(74)80220-4

22. Porrello ER, Mahmoud AI, Simpson E, Hill JA, Richardson JA, Olson EN, Sadek HA. Transient Regenerative Potential of the Neonatal Mouse Heart. Science. 2011;331(6020):1078–1080. http://www.sciencemag.org/cgi/doi/10.1126/science.1200708. doi:10.1126/science.1200708

23. Bertsch S, Marks F. A comparative study on wound-healing in neonatal and adult mouse epidermis in vivo. Cell and tissue kinetics. 1982;15(1):81–7. http://www.ncbi.nlm.nih.gov/pubmed/7060084

24. Cox BC, Chai R, Lenoir A, Liu Z, Zhang L, Nguyen D-H, Chalasani K, Steigelman KA, Fang J, Rubel EW, et al. Spontaneous hair cell regeneration in the neonatal mouse cochlea in vivo. Development. 2014;141(7):1599–1599. http://dev.biologists.org/cgi/doi/10.1242/dev.109421. doi:10.1242/dev.109421

25. Ansorge HL, Hsu JE, Edelstein L, Adams S, Birk DE, Soslowsky LJ. Recapitulation of the achilles tendon mechanical properties during neonatal development: A study of differential healing during two stages of development in a mouse model. Journal of Orthopaedic Research. 2012 Mar [accessed 2016 May 17];30(3):448–56. http://www.ncbi.nlm.nih.gov/pubmed/22267191. doi:10.1002/jor.21542

26. Howell K, Chien C, Bell R, Laudier D, Tufa SF, Keene DR, Andarawis-Puri N, Huang AH. Novel Model of Tendon Regeneration Reveals Distinct Cell Mechanisms Underlying Regenerative and Fibrotic Tendon Healing. Scientific Reports. 2017 [accessed 2017 Apr 27];7:45238. http://www.nature.com/articles/srep45238. doi:10.1038/srep45238

27. Taye N, Karoulias SZ, Hubmacher D. The “other” 15–40%: The Role of Non-Collagenous Extracellular Matrix Proteins and Minor Collagens in Tendon. Journal of Orthopaedic Research. 2019 [accessed 2020 Jan 8];38(1):23–35. https://onlinelibrary.wiley.com/doi/abs/10.1002/jor.24440. doi:10.1002/jor.24440

28. Birk DE, Nurminskaya M V., Zycband EI. Collagen fibrillogenesis in situ: Fibril segments undergo post-depositional modifications resulting in linear and lateral growth during matrix development. Developmental Dynamics. 1995 [accessed 2020 Dec

7];202(3):229–243. https://pubmed.ncbi.nlm.nih.gov/7780173/. doi:10.1002/aja.1002020303

29. Birk DE, Zycband EI, Woodruff S, Winkelmann DA, Trelstad RL. Collagen fibrillogenesis in situ: Fibril segments become long fibrils as the developing tendon matures. Developmental Dynamics. 1997 [accessed 2016 May 31];208(3):291–298. http://doi.wiley.com/10.1002/%28SICI%291097-0177%28199703%29208%3A3%3C291%3A%3AAID-AJA1%3E3.0.CO%3B2-D. doi:10.1002/(SICI)1097-0177(199703)208:3<291::AID-AJA1>3.0.CO;2-D

30. Zhang G, Young BB, Ezura Y, Favata M, Soslowsky LJ, Chakravarti S, Birk DE. Development of tendon structure and function: Regulation of collagen fibrillogenesis. Journal of Musculoskeletal Neuronal Interactions. 2005 [accessed 2017 Aug 10];5(1):5–21. https://pubmed.ncbi.nlm.nih.gov/15788867/. doi:10.1016/j.biomaterials.2010.02.062

31. Birk DE, Mayne R. Localization of collagen types I, III and V during tendon development. Changes in collagen types I and III are correlated with changes in fibril diameter. European Journal of Cell Biology. 1997 [accessed 2020 Dec 16];72(4):352–361. https://pubmed.ncbi.nlm.nih.gov/9127735/

32. Zhang G, Young BB, Birk DE. Differential expression of type XII collagen in developing chicken metatarsal tendons. Journal of Anatomy. 2003 [accessed 2020 Dec 16];202(5):411–420. https://pubmed.ncbi.nlm.nih.gov/12739618/. doi:10.1046/j.1469-7580.2003.00174.x

33. Young BB, Gordon MK, Birk DE. Expression of type XIV collagen in developing chicken tendons: Association with assembly and growth of collagen fibrils. Developmental Dynamics. 2000 [accessed 2020 Dec 16];217(4):430–439.

https://pubmed.ncbi.nlm.nih.gov/10767087/. doi:10.1002/(SICI)1097-0177(200004)217:4<430::AID-DVDY10>3.0.CO;2-5

34. Ansorge HL, Meng X, Zhang G, Veit G, Sun M, Klement JF, Beason DP, Soslowsky LJ, Koch M, Birk DE. Type XIV collagen regulates fibrillogenesis: Premature collagen fibril growth and tissue dysfunction in null mice. Journal of Biological Chemistry. 2009 [accessed 2016 Jul 18];284(13):8427–8438. http://www.ncbi.nlm.nih.gov/pubmed/19136672. doi:10.1074/jbc.M805582200

35. Zhang G, Ezura Y, Chervoneva I, Robinson PS, Beason DP, Carine ET, Soslowsky LJ, Iozzo R V., Birk DE. Decorin regulates assembly of collagen fibrils and acquisition of biomechanical properties during tendon development. Journal of Cellular Biochemistry. 2006 [accessed 2017 Aug 10];98(6):1436–1449. http://doi.wiley.com/10.1002/jcb.20776. doi:10.1002/jcb.20776

36. Scott JE, Orford CR, Hughes EW. Proteoglycan-collagen arrangements in developing rat tail tendon. An electron-microscopical and biochemical investigation. Biochemical Journal. 1981 [accessed 2020 Dec 16];195(3):573–581. https://pubmed.ncbi.nlm.nih.gov/6459082/. doi:10.1042/bj1950573

37. Watanabe M, Nojima M, Shibata T, Hamada M. Maturation-related biochemical changes in swine anterior cruciate ligament and tibialis posterior tendon. Journal of Orthopaedic Research. 1994 [accessed 2020 Dec 16];12(5):672–682. https://pubmed.ncbi.nlm.nih.gov/7931784/. doi:10.1002/jor.1100120510

38. Lo IKY, Marchuk LL, Leatherbarrow KE, Frank CB, Hart DA. Collagen fibrillogenesis and mRNA levels in the maturing rabbit medial collateral ligament and patellar tendon.

Connective Tissue Research. 2004 [accessed 2020 Dec 16];45(1):11–22. https://pubmed.ncbi.nlm.nih.gov/15203936/. doi:10.1080/03008200490278070

39. Moore MJ, De Beaux A. A quantitative ultrastructural study of rat tendon from birth to maturity. Journal of anatomy. 1987 [accessed 2020 Dec 20];153:163–9. http://www.ncbi.nlm.nih.gov/pubmed/3429315

40. Ansorge HL, Adams SM, Birk DE, Soslowsky LJ. Mechanical, compositional and structural properties of the post-natal mouse Achilles tendon. Annals of Biomedical Engineering. 2011 [accessed 2016 May 17];39(7):1904–1913. http://www.ncbi.nlm.nih.gov/pubmed/21431455. doi:10.1007/s10439-011-0299-0.Mechanical

41. Molloy T, Wang Y, Murrell GAC. The roles of growth factors in tendon and ligament healing. Sports Medicine. 2003 [accessed 2021 Apr 25];33(5):381–394. https://link-springer-com.proxy.library.upenn.edu/article/10.2165/00007256-200333050-00004. doi:10.2165/00007256-200333050-00004

42. Hope M, Saxby TS. Tendon Healing. Foot and Ankle Clinics. 2007;12(4):553–567. doi:10.1016/j.fcl.2007.07.003

43. Murphy PG, Loitz BJ, Frank CB, Hart DA. Influence of exogenous growth factors on the synthesis and secretion of collagen types I and III by explants of normal and healing rabbit ligaments. Biochemistry and cell biology. 1994 [accessed 2021 Nov 27];72(9–10):403–409. https://cdnsciencepub.com/doi/abs/10.1139/o94-054. doi:10.1139/o94-054

44. Sharma P, Maffulli N. Biology of tendon injury: Healing, modeling and remodeling. Journal of Musculoskeletal Neuronal Interactions. 2006 [accessed 2016 Nov

21];6(2):181–190. http://www.ncbi.nlm.nih.gov/pubmed/16849830. doi:10.1016/j.math.2014.02.002

45. Gelberman RH, Steinberg D, Amiel D, Akeson W. Fibroblast chemotaxis after tendon repair. Journal of Hand Surgery. 1991 [accessed 2021 Nov 27];16(4):686–693. http://www.jhandsurg.org/article/036350239190195H/fulltext. doi:10.1016/0363-5023(91)90195-H

46. Leadbetter WB. Cell-matrix response in tendon injury. Clinics in sports medicine. 1992 [accessed 2021 Nov 27];11(3):533–578. https://pubmed.ncbi.nlm.nih.gov/1638640/. doi:10.1016/s0278-5919(20)30507-x

47. Thomopoulos S, Hattersley G, Rosen V, Mertens M, Galatz L, Williams GR, Soslowsky LJ. The localized expression of extracellular matrix components in healing tendon insertion sites: An in situ hybridization study. Journal of Orthopaedic Research. 2002 [accessed 2016 May 23];20(3):454–463. http://www.ncbi.nlm.nih.gov/pubmed/12038618. doi:10.1016/S0736-0266(01)00144-9

48. Berglund M, Reno C, Hart DA, Wiig M. Patterns of mRNA Expression for Matrix Molecules and Growth Factors in Flexor Tendon Injury: Differences in the Regulation Between Tendon and Tendon Sheath. Journal of Hand Surgery. 2006 [accessed 2021 Nov 27];31(8):1279–1287. http://www.jhandsurg.org/article/S0363502306006927/fulltext. doi:10.1016/j.jhsa.2006.06.011

49. Sklenka AM, Levy MS, Boivin GP. Effect of age on collagen fibril diameter in rabbit patellar tendon repair. Comparative Medicine. 2006;56(1):8–11.

50. Postacchini F, Martino C De. Regeneration of rabbit calcaneal tendon maturation of collagen and elastic fibers following partial tenotomy. Connective Tissue Research. 1980

[accessed 2021 Nov 27];8(1):41–47. https://www.tandfonline.com/doi/abs/10.3109/03008208009152120. doi:10.3109/03008208009152120

51. Ehrlich HP, Lambert PA, Saggers GC, Myers RL, Hauck RM. Dynamic changes appearing in collagen fibers during intrinsic tendon repair. Annals of Plastic Surgery. 2005 [accessed 2021 Nov 27];54(2):201–206. https://journals.lww.com/annalsplasticsurgery/Fulltext/2005/02000/Dynamic_Changes_Appearing_in_Collagen_Fibers.18.aspx. doi:10.1097/01.sap.0000141380.52782.db

52. Gimbel JA, Van Kleunen JP, Mehta S, Perry SM, Williams GR, Soslowsky LJ. Supraspinatus tendon organizational and mechanical properties in a chronic rotator cuff tear animal model. Journal of Biomechanics. 2004;37(5):739–749. doi:10.1016/j.jbiomech.2003.09.019

53. Howell KL, Kaji DA, Li TM, Montero A, Yeoh K, Nasser P, Huang AH. Macrophage depletion impairs neonatal tendon regeneration. FASEB Journal. 2021 [accessed 2021 Nov 27];35(6). https://pubmed.ncbi.nlm.nih.gov/33982337/. doi:10.1096/fj.202100049R

CHAPTER 2: POST-INJURY TENDON MECHANICS ARE NOT AFFECTED BY TAMOXIFEN TREATMENT

2.1 Introduction

The incidence of tendon injury is rising due to an increasingly active and aging population over recent decades.[1] Accompanying the increasing rates of tendon injury is a growing interest in the mechanisms involved in tendon healing, along with the development of models to better address these questions. The development of powerful biological tools in genetic mouse models allows for manipulation of the mouse genome, giving researchers the ability to create loss-of-function and gain-of-function mutations with temporal and spatial control.[2,3] The tamoxifen (TM)-inducible CreERT2 system is an effective tool in achieving temporal and spatial control over the genome that functions by Cre-mediated genetic recombination between loxP sequences of floxed alleles.[4,5] In this system, TM metabolizes into 4-hydroxytamoxifen, which binds to the mutant ligand-binding domain of the estrogen receptor and enables translocation of the CreERT2 complex into the nucleus to initiate Cre-mediated genetic recombination.[6] The ability for TM to act as an estrogen receptor agonist and antagonist opens up the possibility for unintended consequences when used in preclinical mouse models.

Though the potential unintended effects of TM have been studied in other tissues, the effects of TM on tendon healing have not been sufficiently explored. Studies exploring the effects of TM reveal that the outcomes are highly variable, providing evidence for both profibrotic and antifibrotic properties.[7,8] TM has also been shown to interfere with major regulators of the inflammatory and healing responses, with disruptions in inflammation via suppression of TGF-β signaling and an improved healing response in the endothelium through upregulation of ERα.[9,10] Additionally, administration

of TM has altered proliferation of epithelial cells, further highlighting the importance of study the effects of TM on tendon healing.[10,11] The variability in the effects of TM in different tissues and physiological states necessitates additional characterization within tendon tissue and, more specifically, within the various applications and protocols of TM to specific types of studies in tendon.

A recent study explored the effects of TM on tendon homeostasis and healing, where two different TM treatment regimens were utilized – one where TM was administered a week before tendon injury, and a second where TM was administered at the time of injury and throughout the healing process for 2 weeks.[12] These protocols were specifically chosen to mimic standard protocols that label cells prior to injury and throughout injury, respectively. However, given the variability within the response to tamoxifen in various contexts, it is also vital to know the effects of tamoxifen when it is applied with an optimized dose during a short duration at the time of injury for studies that explore the specific roles of genes during tendon healing. These studies are important for determining the roles of specific genes during the tendon healing process without the confounding effects on development that are associated with conventional knockout models, but it is necessary to clearly establish the limitations associated with TM-inducible Cre models so that better informed decisions can be made when weighing the advantages and disadvantages of each genetic knockdown model.

Therefore, the objective of this study is to determine if TM, in a specific dosing regimen, disrupts the tendon healing process in an established mouse patellar tendon injury model.[13] To delineate the effects of TM from just the corn oil (CO) delivery vehicle, we utilized a group that received TM injections with CO, a group that received CO injections with no TM, and a control group that did not receive any injections. We hypothesized that the use of TM, but not CO, will negatively impact the tendon healing

process and produce a mechanically inferior tendon with alterations in cellularity and cellular nuclear shape.

2.2 Methods

2.2.1 Animals, Injury Model, & Injections

This study was approved by the University of Pennsylvania Institutional Animal Care and Use Committees. Female wild-type mice with a C57/BL6 background (Charles River, n=8/group, n=24 total) were utilized and separated into three treatment groups – corn oil injections with tamoxifen (TM, 4.5mg/40g body weight), corn oil injections (CO), and no treatment (WT). The TM and CO groups received three consecutive daily intraperitoneal injections, with the final injection occurring on the day of injury when the mice were 120 days old. The mice underwent bilateral surgery as described.[13,14] Briefly, an incision was made near the knee, then longitudinal incisions were made on either side of the patellar tendon. A rubber-coated backing was placed beneath the patellar tendon and a full thickness, partial-width (~60%) transection was made using a 0.75 mm biopsy punch. The skin was sutured, and the animals were allowed to return to cage activity. The mice were sacrificed three weeks after injury. All samples were randomly assigned to the assays after sacrifice, and all personnel were blinded during data collection and analysis.

2.2.2 Tendon Biomechanics and Collagen Fiber Realignment

Right patellar tendons were prepared for mechanical testing (n=8/group) as described.[15] Briefly, patella-tendon-tibia complexes were dissected, then scanned using a custom laser device to measure cross-sectional area.[16] Verhoeff's stain was used to apply stain lines at the tibial insertion, 1 mm and 2 mm from the tibial insertion, and at the distal patella for optical strain tracking. The tibia was secured in a custom 3D-printed

pot using poly(methyl methacrylate). Custom fixtures were used to secure the pot during mechanical testing.

During testing, tendons were loaded into a 1x phosphate-buffered saline bath at 37°C secured to a tensile testing system (Instron 5848, Instron, Norwood, MA) integrated with an established cross-polarized light setup.[17,18] The viscoelastic testing protocol consisted of preconditioning, stress relaxations (3%, 4%, and 5% strain) each followed by a series of frequency sweeps (0.1, 1, 5, and 10 Hz), a return to gage length for 60 s, and ending with a ramp-to-failure at a strain rate of 0.1%/s. Series of image maps, each consisting of 18 images, were taken throughout the testing protocol for collagen fiber realignment and optical strain tracking data.[17] Collagen fiber realignment, outputted as circular variance, was calculated separately for the tendon midsubstance and insertion using a custom program, and has an inverse relationship with the realignment of collagen fibers (Matlab, Natick, MA).[19]

Maximum stress was calculated from stress-strain data. Optical tracking was used to compute midsubstance and insertion modulus (Matlab, Natick, MA). Dynamic modulus (E*) and tan (δ), representing the phase shift in the stress-strain relationship during dynamic loading, were calculated at each strain-frequency combination.

2.2.3 Cellularity and Nuclear Shape

For histological analysis, the left knee joint was isolated by cutting through the femur and tibia at the time of sacrifice (n=4/group). The knee was flexed to 90°, placed into a cassette, fixed in formalin, decalcified in formic acid, and processed using standard paraffin histological techniques. Samples were embedded in paraffin, and sections were cut at 7 μm thickness before staining with hematoxylin and eosin.

Cellularity (1 – fewer cells, 3 – more cells) and nuclear shape (1 – spindle, 2 – mixed, 3 – round) were assessed using semi-quantitative analysis by blinded graders.

2.2.4 Statistics

A one-way ANOVA with Bonferroni post-hoc analysis was used to evaluate the effect of treatment on tendon mechanics. Collagen fiber realignment data was analyzed using a two-way ANOVA with Bonferroni post hoc analysis to determine the effects of treatment group and tendon strain. Collagen fiber realignment comparisons between strain levels were only performed on consecutive strain measurements (i.e., 1% vs 3%, 3% vs 5%, 5% vs 7%). All the data compared using a one- or two-way ANOVA were analyzed for normality using the Shapiro-Wilk test. Cellularity and nuclear shape were evaluated using the Kruskal-Wallis test with Dunn's multiple comparison test. Statistical significance was set at $p<0.05$.

2.3 Results

2.3.1 Tendon Biomechanics & Collagen Fiber Realignment

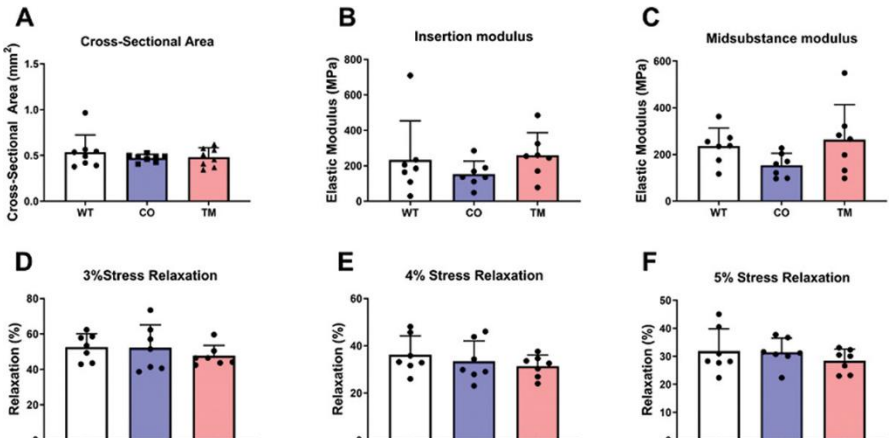

Figure 7. Patellar tendons from mice treated with CO or TM showed no differences in cross-sectional area (a), insertion modulus (b), or midsubstance modulus (c) compared to WT mice that received no treatment. The lack of changes to patellar tendon mechanics after CO or TM treatment were consistent after stress relaxations were performed at 3%, 4%, and 5% strain (d–f).

No changes in midsubstance modulus or insertion modulus were found between any of the treatment groups (Fig. 7A-

B). Similarly, analysis of the viscoelastic mechanics showed no changes between treatment groups for the stress relaxations at 3%, 4%, and 5% strain (Fig. 7C-E), and no changes in dynamic modulus or phase shift at these same strains during the frequency sweeps at 0.1, 1, 5, or 10 Hz (Fig. 8).

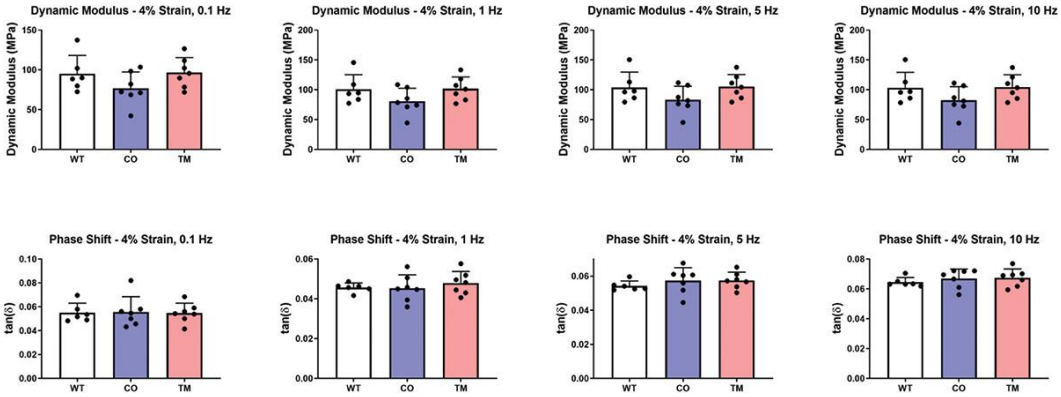

Figure 8. Dynamic loading of mouse patellar tendons, consisting of a series of frequency sweeps at 0.1, 1, 5, and 10 Hz while the samples were at 3%, 4%, and 5%, strain, revealed no changes to dynamic modulus or phase shift between treatment groups across the entire spectrum of loading frequencies and strain levels (3% and 5% strain not shown).

Analysis of collagen fiber realignment during tendon loading revealed no differences between the treatment groups in the insertion or midsubstance regions of the tendons (Fig. 9). Strain level was a significant factor within the ANOVA, with all treatment groups showing increased tendon realignment between 1% and 3% strain, but no changes between 3% and 5% strain or 5% and 7% strain.

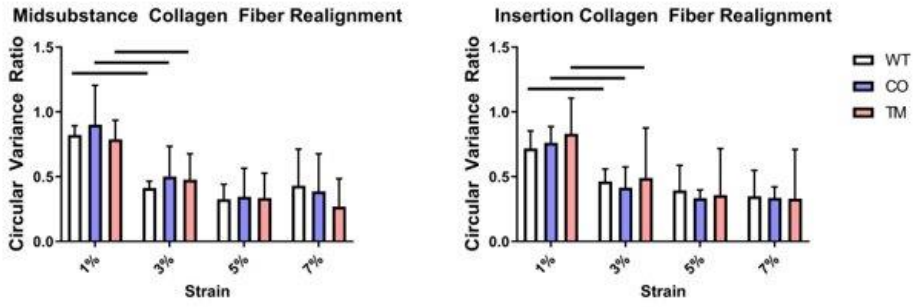

Figure 9. Increased collagen fiber realignment was present between 1% and 3% strain in all treatment groups in the tendon midsubstance and insertion. No differences in realignment were found within the treatment groups between 3%, 5%, or 7% strain, and no differences were found between the treatment groups within each strain level.

2.3.2 Cellularity and Nuclear Shape

There were no differences in cellularity or nuclear shape between the WT, CO, or TM treated groups (Fig. 10).

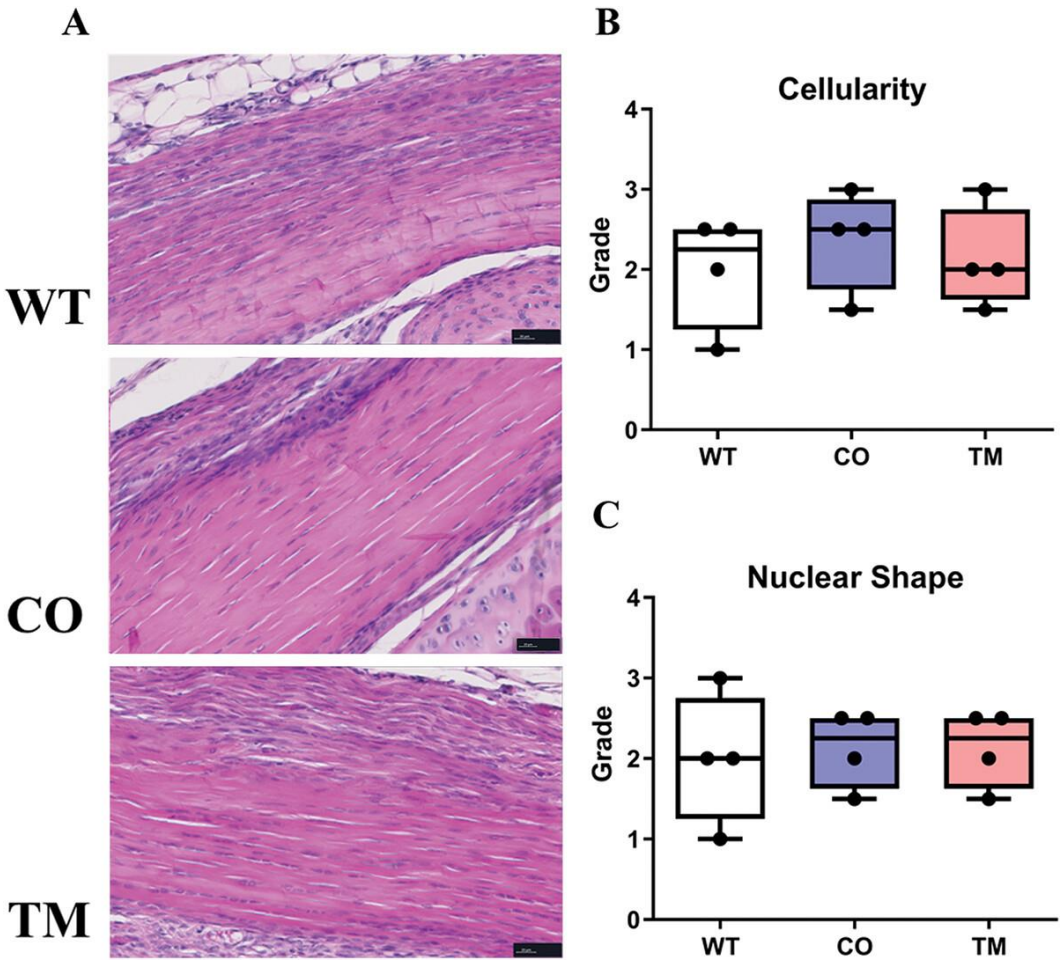

Figure 10. (a) Representative images of mouse patellar tendons stained with hematoxylin and eosin. (b) Semi-quantitative analysis did not reveal any changes in cellularity or cell shape between mice in the WT, TM, or CO groups. Scale bars = 20 µm.

2.4 Discussion

The TM-inducible CreERT2 system is a powerful tool that allows for the spatial and temporal manipulation of genetics. Due to the ability for TM to act as an estrogen receptor agonist and antagonist, it is critical to consider the possible confounding effects that result from administering TM. The objective of this study was to explore the effects of TM and CO on tendon healing by analyzing tendon mechanics, cellularity, and cellular

nuclear shape. Contrary to our hypothesis, the use of TM and CO did not affect tendon mechanics, cellularity, or cellular nuclear shape at three weeks post-injury. The absence of changes in mechanics are consistent with a recent study examining the healing response in tendon after TM and CO treatment that found minimal changes in tendon mechanics and no changes in functional parameters relating to tendon gliding function after 14 days of healing, where a reduction in maximum load in females was the only mechanics parameter that decreased after TM treatment.[12] Interestingly, they also noted that long-term corn oil treatments that were applied throughout the healing response disrupted tendon homeostasis in the contralateral limb after injury.[12] Overall, these initial studies in tendon reveal minimal changes to the healing response after TM injection. However, the disruption in tendon homeostasis associated with long-term CO treatment highlights the importance of optimizing TM and CO dose to ensure that only the minimally viable amount is used in a study.

The absence of changes to the tendon healing response after use of TM in our study is surprising given the known effects of TM in other tissues. A previous study in mice noted that TM induced hernias in male, but not female mice, with major structural abnormalities in the lower abdominal wall due to increased activation of MMP2/13 and decreased collagen II.[20] A major difference between this study and our current study is that TM was administered via chow with no feeding limitations for 5 weeks, which allows for the mice to receive a less controlled and potentially much higher dose of TM than what is needed for TM-inducible knockdown models. Another study examined the effects of TM on cerulein-induced pancreatic fibrogenesis, where TM was administered via oral gavage for 5 consecutive days, resulting in the mice receiving approximately 300% of the TM administered in our current study.[21] The authors noted that the fibrotic response to TM treatment was sex-specific and time-dependent, where a higher fibrotic index was

found in female mice when cerulein was applied 3 days after the TM treatment was finished, but the fibrotic index returned back to control levels when cerulein was applied 1 and 2 weeks after the TM treatment.[21] Interestingly, the effects seemed to oscillate in female mice, where an increase in the fibrotic index was also found when cerulein was applied three weeks after the TM treatment.[21] Sex differences were also noted, where tamoxifen generally decreased the fibrotic index in male mice.[21] These same patterns generally held when myofibroblasts and inflammatory cells were quantified after treatment with TM and cerulein.[21] While we did not directly analyze the tendons in our current study for an increased fibrotic response, the lack of changes in tendon mechanics after injury imply that any pro- or anti-fibrotic effects from TM were minimal. It was also notable that no changes to cellularity were found after tendon injury, which deviates from the results found when examining pancreatic tissue. The variability in the response to TM among various tissues highlights the need for additional studies that examine the response in tendon after use of TM in additional contexts, including use of TM during tendon development, homeostasis, aging, long-term tendon healing, and any injection protocols that use higher levels of TM or include long-term treatment with TM and CO.

This study does have limitations. The effect of TM on tendon healing was assessed by analyzing tendon mechanics and basic histology that only examined cellularity and cellular nuclear shape. While the primary goal of this study was to specifically examine tendon mechanical properties, additional gene expression analysis could be performed to further determine the cellular response to TM treatment during tendon healing. Additionally, only female mice were utilized in this study. Due to the role of TM as an estrogen receptor agonist and antagonist, the effects may be sex specific. Finally, only one injection protocol and TM dose was utilized though our study

determined that this protocol is safe. A study design with different TM doses or an injection protocol at different time points relative to tendon injury may yield different results.

This study reveals additional insight into the effects of TM on tendon healing, showing no differences across any of the measured mechanics or histological parameters between groups that received TM, the CO vehicle control, or no treatment at time of injury. Extrapolating these results to alternative TM injection protocols should be done with caution since a narrow range of conditions were explored. Future tendon injury studies utilizing TM should optimize the dose to reduce the number of unintended effects that could arise due to the role of TM as an estrogen receptor agonist and antagonist. Additionally, any future studies should ensure that proper controls are used to further reduce impact of unintended consequences that the use of TM could have on the tendon healing process.

2.5 References

1. Lantto I, Heikkinen J, Flinkkilä T, Ohtonen P, Leppilahti J. Epidemiology of Achilles tendon ruptures: Increasing incidence over a 33-year period. Scandinavian Journal of Medicine and Science in Sports. 2015 [accessed 2020 Nov 10];25(1):e133–e138. https://pubmed.ncbi.nlm.nih.gov/24862178/. doi:10.1111/sms.12253

2. Lakso M, Sauer B, Mosinger B, Lee EJ, Manning RW, Yu SH, Mulder KL, Westphal H. Targeted oncogene activation by site-specific recombination in transgenic mice. Proceedings of the National Academy of Sciences of the United States of America. 1992 [accessed 2020 Nov 10];89(14):6232–6236. /pmc/articles/PMC49474/?report=abstract. doi:10.1073/pnas.89.14.6232

3. Lobe CG, Nagy A. Conditional genome alteration in mice. BioEssays. 1998 [accessed 2020 Nov 10];20(3):200–208. https://onlinelibrary.wiley.com/doi/full/10.1002/%28SICI%291521-1878%28199803%2920%3A3%3C200%3A%3AAID-BIES3%3E3.0.CO%3B2-V. doi:10.1002/(SICI)1521-1878(199803)20:3<200::AID-BIES3>3.0.CO;2-V

4. Metzger D, Clifford J, Chiba H, Chambon P. Conditional site-specific recombination in mammalian cells using a ligand- dependent chimeric Cre recombinase. Proceedings of the National Academy of Sciences of the United States of America. 1995 [accessed 2020 Nov 10];92(15):6991–6995. /pmc/articles/PMC41457/?report=abstract. doi:10.1073/pnas.92.15.6991

5. Schwenk F, Kühn R, Angrand PO, Rajewsky K, Stewart AF. Temporally and spatially regulated somatic mutagenesis in mice. Nucleic Acids Research. 1998 [accessed 2020 Nov 10];26(6):1427–1432. /pmc/articles/PMC147429/?report=abstract. doi:10.1093/nar/26.6.1427

6. Barbieri RL. The Breast. In: Yen & Jaffe's Reproductive Endocrinology. Elsevier; 2009. p. 235–248. https://www.sciencedirect.com/topics/medicine-and-dentistry/1-1-2-triphenylethylene-derivative. doi:10.1016/B978-1-4160-4907-4.00010-3

7. Nakai M, Uchida K, Teuscher C. The development of male reproductive organ abnormalities after neonatal exposure to tamoxifen is genetically determined. Journal of Andrology. 1999 [accessed 2020 Nov 10];20(5):626–634. https://onlinelibrary.wiley.com/doi/full/10.1002/j.1939-4640.1999.tb02564.x. doi:10.1002/j.1939-4640.1999.tb02564.x

8. Tucker HLM, Holdridge J, Parsons CLM, Akers RM. Excess deposition of collagen in mammary glands of tamoxifen-treated Holstein heifers is associated with impaired mammary growth. Domestic Animal Endocrinology. 2018 [accessed 2020 Nov 10];65:49–55. https://pubmed.ncbi.nlm.nih.gov/29894894/. doi:10.1016/j.domaniend.2018.05.006

9. Mao D, Mi J, Pan X, Li F, Rui Y. Tamoxifen inhibits the progression of trauma-induced heterotopic ossification in mice. Medical Science Monitor. 2019 [accessed 2020 Nov 10];25:7872–7881. /pmc/articles/PMC6820362/?report=abstract. doi:10.12659/MSM.916733

10. Zahreddine R, Davezac M, Smirnova NF, Buscato M, Lhuillier E, Lupieri A, Solinhac R, Vinel A, Vessieres E, Henrion D, et al. Tamoxifen Accelerates Endothelial Healing by Targeting ERα in Smooth Muscle Cell. Circulation Research. 2020 Oct 5 [accessed 2020 Nov 10]. https://pubmed.ncbi.nlm.nih.gov/33012251/. doi:10.1161/circresaha.120.317062

11. A A, C F, I R-L, G F, M A, M B, C O, H B, H L, P G, et al. The AF-1 activation function of estrogen receptor α is necessary and sufficient for uterine epithelial cell

proliferation in vivo. Endocrinology. 2013 [accessed 2021 Aug 26];154(6):2222–2233. https://pubmed.ncbi.nlm.nih.gov/23580568/. doi:10.1210/EN.2012-2059

12. Best KT, Studentsova V, Ackerman JE, Nichols AEC, Myers M, Cobb J, Knapp E, Awad HA, Loiselle AE. Effects of tamoxifen on tendon homeostasis and healing: Considerations for the use of tamoxifen-inducible mouse models. Journal of Orthopaedic Research. 2020 Jun 9 [accessed 2020 Nov 10]:jor.24767. https://onlinelibrary.wiley.com/doi/abs/10.1002/jor.24767. doi:10.1002/jor.24767

13. Beason DP, Kuntz AF, Hsu JE, Miller KS, Soslowsky LJ. Development and evaluation of multiple tendon injury models in the mouse. Journal of Biomechanics. 2012 [accessed 2016 Jul 11];45(8):1550–1553. http://www.ncbi.nlm.nih.gov/pubmed/22405494. doi:10.1016/j.jbiomech.2012.02.022

14. Dunkman AA, Buckley MR, Mienaltowski MJ, Adams SM, Thomas SJ, Kumar A, Beason DP, Iozzo R V, Birk DE, Soslowsky LJ. The injury response of aged tendons in the absence of biglycan and decorin. Matrix Biology. 2014 [accessed 2016 Jul 13];35:232–238. http://www.ncbi.nlm.nih.gov/pubmed/24157578. doi:10.1016/j.matbio.2013.10.008

15. Dunkman AA, Buckley MR, Mienaltowski MJ, Adams SM, Thomas SJ, Satchell L, Kumar A, Pathmanathan L, Beason DP, Iozzo R V, et al. The tendon injury response is influenced by decorin and biglycan. Annals of Biomedical Engineering. 2014 [accessed 2016 Jul 13];42(3):619–630. http://www.ncbi.nlm.nih.gov/pubmed/24072490. doi:10.1007/s10439-013-0915-2

16. Favata M. Scarless Healing in the Fetus: Implications and Strategies for Postnatal Tendon Repair. University of Pennsylvania; 2006.

17. Lake SP, Miller KS, Elliott DM, Soslowsky LJ. Effect of fiber distribution and realignment on the nonlinear and inhomogeneous mechanical properties of human

supraspinatus tendon under longitudinal tensile loading. Journal of Orthopaedic Research. 2009 [accessed 2016 May 31];27(12):1596–1602. http://www.ncbi.nlm.nih.gov/pubmed/19544524. doi:10.1002/jor.20938

18. Robinson KA, Sun M, Barnum CE, Weiss SN, Huegel J, Shetye SS, Lin L, Saez D, Adams SM, Iozzo R V., et al. Decorin and biglycan are necessary for maintaining collagen fibril structure, fiber realignment, and mechanical properties of mature tendons. Matrix Biology. 2017 Sep 5 [accessed 2017 Sep 25]. http://www.sciencedirect.com/science/article/pii/S0945053X17301063?via%3Dihub. doi:10.1016/j.matbio.2017.08.004

19. Miller KS, Connizzo BK, Feeney E, Soslowsky LJ. Characterizing local collagen fiber re-alignment and crimp behavior throughout mechanical testing in a mature mouse supraspinatus tendon model. Journal of Biomechanics. 2012 [accessed 2019 May 30];45(12):2061–2065. https://www.sciencedirect.com/science/article/abs/pii/S0021929012003387. doi:10.1016/J.JBIOMECH.2012.06.006

20. Ma X, Liu Y, Wang Q, Chen Y, Liu M, Li X, Xiang R, Wei Y, Duan Y, Han J. Tamoxifen induces the development of hernia in mice by activating MMP-2 and MMP-13 expression. Biochimica et Biophysica Acta - Molecular Basis of Disease. 2015;1852(5):1038–1048. doi:10.1016/j.bbadis.2015.02.006

21. Li X, Clappier C, Kleiter I, Heuchel R. Tamoxifen affects chronic pancreatitis-related fibrogenesis in an experimental mouse model: an effect beyond Cre recombination. FEBS Open Bio. 2019 [accessed 2020 Nov 25];9(10):1756–1768. https://onlinelibrary.wiley.com/doi/abs/10.1002/2211-5463.12714. doi:10.1002/2211-5463.12714

CHAPTER 3: BIGLYCAN HAS A MAJOR ROLE IN MAINTENANCE OF MATURE TENDON MECHANICS

3.1 Introduction

Tendon is a dense connective tissue composed of highly organized uniaxial collagen fibrils that provides joint stability and transmits force between muscle and bone. It is composed primarily of collagens, water, proteoglycans, glycoproteins, and cells.[1] The composition of the extracellular matrix (ECM) is vital for normal development and maintenance of tendon structure, mechanical properties, and function.[2] Small leucine-rich proteoglycans (SLRPs) have been implicated in regulation of fibrillogenesis, and the resulting establishment of tendon structure and mechanics. The most abundant SLRPs in tendon are decorin and biglycan, two class I SLRPs with structurally similar core proteins with one or two glycosaminosglycan (GAG) chains, respectively, that compete for binding sites on fibrillar collagens.[3,4] While decorin expression constitutes approximately 80% of SLRP expression in tendon,[5] compensatory upregulation has been demonstrated with biglycan after knockdown, indicating functional redundancy between these proteins.[3,6,7]

Previous studies have attempted to determine the roles of decorin and biglycan in mature tendon mechanics and structure using knockout models.[8–13] Overall, these studies consistently demonstrated that decorin and biglycan knockout impacted viscoelastic mechanics and collagen fibril structure, with decorin knockout often resulting in the more severe tendon phenotype while biglycan knockout impacted tendon properties to a lesser degree.[10–13] This led to the suggestion of coordinated role for these SLRPs with biglycan having a more modulatory role during tendon development. However, the precise roles of decorin and biglycan in establishing and maintaining tendon properties during homeostasis is still unclear. A major obstacle in interpreting the

results of these studies is the inability to isolate effects in homeostasis due to the impact of SLRP knockout during tendon development that occurs with the use of conventional knockout models. Tamoxifen (TM) inducible mouse knockdown models provide the ability to temporally control SLRP expression, removing the confounding variable of altered developmental processes when determining the precise roles of decorin and biglycan in maintaining mature, homeostatic tendon mechanical properties and structure.

Our lab has recently used TM-inducible knockdowns to explore changes in tendon mechanics, structure, and composition after loss of decorin and biglycan expression in adult mice.[14] The TM-inducible compound-null decorin and biglycan (I-*Dcn*$^{-/-}$/*Bgn*$^{-/-}$) mouse model was used to define the effects of decorin and biglycan knockout (together) in mature mice 30 days after Cre induction.[14] The absence of decorin and biglycan resulted in inferior mechanical properties and altered collagen fibril structure.[14] However, the individual roles of decorin and biglycan in these changes, and whether one of these was the dominant driver of the changes, remains unknown.

Therefore, the purpose of this study was to determine the individual roles of each molecule in tendon mechanics and structure in mature mice during homeostasis utilizing TM-inducible knockdown of decorin or biglycan for 30 days in mature mice. Conventional knockouts that target decorin and biglycan indicated that decorin is the primary SLRP in developing and maintaining tendon structure and mechanics, while knockout of biglycan had minimal effect on these parameters.[9,10,15] Additionally, biglycan expression is known to peak shortly after birth, while decorin expression stays consistent.[16] Therefore, we hypothesized that knockdown of decorin in mature tendon would result in detrimental changes to tendon mechanics and structure, while knockdown of biglycan would have a lesser effect on these parameters.

3.2 Methods

3.2.1 Mice

Adult female wild type control mice, *Dcn*$^{+/+}$/*Bgn*$^{+/+}$ (WT, n=16) as well as inducible *Dcn*$^{flox/flox}$ (I-*Dcn*$^{-/-}$, n=16), and *Bgn*$^{flox/flox}$ (I-*Bgn*$^{-/-}$, n=16) mice were utilized. The conditional *Dcn*$^{flox/flox}$ and *Bgn*$^{flox/flox}$ mice with a tamoxifen (TM) inducible Cre, (B6.129-Gt(ROSA)26Sortm1(cre/ERT2)Tyj/J, Jackson Labs) have been previously described.[14] All mice were in a C57/BL6 background (Charles River). Female mice were utilized for all groups in this study because *Bgn* is located on the X chromosome. All personnel were blinded during data collection. This study was approved by the University of South Florida and the University of Pennsylvania Institutional Animal Care and Use Committees.

3.2.2 Cre-induction Protocol

I-*Dcn*$^{-/-}$ and I-*Bgn*$^{-/-}$ knockout mice and WT mice received three consecutive daily intraperitoneal tamoxifen injections (4.5 mg/40 g body weight) beginning at 120d, then were euthanized at 150d.[14] WT mice received tamoxifen injections to control for any unintended side effects.

3.2.3 Biomechanics

Patellar tendons (n = 12-14/group) were prepared for mechanical testing as previously described.[17] Briefly, patella-tendon-tibia complexes were dissected, then scanned using a custom laser device to measure cross-sectional area.[18] Verhoeff's stain was used to apply stain lines at the tibial insertion, 1 mm and 2 mm from the tibial insertion, and at the distal patella for optical strain tracking. The tibia was secured in a custom 3D-printed pot using poly(methyl methacrylate). Custom fixtures were used to secure the pot and patella during mechanical testing.

During testing, tendons were loaded into a 1x phosphate-buffered saline bath at 37°C secured to a tensile testing system (Instron 5848, Instron, Norwood, MA) integrated with an established cross-polarized light setup.[14,19] The viscoelastic testing protocol consisted of preconditioning, stress relaxations for 600 seconds at 3%, 4%, and 5% strain with each followed by a series of 10 frequency sweeps at 0.1, 1, 5, and 10 Hz, a return to gage length for 60 s, and ending with a ramp-to-failure at a strain rate of 0.1%/s. A series of image maps, each consisting of 18 images taken at 0.07s intervals with a 12s gap between each image map, were taken throughout the ramp-to-failure for collagen fiber realignment and optical strain tracking data.[19] Collagen fiber realignment, outputted as circular variance, was calculated using a custom program, and has an inverse relationship with the realignment of collagen fibers (Matlab R2015a, Mathworks, Inc., Natick, MA).[20]

Maximum stress was calculated from stress-strain data. Optical tracking was used to compute midsubstance and insertion modulus at the tibial insertion (Matlab R2015a, Mathworks, Inc., Natick, MA). Dynamic modulus (E*) and tan (δ), representing the phase shift in the stress-strain relationship, were calculated at each strain-frequency combination.

3.2.4 Real-time PCR

Patellar tendons were collected at the time of sacrifice and stored under liquid nitrogen. Frozen patellar tendons were cut into small pieces and total RNA was extracted using a RNeasy Micro Kit (QIAGEN). Total RNA (4 ng/well) was subjected to reverse transcription using the High-Capacity cDNA Reverse Transcription Kit (Applied Biosystems) and real-time PCR was performed with Fast SYBR Green PCR master mix (Applied Biosystems) on a StepOnePlus Real Time PCR system (Applied Biosystems).

The primer sequences are listed in Table 1. Each sample was run in duplicate (*n* = 5/group) and data were analyzed using StepOne software c2.0 (Applied Biosystems). b-actin was used as an internal control to standardize the amount of sample total RNA.

Table 1. Primer sequences used for real-time PCR.

	Forward Primer	Reverse Primer
Dcn	TGAGCTTCAACAGCATCACC	AAGTCATTTTGCCCAACTGC
Bgn	CTACGCCCTGGTCTTGGTAA	ACTTTGCGGATACGGTTGTC
Fmod	GAAGGGTTGTTACGCAAATGG	AGATCACCCCCTAGTCTGGGTTA
Lum	TCCACTTCCAAAGTCCCTGCAAGA	AAGCCGAGACAGCATCCTCTTTGA
Kera	CCTGGAAAGCAAGGTGCTGTA	TCATAGGCCTGTCTCACACTCTGT
Col1a1	CTTCACCTACAGCACCCTTGTG	TGACTGTCTTGCCCCAAGTTC
β-actin	AGATGACCCAGATCATGTTTGAGA	CACAGCCTGGATGGCTACGT

3.2.5 Immuno-blots

Decorin and biglycan content was analyzed immuno-chemically using a Wes™ automated Western blotting system (ProteinSimple, San Jose, CA). Tendons were dissected at day 150. Individual mice (n=3) were used for each genotype. Two tendons from each mouse were cut into small pieces and protein was extracted using an extraction buffer composed of 4 M guanidine-HCl, 50 mM sodium acetate, pH 5.8 with proteinase inhibitor (Thermo Scientific, Waltham, MA) at 4°C for 48 hr with shaking. The extraction was clarified by centrifugation and then went through 7K MWCO Zeba Spin Desalting Columns (Peirce Biotechnology, Rockford, IL) to change to the digestion buffer containing 150 mM Tris-HCl, 150 mM NaCl, pH 7.3. Samples were digested with chondroitinase ABC (Seikagaku Biobusiness Corporation, Tokyo, Japan) for 24 hr at

37°C. Total protein concentration was determined using BCA protein assay kit (Pierce Biotechnology, Rockford, IL). Samples were diluted with 0.1× sample buffer (ProteinSimple, San Jose, CA) at a concentration of either 0.2 µg/µl for detecting biglycan or further diluted 10 times for detecting decorin using WES system. Denatured protein samples were loaded into single designated wells of Wes Separation 12-230 kDa 25 Capillary Cartridges, rabbit anti-mouse decorin (LF113, 1:500 dilution, provided by Dr. L. Fisher, NIH-NIDCR) antibody or biglycan antibody (LF159, 1:100 dilution, provided by Dr. L. Fisher, NIH-NIDCR) and the Wes anti-rabbit detection module was used for detection. Quantification by densitometry was performed using the area of the targeted protein and normalized to total protein amount, which was analyzed by loading an equal amount of protein to a separate capillary cartridge and detected with the Wes total protein detection module. All Wes reagents (separation module and detection modules) were purchased from ProteinSimple and the Wes assay was carried out following the manufacturer's instructions. Data analyses were performed using the Compass Software (ProteinSimple).

3.2.6 Histology

For histological analysis (n = 4/group) the knee joint was isolated by cutting through the femur and tibia at the time of sacrifice. The knee was flexed to 90°, placed into a cassette, fixed in formalin, and processed using standard paraffin histological techniques. Samples were embedded in paraffin and sections were cut at 7 µm thickness before staining with hematoxylin and eosin. Two sections were imaged per sample, then cell nuclear shape and cellularity were quantified within a 2000 µm x1500 µm region of interest (ROI) using commercial software (BIOQUANT Image Analysis Corporation, Nashville, TN).

3.2.7 Transmission Electron Microscopy (TEM)

Patellar tendons from 4 different mice per group were analyzed using TEM. Samples were fixed *in situ* using standard methods.[14,21,22] Post-staining with 2% aqueous uranyl acetate followed by 1% phosphotungstic acid, pH 3.2, was utilized for contrast enhancement. Cross sections through the midsubstance of the patellar tendons were examined at 80 kV using a JEOL 1400 transmission electron microscope. Images were digitally captured at an instrument magnification of 60,000x using an Orius widefield sidemount CCD camera at a resolution of 3648 x 2672. The digital images were masked and transferred to a RM Biometrics-Bioquant Image Analysis System (Memphis, TN) for analysis. Image magnification was calibrated using a line grating replica (PELCO®, Product No. 606). Fibril diameter analyses were completed using images from the central portion of the tendon. All fibrils within a 2800 nm x 2000 nm ROI on the digitized image were analyzed. Non-overlapping ROIs were placed based on fibril orientation (i.e., cross section) and absence of cells. Diameters were measured along the minor axis of the fibril. For measurements of fibril density, the total number of fibrils within the ROI was normalized for area.

3.2.8 Statistics

All data was tested for normality using the Shapiro-Wilk test. For all biomechanics measurements and gene and protein content, a one-way ANOVA across genotype with Bonferroni post-hoc test was performed. Collagen realignment data was analyzed using a two-way ANOVA across genotype and repeated strain level with Bonferroni post-hoc tests. Nuclear aspect ratio, cellularity, and fibril diameter distributions were compared using Kolmogorov-Smirnov tests with Bonferroni post-hoc. Statistical significance was set at $p<0.05$.

3.3 Results

3.3.1 Gene Expression and Protein Content

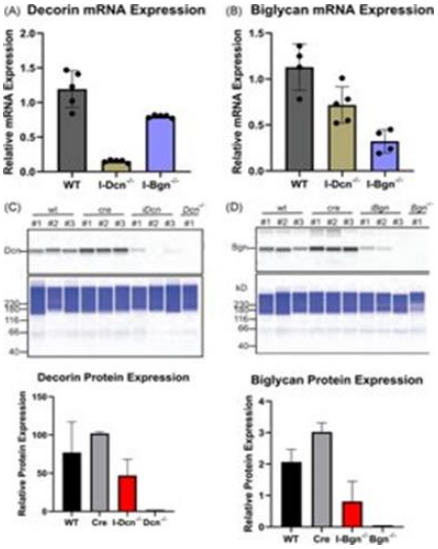

Figure 12. *(A) Dcn mRNA expression was reduced in the I-*Dcn$^{-/-}$ *patellar tendons and (B) Bgn mRNA expression was reduced in the I-*Bgn$^{-/-}$ *patellar tendons after tamoxifen treatment. (C) The immunoblots revealed reduced decorin and (D) biglycan protein content in the I-*Dcn$^{-/-}$ *and I-*Bgn$^{-/-}$ *groups, respectively. mRNA, messenger RNA*

Both decorin and biglycan mRNA expression were knocked down in the patellar tendon 30 days after Cre induction in the mature I-*Dcn*$^{-/-}$ and I-*Bgn*$^{-/-}$ mice (Fig. 11A-B). Both groups showed consistent results with reduced protein content for decorin and biglycan in their respective knockdown groups 30 days after induction (Fig. 11C-D). Both knockdown groups were reduced compared to control groups. However, conventional knockout protein content was higher than what was observed in the traditional knockout mice. Presumably this is due to incomplete turnover of SLRPs deposited prior to knockdown. There was no evidence of compensatory upregulation of biglycan in I-*Dcn*$^{-/-}$ or decorin in I-*Bgn*$^{-/-}$ mice (Fig. 11A-B). The lack of compensation after knockdown of decorin and biglycan in our mouse models gives us confidence that the changes in phenotype are due to reduced content of the target protein, and not obscured by the functional redundancy between decorin and biglycan.

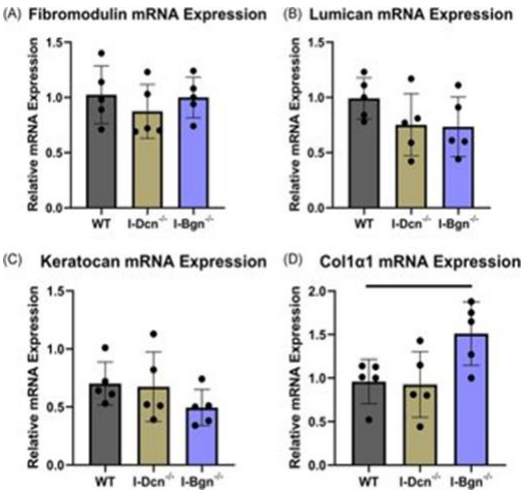

Figure 11. There were no changes in mRNA expression levels of (A) Fmod, (B) Lum, and (C) Kera after knockdown of decorin or biglycan. (D) Upregulation of Col1α1 was observed after biglycan knockdown. mRNA, messenger RNA

The expression of closely related class II SLRPs known to have roles in fibrillogenesis, fibromodulin (*Fmod*), lumican (*Lum*), and

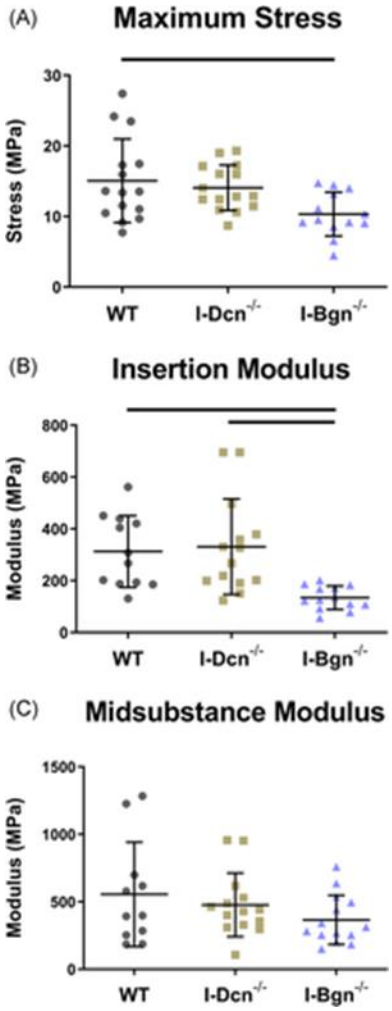

Figure 13. (A) Maximum stress and (B) insertion modulus were significantly reduced after biglycan knockdown, while these properties were unaffected after decorin knockdown. (C) Midsubstance modulus was not affected in the I-Dcn$^{-/-}$ or I-Bgn$^{-/-}$ groups

keratocan (*Kera*), were analyzed to determine if any compensatory alterations in expression occurred because of decorin of biglycan knockdown. No significant changes in mRNA expression of *Fmod, Lum,* or *Kera* were observed after knockdown of decorin or biglycan (Fig.12A-C). Collagen I expression was examined after knockdown using the alpha1(I) chain of collagen I as a marker. Expression in I-*Dcn*$^{-/-}$ mice was comparable to that in WT control mice. However, there was a significant increase in collagen I expression I-*Bgn*$^{-/-}$ tendons compared to WT (Fig. 12D).

3.3.2 Biomechanical Properties

The quasistatic and viscoelastic biomechanical properties of the mouse patellar tendons were evaluated. Quasistatic mechanics analysis revealed decreased maximum stress in the I-*Bgn*$^{-/-}$ group vs WT, while no changes were seen in I-*Dcn*$^{-/-}$ (Fig. 13A). Insertion modulus showed a decrease in I-*Bgn*$^{-/-}$ compared to WT and I-*Dcn*$^{-/-}$ (Fig. 13B), while there were no differences between any groups in the midsubstance modulus (Fig. 13C). The tendons primarily failed at the tibial insertion with no sign of bony avulsion.

Viscoelastic mechanics were evaluated at 3%, 4%, and 5% (Fig. 14A-C) strain, correlating with the toe, transition, and linear regions of the stress-strain curve for mouse patellar tendons, respectively. Further supported by the quasistatic mechanics results,

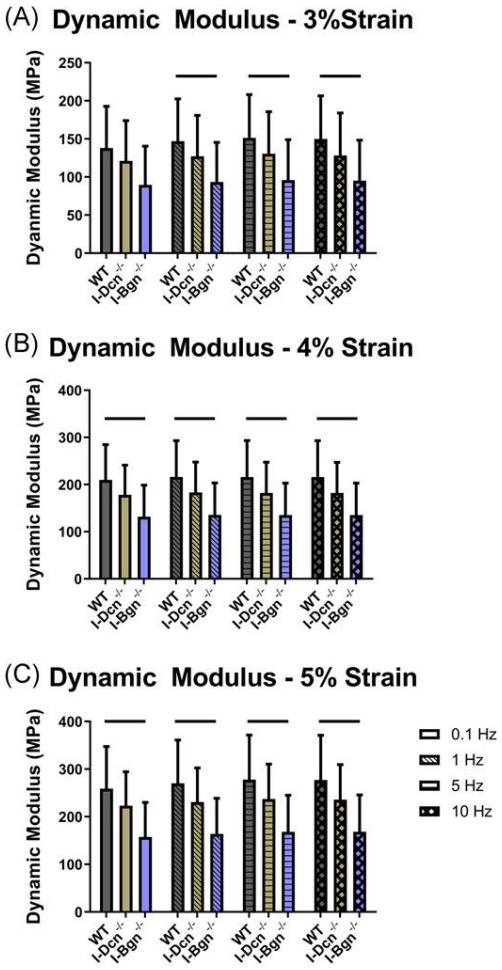

Figure 14. Dynamic modulus decreased at (A) 3%, (B) 4%, and (C) 5% strain in the I-Bgn$^{-/-}$ group, indicating a reduced ability to resist deformation during dynamic loading. These results are consistent across all loading frequencies except for 0.1 Hz at 3% strain where no changes were present in the I-Bgn$^{-/-}$ tendons. No changes in dynamic modulus were observed after knockdown of decorin

viscoelastic properties were reduced in the I-*Bgn*$^{-/-}$ group. Dynamic modulus was reduced in the absence of biglycan at all strains and frequencies compared to WT, except for 3% strain at 0.1 Hz (Fig. 14A). No changes to dynamic modulus were found in the absence of decorin, and no changes in phase shift were found between groups at any strain (not shown). Additionally, the stress relaxation tests showed a decrease in the percent relaxation between I-*Bgn*$^{-/-}$ and I-*Dcn*$^{-/-}$ at all strains and decreases between I-*Bgn*$^{-/-}$ and WT at 4% and 5% strain (Fig. 15).

Collagen fiber realignment was altered in the absence of both decorin and biglycan (Fig. 16). In the midsubstance and insertion, I-Dcn$^{-/-}$ realignment was delayed, while I-*Bgn*$^{-/-}$ realignment occurred over a larger range of strains (Fig. 16A). I-*Bgn*$^{-/-}$ also showed increased levels of realignment in the midsubstance compared to I-*Dcn*$^{-/-}$ at 3-5% strain, and increased midsubstance realignment compared to WT at 3-5%, 5-7%, and 7-9% strain. Results were similar in the insertion, with the absence of biglycan resulting in increased realignment at 3-5%, 5-7%, and 7-9% strain compared to both WT and I-*Dcn*$^{-/-}$ (Fig. 16B).

Figure 15. During the stress relaxation test at 3% strain, the percent relaxation of I-Bgn$^{-/-}$ tendons decreased compared to the I-Dcn$^{-/-}$ group. The percent relaxation of the I-Bgn$^{-/-}$ tendons also decreased at 4% and 5% strain relative to the I-Dcn$^{-/-}$ and WT groups.

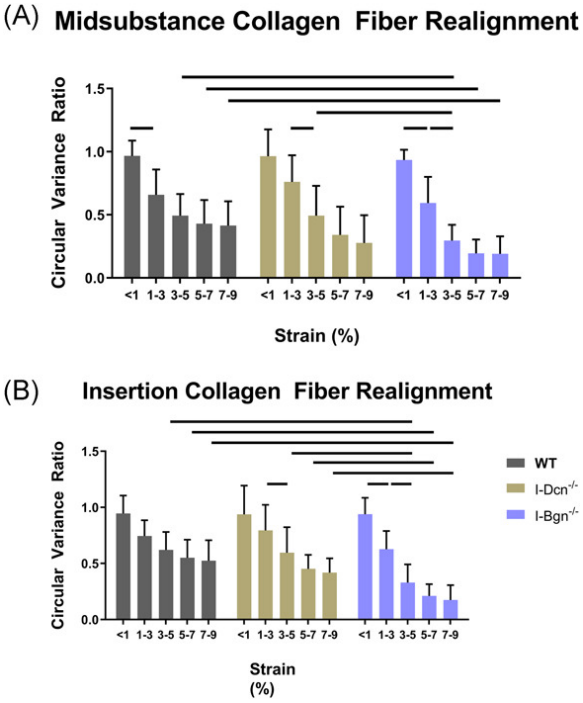

Figure 16. Knockdown of decorin delayed collagen fiber realignment in the (A) midsubstance and (B) insertion regions of the tendons. Knockdown of biglycan caused fiber realignment to occur over a larger range of strains and to a greater extent than the I-Dcn$^{-/-}$ and WT groups in both regions of the tendon.

3.3.3 Histology

Histological analysis revealed no gross differences after SLRP knockdown. However, a decrease in nuclear aspect ratio was found in the absence of biglycan compared to WT and I-*Dcn*$^{-/-}$, indicating a more spindle-like nuclear shape (Fig. 17). No changes were seen in cellularity (not shown).

3.3.4 Transmission Electron Microscopy

Tendon collagen fibril diameters were measured 30 days after Cre induction in I-*Dcn*$^{-/-}$ and I-*Bgn*$^{-/-}$ and compared to controls using TEM. Overall collagen fibril structure was similar between WT, I-*Dcn*$^{-/-}$, and I-*Bgn*$^{-/-}$ with circular cross-sectional profiles (Fig. 18A). However, I-*Dcn*$^{-/-}$ and I-*Bgn*$^{-/-}$ had increased fibril diameters compared to WT tendons (Fig. 18B and C). Median collagen fibril diameter was increased in I-*Dcn*$^{-/-}$ and I-*Bgn*$^{-/-}$ versus WT (108.4 nm, 106.0 nm, and

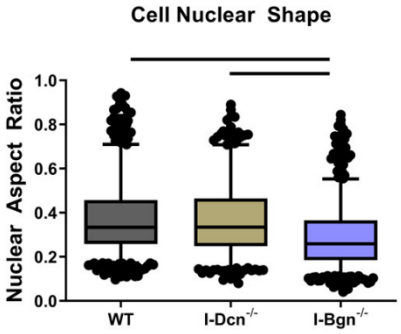

Figure 17. *Nuclear aspect ratio decreased in the I-*Bgn$^{-/-}$ *group compared to WT and I-*Dcn$^{-/-}$ *groups.*

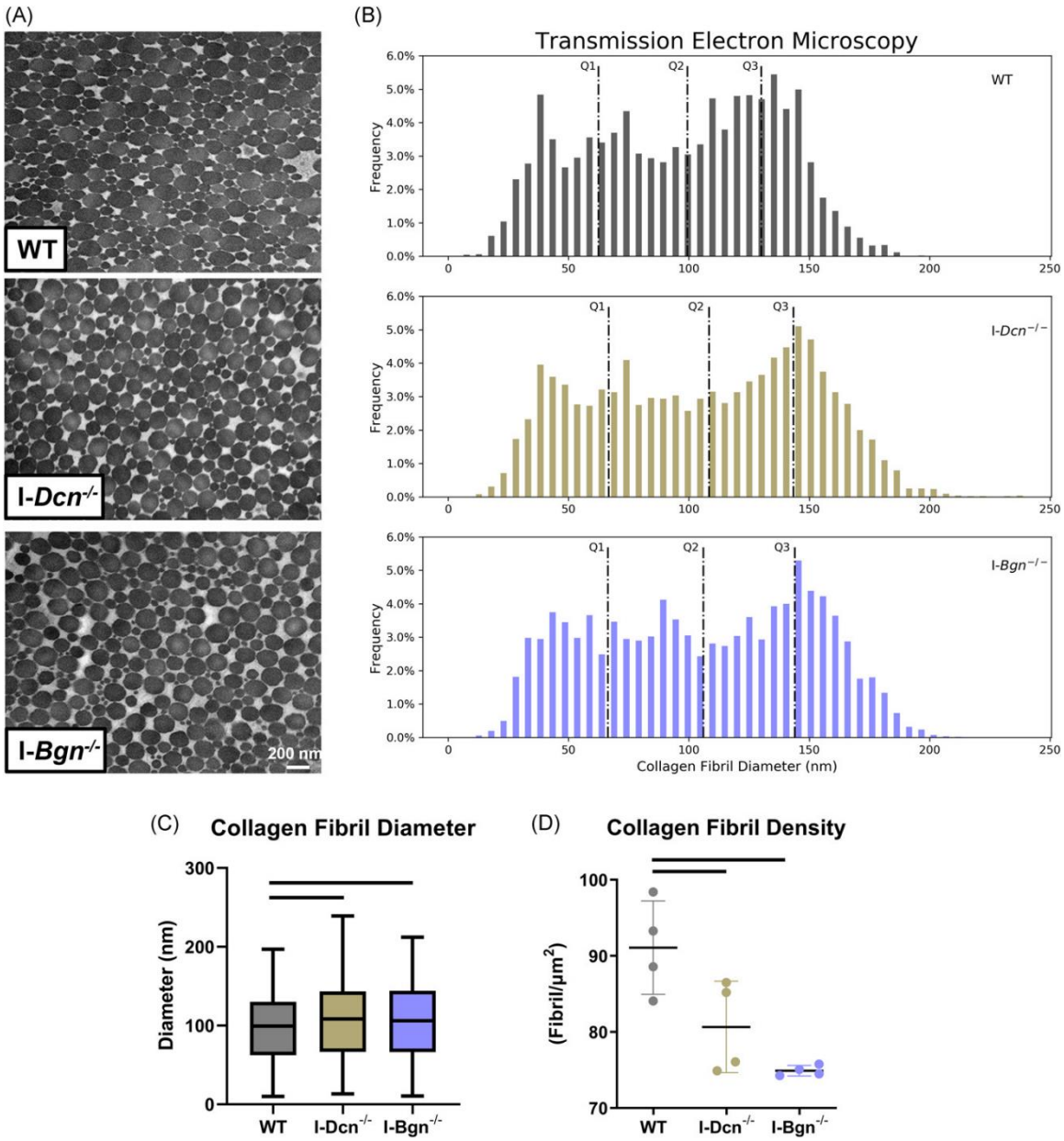

Figure 18. Transmission electron microscopy revealed increased collagen fibril diameter and decreased fibril density after SLRP knockdown. (A) All groups displayed circular cross-sectional collagen fibril profiles. (B) Knockdown of decorin and biglycan resulted in similar increases across all fibril diameter quartiles relative to WT, (C) resulting in an overall increase in collagen fibril diameter and (D) decrease in collagen fibril density. SLRP, small leucine-rich proteoglycans

99.4 nm, respectively). Similar increases were found for quartiles 1 (66.7 nm, 66.4 nm, and 62.4 nm) and 3 (143.4 nm, 144.0 nm, and 130.1 nm). Collagen fibril density was also decreased in I-*Dcn*$^{-/-}$ and I-*Bgn*$^{-/-}$ compared to WT (Fig. 18D). Overall, the inducible

knockdown groups had altered collagen fibril diameters with broader distributions versus WT, but the I-*Dcn*$^{-/-}$ and I-*Bgn*$^{-/-}$ distributions were comparable.

3.4 Discussion

The objective of this study was to determine the regulatory roles of decorin and biglycan on tendon mechanics and structure during tendon homeostasis. We used TM-inducible models in skeletally mature mice to avoid the confounding variables associated with conventional knockouts that arise from undergoing development with altered expression. Similar to the present study, our previous work used a TM-inducible compound decorin/biglycan (I-*Dcn*$^{-/-}$/*Bgn*$^{-/-}$) knockdown mouse model to determine the regulatory roles of decorin and biglycan in maintaining structure and function in mature tendons.[14] The I-*Dcn*$^{-/-}$/*Bgn*$^{-/-}$ tendons revealed structural alterations compared to WT controls that occurred at the collagen fibril level, with a general increase across the entire fibril diameter distribution and a population of unusually large fibrils.[14] These changes to I-*Dcn*$^{-/-}$/*Bgn*$^{-/-}$ collagen fibril structure were similar to what was observed in conventional decorin-null tail tendons, which also produced a collagen fibril diameter distribution that was larger than WT across the entire distribution and included a population of unusually large fibrils.[15,23] Due to the similarities in structural changes between I-*Dcn*$^{-/-}$/*Bgn*$^{-/-}$ and decorin-null tendons we hypothesized that the I-*Dcn*$^{-/-}$/*Bgn*$^{-/-}$ model may reflect the decorin-null phenotype. Since biglycan expression normally decreases after development[15,16] we also hypothesized that decorin may be the primary regulator of tendon homeostasis at maturity while biglycan has either no regulatory role or a minor role. Based on these insights, in our present study we hypothesized that knockdown of decorin would result in detrimental alterations to tendon mechanics and structure, while biglycan knockdown would have no effect on these parameters.

The validity of our knockdown models was confirmed with substantial reductions in mRNA expression and protein content for decorin and biglycan in the I-*Dcn*$^{-/-}$ and I-*Bgn*$^{-/-}$ groups, respectively. No changes in gene expression were found in any of the fibril-associated class I or II SLRPs due to decorin or biglycan knockdown. This suggests that our I-*Dcn*$^{-/-}$ and I-*Bgn*$^{-/-}$ mice are effective models to study the regulatory roles of Dcn and Bgn in tendon since there are no compensatory upregulation of the class II SLRPs that have similarities in structure and function.

Contrary to our hypothesis, induced knockdown of decorin resulted in no changes to tendon mechanics. The only change to mechanics observed in I-*Dcn*$^{-/-}$ tendons was higher collagen realignment in the midsubstance between 3-5% strain compared to WT. Surprisingly, knockdown of biglycan resulted in broad changes to tendon mechanics. I-*Bgn*$^{-/-}$ tendons revealed changes to quasistatic and viscoelastic mechanics, with reductions in insertion modulus, maximum stress, dynamic modulus, and stress relaxation compared to WT. Collagen realignment of I-*Bgn*$^{-/-}$ tendons differed from the I-*Dcn*$^{-/-}$ tendons, with realignment occurring between 1%, 3%, and 5% strain and having a more aligned matrix from 5-9% strain in the midsubstance and insertion compared to WT and I-*Dcn*$^{-/-}$. The collagen realignment observed in I-*Bgn*$^{-/-}$ tendons is analogous to the realignment demonstrated by I-*Dcn*$^{-/-}$/*Bgn*$^{-/-}$ tendons, which also increased collagen realignment between 1%, 3%, and 5% strain and increased collagen fiber realignment from 5-9% strain compared to WT.[14] There were further similarities between I-*Bgn*$^{-/-}$ and I-*Dcn*$^{-/-}$/*Bgn*$^{-/-}$ tendons during dynamic loading, where both models produced a lower dynamic modulus compared to WT tendons at loading frequencies of 0.1, 1, 5, and 10 Hz.[14] Overall, these data suggest that biglycan is playing an active

regulatory role during tendon homeostasis that is comparable, if not more significant than, the role of decorin.

These results are surprising and in contrast to previous studies that showed conventional biglycan knockouts have little effect on tendon properties. Specifically, a previous study using conventional heterozygote and null biglycan knockout mice evaluated at 5 months of age demonstrated an increased dynamic modulus with no changes to quasistatic mechanics or fibril diameter.[9] Conversely, knockout of decorin has previously revealed a greater effect on tendon mechanics including increased dynamic modulus, decreased phase shift, and increased stress relaxation.[8] Another study examined decorin and biglycan knockout in mouse tail fascicles, patellar tendons, and flexor digitorum longus (FDL) tendons and found the results to be highly tendon dependent.[13] Knockout of biglycan had no effect on quasistatic or viscoelastic properties in the tendon tail fascicle or patellar tendon, but a reduction in maximum stress and modulus was found in the FDL.[13] Decorin knockout increased quasistatic mechanics in the patellar tendon and FDL and increased percent relaxation in the patellar tendon.[13] The differential effects of decorin and biglycan knockout found in this study were attributed to differences in tendon location and function. Given the advantages of TM-inducible SLRP knockdown models including normal tendon development and no changes to SLRP expression, the data from the current study are likely more reliable to determine the effects of decorin and biglycan knockdown on tendon structure and mechanics than what has been described using traditional knockdown models.

The changes seen after knockdown of decorin and biglycan could also be due to tissue remodeling mediated by higher levels of TGF-β. Both decorin and biglycan can bind to TGF-β, which reduces TGF-β activity in the tissue. The inhibition of TGF-β via

decorin and biglycan binding occurs in a dose-dependent manner, and the affinity to TGF-β is similar between decorin and biglycan.[24] An increase in pro-fibrotic TGF-β-mediated tissue remodeling would be expected after knockdown of decorin or biglycan. However, given the high expression levels of decorin relative to biglycan in the tendon ECM, we would expect TGF-β activity to have a larger impact on the mechanics of I-*Dcn*$^{-/-}$ tendons than on the I-Bg*n*$^{-/-}$ tendons. It is possible that decorin or biglycan expression combined with fibromodulin is sufficient in preventing extensive remodeling by TGF-β since fibromodulin is more effective at sequestering TGF-β activity because of the ability to bind to both the active and latent forms of TGF-β.[25]

The structural changes associated with knockdown of decorin and biglycan were similar at the collagen fibril level with an increase in collagen fibril diameter and decreased collagen fibril density compared to WT. These changes to the tendon microstructure are likely due to the roles of decorin and biglycan in collagen fibrillogenesis. Decorin and biglycan play vital roles throughout the development of tendon structure, and this is attributed to the coordinate interactions between these two proteins during collagen fibrillogenesis. Knockout of decorin or biglycan has produced alterations to the collagen fibril diameter distribution and irregularly shaped fibrils that are maintained throughout adulthood. Additionally, decorin and biglycan play important roles in stabilizing mature collagen fibrils by preventing lateral fusion of smaller diameter fibrils. This study provides additional evidence that decorin and biglycan play vital roles in maintaining tendon microstructure in mature tissue.

Biglycan knockdown also produced surprising histology results. Previous studies showed an absence of changes to cellularity and nuclear shape with both decorin and biglycan knockout,[14] while the inducible biglycan knockdown in the current study

revealed decreased nuclear shape, which is associated with decreased cellular activity in tendon. A potential mechanism to explain the changes found in tendon after biglycan knockdown is the role of biglycan in maintaining the tendon stem/progenitor cell (TSPC) niche.[26] TSPCs reside in a niche that is surrounded predominantly by ECM proteins. Evidence suggests that biglycan, and not decorin, plays a major role in the maintenance of this niche by regulating tendon progenitor differentiation, inflammation, and sequestering growth factors. Disruption of the TSPC niche using *Bgn*$^{0/-}$*Fmod*$^{-/-}$ knockout mice resulted in an increase in the quantity of TSPCs and dysregulation in the balance of cytokines.[26] Additonal evidence also suggests that disruption of the tissue niche in tendon can result in a switch from homeostasis to tissue degradation that is mediated by activation of the immune response, production of ROS, and activation proteolytic enzymes.[27] A possible reason for the decreased mechanics observed in the I-*Bgn*$^{-/-}$ tendons is that knockdown of biglycan disrupted the tissue niche, which triggered a switch from homeostasis to a degenerative state.

This study is not without limitations. Our use of an inducible knockout model combined with the 30-day timeline does not ensure total knockout and clearance of the decorin and biglycan proteins. However, the tissue turnover rate of decorin and biglycan are approximately 18 days and 14 days, respectively, ensuring that this timeline is sufficient for reduced protein content in our models.[28,29] This data is in agreement with the protein content data in this study. Additionally, this study examined a targeted set of markers, comprised of collagens and fibril associated SLRPs, while investigating the roles of decorin and biglycan in the maintenance of tendon structure and mechanics. Utilizing proteomics to capture all the protein content changes associated with decorin and biglycan knockdown would give a broader view of the molecular mechanisms at

play. Finally, our histology results revealed changes in cellular phenotype because of biglycan knockdown. Future work analyzing various aspects of cellular behavior after knockdown of decorin or biglycan, for example cellular proliferation, senescence, apoptosis, and matrix production, would provide further insight into the roles of decorin and biglycan in cellular maintenance and signaling during homeostasis.

Our novel inducible I-*Dcn*$^{-/-}$ and I-*Bgn*$^{-/-}$ mouse models allowed for the analysis of decorin and biglycan knockdown in adult tendons without the confounding variables of SLRP knockout during development. Surprisingly, knockdown of biglycan resulted in alterations to tendon mechanics, and structure, while knockdown of decorin had no effects on mechanics and minor effects on tendon structure. This provides evidence against the idea that decorin plays the dominant role among SLRPs in tendon maintenance while biglycan has a minor modulatory role. Results from this study highlight the importance of TM-inducible models in evaluating the role of proteins in adult models. Future work will explore the effects of TM-inducible decorin and biglycan knockdown in aged tendons.

3.5 References

1. Taye N, Karoulias SZ, Hubmacher D. 2019. The “other” 15–40%: The Role of Non-Collagenous Extracellular Matrix Proteins and Minor Collagens in Tendon. J. Orthop. Res. 38(1):23–35 [cited 2020 Jan 8] Available from: https://onlinelibrary.wiley.com/doi/abs/10.1002/jor.24440.

2. Kjaer M. 2004. Role of Extracellular Matrix in Adaptation of Tendon and Skeletal Muscle to Mechanical Loading. Physiol. Rev. 84(2):649–698 Available from: http://physrev.physiology.org/cgi/doi/10.1152/physrev.00031.2003.

3. Zhang G, Young BB, Ezura Y, et al. 2005. Development of tendon structure and function: Regulation of collagen fibrillogenesis. J. Musculoskelet. Neuronal Interact. 5(1):5–21 [cited 2017 Aug 10] Available from: https://pubmed.ncbi.nlm.nih.gov/15788867/.

4. Iozzo R V. 1999. The biology of the small leucine-rich proteoglycans. Functional network of interactive proteins. J. Biol. Chem. 274(27):18843–18846 [cited 2016 Aug 31] Available from: http://www.jbc.org/cgi/doi/10.1074/jbc.274.27.18843.

5. Samiric T, Ilic MZ, Handley CJ. 2004. Characterisation of proteoglycans and their catabolic products in tendon and explant cultures of tendon. Matrix Biol. 23(2):127–140.

6. Casar JC, McKechnie BA, Fallon JR, et al. 2004. Transient up-regulation of biglycan during skeletal muscle regeneration: Delayed fiber growth along with decorin increase in biglycan-deficient mice. Dev. Biol. 268(2):358–371.

7. Dunkman AA, Buckley MR, Mienaltowski MJ, et al. 2013. Decorin expression is

important for age-related changes in tendon structure and mechanical properties. Matrix Biol. 32(1):3–13 [cited 2016 Aug 26] Available from: http://www.ncbi.nlm.nih.gov/pubmed/23178232.

8. Dourte LM, Pathmanathan L, Jawad AF, et al. 2012. Influence of decorin on the mechanical, compositional, and structural properties of the mouse patellar tendon. J. Biomech. Eng. 134(3):031005 [cited 2016 Jul 18] Available from: http://www.ncbi.nlm.nih.gov/pubmed/22482685.

9. Dourte LM, Pathmanathan L, Mienaltowski MJ, et al. 2013. Mechanical, compositional, and structural properties of the mouse patellar tendon with changes in biglycan gene expression. J. Orthop. Res. 31(9):1430–1437 [cited 2017 Aug 10] Available from: http://www.ncbi.nlm.nih.gov/pubmed/23592048.

10. Gordon J, Freedman BR, Zuskov A, et al. 2015. Achilles tendons from decorin- and biglycan-null mouse models have inferior mechanical and structural properties predicted by an image-based empirical damage model. J. Biomech. 48(10):2110–5 [cited 2016 Jul 13] Available from: http://www.ncbi.nlm.nih.gov/pubmed/25888014.

11. Connizzo BK, Sarver JJ, Birk DE, et al. 2013. Effect of age and proteoglycan deficiency on collagen fiber re-alignment and mechanical properties in mouse supraspinatus tendon. J. Biomech. Eng. 135(2):021019 [cited 2016 Aug 26] Available from: http://www.ncbi.nlm.nih.gov/pubmed/23445064.

12. Elliott DM, Robinson PS, Gimbel JA, et al. 2003. Effect of altered matrix proteins on quasilinear viscoelastic properties in transgenic mouse tail tendons. Ann. Biomed. Eng. 31(5):599–605 [cited 2018 Dec 6] Available from:

http://link.springer.com/10.1114/1.1567282.

13. Robinson PS, Huang T-F, Kazam E, et al. 2005. Influence of Decorin and Biglycan on Mechanical Properties of Multiple Tendons in Knockout Mice. J. Biomech. Eng. 127(1):181 Available from: http://biomechanical.asmedigitalcollection.asme.org/article.aspx?articleid=1413750.

14. Robinson KA, Sun M, Barnum CE, et al. 2017. Decorin and biglycan are necessary for maintaining collagen fibril structure, fiber realignment, and mechanical properties of mature tendons. Matrix Biol. [cited 2017 Sep 25] Available from: http://www.sciencedirect.com/science/article/pii/S0945053X17301063?via%3Dihub.

15. Zhang G, Ezura Y, Chervoneva I, et al. 2006. Decorin regulates assembly of collagen fibrils and acquisition of biomechanical properties during tendon development. J. Cell. Biochem. 98(6):1436–1449 [cited 2017 Aug 10] Available from: http://doi.wiley.com/10.1002/jcb.20776.

16. Ansorge HL, Adams SM, Birk DE, Soslowsky LJ. 2011. Mechanical, compositional and structural properties of the post-natal mouse Achilles tendon. Ann. Biomed. Eng. 39(7):1904–1913 [cited 2016 May 17] Available from: http://www.ncbi.nlm.nih.gov/pubmed/21431455.

17. Dunkman AA, Buckley MR, Mienaltowski MJ, et al. 2014. The tendon injury response is influenced by decorin and biglycan. Ann. Biomed. Eng. 42(3):619–630 [cited 2016 Jul 13] Available from:

http://www.ncbi.nlm.nih.gov/pubmed/24072490.

18. Favata M. 2006. Scarless Healing in the Fetus: Implications and Strategies for Postnatal Tendon Repair.

19. Lake SP, Miller KS, Elliott DM, Soslowsky LJ. 2009. Effect of fiber distribution and realignment on the nonlinear and inhomogeneous mechanical properties of human supraspinatus tendon under longitudinal tensile loading. J. Orthop. Res. 27(12):1596–1602 [cited 2016 May 31] Available from: http://www.ncbi.nlm.nih.gov/pubmed/19544524.

20. Miller KS, Connizzo BK, Feeney E, Soslowsky LJ. 2012. Characterizing local collagen fiber re-alignment and crimp behavior throughout mechanical testing in a mature mouse supraspinatus tendon model. J. Biomech. 45(12):2061–2065 [cited 2019 May 30] Available from: https://www.sciencedirect.com/science/article/abs/pii/S0021929012003387.

21. Birk DE, Trelstad RL. 1986. Extracellular compartments in tendon morphogenesis: Collagen fibril, bundle, and macroaggregate formation. J. Cell Biol. 103(1):231–240 [cited 2017 Aug 10] Available from: http://www.ncbi.nlm.nih.gov/pubmed/3722266.

22. Birk DE, Zycband EI, Woodruff S, et al. 1997. Collagen fibrillogenesis in situ: Fibril segments become long fibrils as the developing tendon matures. Dev. Dyn. 208(3):291–298 [cited 2016 May 31] Available from: http://doi.wiley.com/10.1002/%28SICI%291097-0177%28199703%29208%3A3%3C291%3A%3AAID-AJA1%3E3.0.CO%3B2-D.

23. Corsi A, Xu T, Chen XD, et al. 2002. Phenotypic effects of biglycan deficiency are linked to collagen fibril abnormalities, are synergized by decorin deficiency, and mimic Ehlers-Danlos-like changes in bone and other connective tissues. J. Bone Miner. Res. 17(7):1180–1189.

24. Kolb M, Margetts PJ, Sime PJ, Gauldie J. 2001. Proteoglycans decorin and biglycan differentially modulate TGF-β-mediated fibrotic responses in the lung. Am. J. Physiol. - Lung Cell. Mol. Physiol. 280(6 24-6) [cited 2021 Dec 11] Available from: https://journals.physiology.org/doi/abs/10.1152/ajplung.2001.280.6.L1327.

25. Hildebrand A, Romaris M, Rasmussen LM, et al. 1994. Interaction of the small interstitial proteoglycans biglycan, decorin and fibromodulin with transforming growth factor β. Biochem. J. 302(2):527–534 [cited 2021 Dec 11] Available from: /pmc/articles/PMC1137259/?report=abstract.

26. Bi Y, Ehirchiou D, Kilts TM, et al. 2007. Identification of tendon stem/progenitor cells and the role of the extracellular matrix in their niche. Nat. Med. 13(10):1219–1227.

27. Wunderli SL, Blache U, Beretta Piccoli A, et al. 2020. Tendon response to matrix unloading is determined by the patho-physiological niche. Matrix Biol. 89:11–26.

28. Burton-Wurster N, Liu W, Matthews GL, et al. 2003. TGF beta 1 and biglycan, decorin, and fibromodulin metabolism in canine cartilage. Osteoarthr. Cartil. 11(3):167–176.

29. Blumberg P, Brenner R, Budny S, Kresse H. 1997. Increased turnover of small

proteoglycans synthesized by human osteoblasts during cultivation with ascorbate and β-glycerophosphate. Calcif. Tissue Int. 60(6):554–560.

CHAPTER 4: DECORIN KNOCKDOWN IS BENEFICIAL FOR AGED TENDONS IN THE PRESENCE OF BIGLYCAN EXPRESSION

4.1 Introduction

Tendon is a hierarchically organized tissue composed of highly aligned extracellular matrix (ECM) whose predominant function is to transmit tensile forces from muscle to bone. The primary unit of the tendon is the tendon fibril, a heteropolymeric structure assembled from multiple fibril-forming collagens, glycoproteins, glycosaminoglycans (GAGs), and proteoglycans.[1] A major component of proteoglycans in tendon are small leucine-rich proteoglycans (SLRPs), which are a class of proteins involved in a variety of biological processes, including collagen fibrillogenesis, tissue turnover, and cell signal transduction.[2] Decorin (Dcn) and biglycan (Bgn) are two highly expressed fibril associated class I SLRPs that assist in the development and maintenance of tendon structure during development, homeostasis, healing, and aging by binding fibrillar collagens and regulating fibrillogenesis.[3–8] Fibromodulin, lumican, and keratocan are class II SLRPs that are structurally and functionally similar to decorin and biglycan, and regulate fibrillogenesis by binding to fibrillar collagens. Gene clustering balances the expression of these SLRPs, creating a regulatory network among these molecules. This regulatory network can result is compensatory upregulation of other SLRPs after knockdown of one of these genes. Due to the functional redundancy between fibril associated SLRPs during fibrillogenesis, it is important to investigate the expression of all these molecules when using knockdown models to better understand these relationships. Given the wide range of processes in which these proteins are involved, a complete definition of their individual and synergistic roles is required for developing novel treatments to address tendon pathologies.

With an increasingly aging and active population, the incidence of tendon injury is on the rise.[9] Tendon aging is typically characterized by changes to mechanics and structure, including decreased stiffness, modulus, and alterations to collagen fibril diameter.[7,10] While the mechanisms that cause tissue to become more susceptible to injury with increased age are largely unknown, SLRPs are known regulators of collagen fibril organization and matrix assembly in tendon, and could play a role in the age-related changes to tendon mechanics and structure. Previous work using traditional (non-inducible) mouse knockout models found that knockout of decorin ameliorated the age-related alterations to mechanics and structure that is normally observed in tendon, while minimal changes were associated with knockout of biglycan.[7] The traditional knockout models used previously found upregulation of lumican after biglycan knockout, potentially masking the true roles of biglycan during aging, and did not allow for temporal control of SLRP expression.

While studies have been conducted to explore the roles of decorin and biglycan in tendon aging, these results are confounded due to the limitations inherent to traditional knockouts that cannot isolate effects during aging from developmental effects. Recently, our lab has utilized tamoxifen-inducible decorin, biglycan, and compound decorin and biglycan knockdown mouse models to provide temporal control over SLRP expression. The compound model was initially used to determine the roles of decorin and biglycan during tendon homeostasis in mature mice 30 days after Cre induction. Despite the short timeline, the model successfully resulted in reduced decorin and biglycan gene and protein expression levels, as well as a decrease in mechanical and structural properties of the mouse patellar tendon.[11] The present study extends this work by utilizing tamoxifen-inducible decorin, biglycan, and the compound decorin and biglycan

knockdown models to study the effects of these proteins on tendon structure and function in aged tendons without disrupting tendon development.

Therefore, the objective of this study was to determine the effects of decorin and biglycan knockdown on tendon structure and mechanics in aged (300d) and geriatric (570d) tendons. We hypothesized that the targeted knockdown of decorin and compound knockdown of both decorin and biglycan in aged and geriatric mice would result in improved tendon mechanical properties compared to biglycan knockdown and wild type (WT) control mice. We also expected to find alterations to tendon fibril structure after decorin or biglycan knockdown, while the compound decorin/biglycan knockdown mice were expected to have a fibril phenotype identical to the decorin knockdown mice. Further, we hypothesized that the differences present in the aged tendons would be exacerbated in the geriatric tendons. Overall, our findings revealed that knockdown of decorin attenuates the decline in tendon mechanics associated with aging in aged, but not geriatric, mice, and knockdown of decorin and biglycan produced tendons with increased viscoelastic mechanics with age.

4.2 Methods

4.2.1 Animal Backgrounds & Cre Excision

This study was approved by the University of Pennsylvania and University of South Florida Institutional Animal Care and Use Committees. Female $Dcn^{+/+}/Bgn^{+/+}$ control (WT, n=16/age), $Dcn^{flox/flox}$ (I-$Dcn^{-/-}$, n=16/age), $Bgn^{flox/flox}$ (I-$Bgn^{-/-}$, n=16/age), and compound $Dcn^{flox/flox}/Bgn^{flox/flox}$ (I-$Dcn^{-/-}/Bgn^{-/-}$, n=16/age), mice with a tamoxifen (TM) inducible Cre, (B6.129-Gt(ROSA)26Sortm1(cre/ERT2)Tyj/J, Jackson Labs) were utilized (Supplemental Fig. 1). Cre excision of the conditional alleles was induced in mature (120 day) mice with three consecutive daily IP injections of tamoxifen (4.5mg/40g body

weight). WT mice were given TM injections to control for potential side effects. Mice were euthanized at 300 and 570 days of age (n=16/group/age).

4.2.2 SLRP & Collagen I Gene Expression

Patellar tendons were collected after sacrifice and preserved under liquid nitrogen. The frozen patellar tendons were cut into small pieces, then total RNA was extracted using a RNeasy Micro Kit (Qiagen). Total RNA (4 ng/well) was subjected to reverse transcription using the High-Capacity cDNA Reverse Transcription Kit (Applied Biosystems) and real-time PCR was performed with Fast SYBR Green PCR master mix (Applied Biosystems) using a StepOnePlus Real Time PCR system (Applied Biosystems). The primer sequences were as follows: decorin forward primer, 5′-TGAGCTTCAACAGCATCACC-3′, and decorin reverse primer, 5′-AAGTCATTTTGCCCAACTGC-3′; biglycan forward primer, 5′-CTACGCCCTGGTCTTGGTAA-3′, and biglycan reverse primer, 5′-ACTTTGCGGATACGGTTGTC-3′; fibromodulin forward primer: 5′-GAAGGGTTGTTACGCAAATGG-3′, and fibromodulin reverse primer: 5′-AGATCACCCCCTAGTCTGGGTTA-3′; lumican forward primer, 5′-TCCACTTCCAAAGTCCCTGCAAGA-3′, and lumican reverse primer, 5′-AAGCCGAGACAGCATCCTCTTTGA-3′; keratocan forward primer, 5′-CCTGGAAAGCAAGGTGCTGTA-3′, and keratocan reverse primer, 5′-TCATAGGCCTGTCTCACACTCTGT-3′; *Col1a1* forward primer, 5′-CTTCACCTACAGCACCCTTGTG-3′, and *Col1a1* reverse primer, 5′-TGACTGTCTTGCCCCAAGTTC; β-actin forward primer, 5′-AGATGACCCAGATCATGTTTGAGA-3′ and β-actin reverse primer, 5′-CACAGCCTGGATGGCTACGT-3′. The samples were run in duplicate (n = 3-4/group),

then the data were analyzed with StepOne software c2.0 (Applied Biosystems). The amount of sample total RNA was standardized by using β-actin as an internal control.

4.2.3 Tendon Biomechanics and Collagen Fiber Realignment

Right patellar tendons were prepared for mechanical testing (n=10-16/genotype/age) as described.[6] Briefly, patella-tendon-tibia complexes were dissected, then scanned using a custom laser device to measure cross-sectional area[39] Verhoeff's stain was used to apply stain lines at the tibial insertion, 1 mm and 2 mm from the tibial insertion, and at the distal patella for optical strain tracking. The tibia was secured in a custom 3D-printed pot using poly(methyl methacrylate). Custom fixtures were used to secure the pot during mechanical testing.

During testing, tendons were loaded into a 1x phosphate-buffered saline bath at 37°C secured to a tensile testing system (Instron 5848, Instron, Norwood, MA) integrated with an established cross-polarized light setup.[11,40] The viscoelastic testing protocol consisted of preconditioning, stress relaxations (3%, 4%, and 5% strain) each followed by a series of frequency sweeps (0.1, 1, 5, and 10 Hz), a return to gauge length for 60 s, and ending with a ramp-to-failure at a strain rate of 0.1%/s. A series of image maps, each consisting of 18 images, was taken throughout the ramp to failure at 20 s intervals for collagen fiber realignment and optical strain tracking data.[40] Collagen fiber realignment, outputted as circular variance ratio, was calculated separately for the tendon midsubstance and insertion using a custom program, and has an inverse relationship with the realignment of collagen fibers (Matlab, Natick, MA).[41] Circular variance measures the distribution of collagen fiber alignment on the surface of the tendon. The circular variance ratio is the circular variance at a given strain normalized by the circular variance of the same sample at gauge length. Maximum stress was

calculated from stress-strain data. Optical tracking was used to compute midsubstance and insertion modulus (Matlab, Natick, MA). Dynamic modulus and phase shift were calculated at each strain-frequency combination.

4.2.4 Collagen Fibril Diameter

Left patellar tendons were analyzed using TEM (n=4/genotype/age). Samples were fixed *in situ* using Karnovsky's fixative, then dissected from the mouse and placed in Karnovsky's fixative for an additional 2-4 hours.[11,42,43] Post-fixation the samples were rinsed in 0.1M sodium cacodylate buffer, then placed in a 1% osmium tetroxide solution for staining and secondary fixation for 1 hour. Next, the samples were dehydrated using ethanol solutions (ranging from 50% to 100% ethanol in water), then the samples were placed on a shaker for 3 12-hour cycles for epoxy infiltration (ranging from 33% to 100% epoxy resin in propylene oxide) and embedded in fresh epoxy resin before being placed in a 60°C oven overnight for curing. Post-staining with 2% aqueous uranyl acetate followed by 1% phosphotungstic acid, pH 3.2 was utilized for contrast enhancement. Cross sections through the midsubstance of the patellar tendons were examined at 80 kV using a JEOL 1400 transmission electron microscope. Images were digitally captured at an instrument magnification of 60,000x using an Orius widefield sidemount CCD camera at a resolution of 3648 x 2672. The digital images were masked and transferred to a RM Biometrics-Bioquant Image Analysis System (Memphis, TN) for analysis. Image magnification was calibrated using a line grating replica (PELCO®, Product No. 606). Fibril diameter analyses were completed using images from the central portion of the tendon. 10 images were analyzed per animal, and 3500 fibrils were analyzed for each group. All fibrils within a predetermined region of interest (ROI) on the digitized image were analyzed. Non-overlapping ROIs were placed based on fibril orientation (i.e., cross

section) and absence of cells. Diameters were measured along the minor axis of the fibril. For measurements of fibril density, the total number of fibrils within the ROI was normalized for area.

4.2.5 Cell Nuclear Shape and Cellularity

For histological analysis, the left knee joint was isolated by cutting through the femur and tibia at the time of sacrifice (n=4/genotype/age). The knee was flexed to 90°, placed into a cassette, fixed in formalin, and processed using standard paraffin histological techniques. Samples were embedded in paraffin and sections were cut at 7 μm thickness before staining with hematoxylin and eosin. Cell nuclear shape, determined by measuring the nuclear aspect ratio, and cellularity were calculated using commercial software (Bioquant).

4.2.6 Statistics

A two-way ANOVA with Bonferroni post-hoc analysis was used to evaluate the effect of genotype and age on tendon mechanics and cellularity. Realignment data was analyzed using a three-way ANOVA to evaluate the factors of genotype, age, and strain level with Bonferroni post-hoc analysis using the open-source Python package Pingouin.[44] Kolmogorov-Smirnov tests with Bonferroni post-hoc analysis were used in the analysis of collagen fibril diameter and nuclear shape. The significance level was set at $p<0.05$.

4.3 Results

4.3.1 Isolated Knockdown of Decorin and Biglycan Did Not Induce Upregulation of Other Fibril-Associated SLRPs

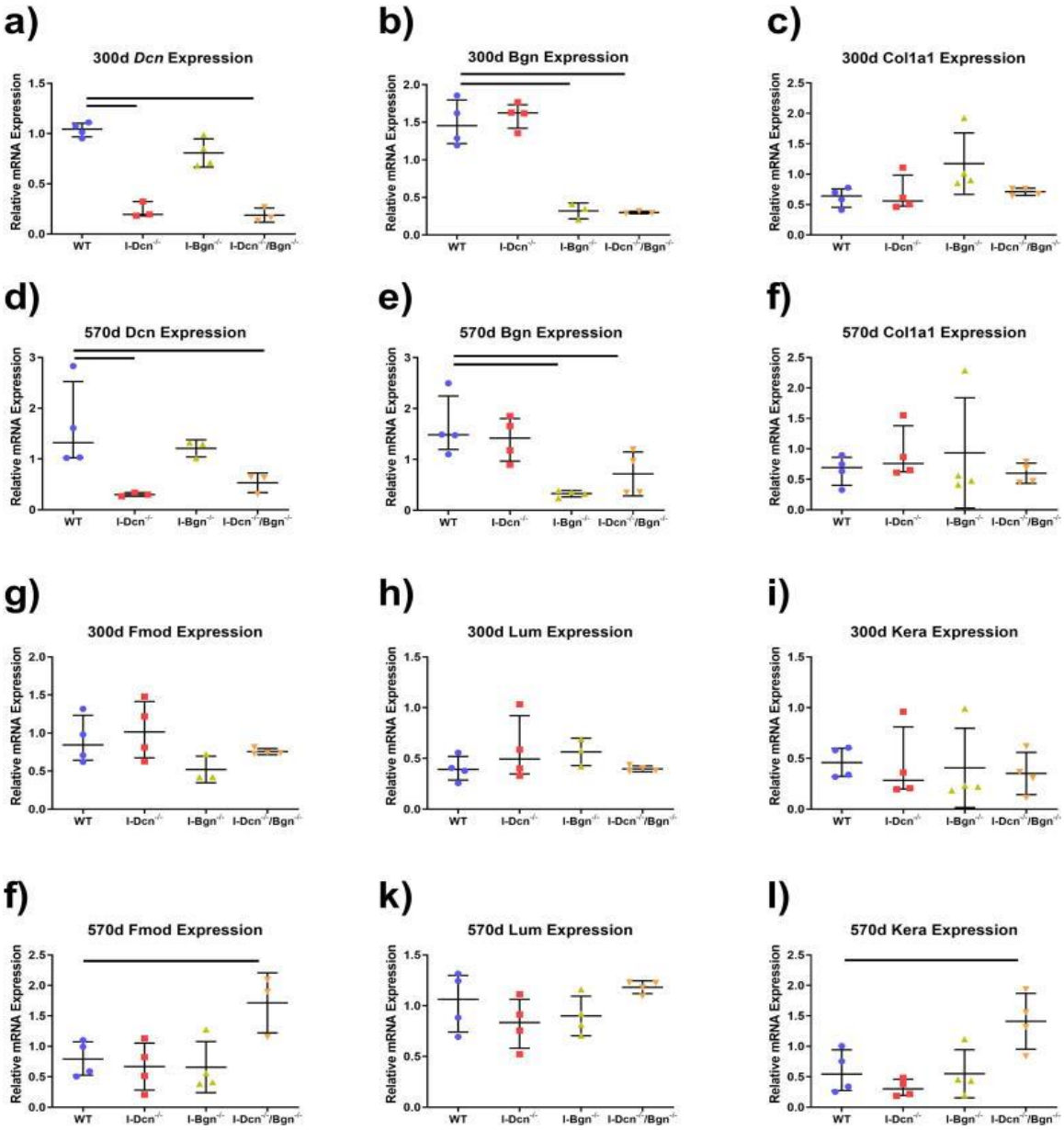

Figure 19. SLRP and Collagen I Gene Expression in Aged and Geriatric Mouse Patellar Tendons. Gene expression was measured at 300 d and 570 d after Cre induction at 120 d (n = 3-4/genotype/age). Knockdown of *Dcn* was confirmed in I-*Dcn*$^{-/-}$ and I-*Dcn*$^{-/-}$/*Bgn*$^{-/-}$ tendons (a, d) and knockdown of Bgn was confirmed for I-*Bgn*$^{-/-}$ and I-*Dcn*$^{-/-}$/*Bgn*$^{-/-}$ tendons (b, e) at 370d and 570d. No upregulation of *Dcn* or *Bgn* was detected in I-*Dcn*$^{-/-}$ or I-*Bgn*$^{-/-}$ tendons, respectively, at 300 d or 570 d (a, b, d, e). No changes in *Col1a1* were detected between genotypes at 300 d or 570 d (c, f). Increased compensatory expression of *Fmod* (j) and *Kera* (l) was detected in I-*Dcn*$^{-/-}$/*Bgn*$^{-/-}$ tendons. Data shown as median with interquartile range.

The expression of various SLRPs were analyzed to investigate compensatory upregulation within our transgenic models. Expression levels confirmed knockdown of decorin and biglycan in the respective transgenic models at 300d and 570d, and no compensation was present among the class I SLRPs in the single-target models (Fig. 19 A-B, D-E). To confirm that the transgenic models did not alter expression of collagen I, *Col1a1* expression was measured, and no changes in expression were found at either timepoint (Fig. 19 C, F). Finally, to determine if compensation was present among the class II SLRPs, we measured fibromodulin, lumican, and keratocan expression. No compensation of class II SLRPs was observed within any of the transgenic models at 300d (Fig. 19 G-I). The lack of class II SLRP compensation was constant for the I-*Dcn*$^{-/-}$ and I-*Bgn*$^{-/-}$ models at 570d (Fig. 19 J-L). Fibromodulin (Fig. 19 J) and keratocan (Fig. 19 L) was upregulated in I-*Dcn*$^{-/-}$/*Bgn*$^{-/-}$ tendons at 570d, while lumican (Fig. 19 K) was not. Overall, each of the transgenic models demonstrated effective knockdown of the target genes, and no compensation of SLRPs was present in the I-*Dcn*$^{-/-}$ or I-*Bgn*$^{-/-}$ models. The compound knockdown of decorin and biglycan was compensated with increased fibromodulin and keratocan expression at 570d.

4.3.2 Decorin and Biglycan Knockdown Increased Viscoelastic Mechanics with Age While Decorin Knockdown Attenuated Age-Related Decline in Mechanics

After determining that minimal masking effects were present from upregulation of SLRPs in our knockdown models, we determined the effects of decorin and biglycan knockdown on tendon mechanics. Before sacrifice, no changes in gait were noted among the mice. I-*Dcn*$^{-/-}$ tendons had an increased midsubstance modulus at 300d (Fig.

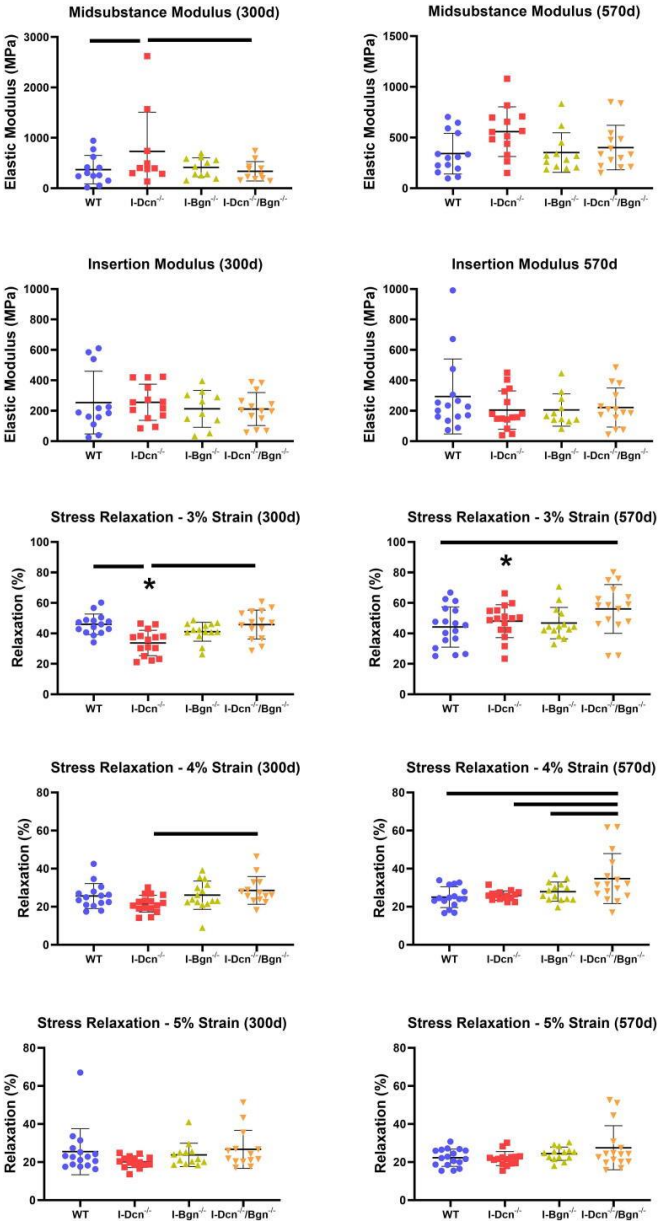

Figure 20. Patellar Tendon Modulus and Stress Relaxation After Decorin and Biglycan Knockdown. During mechanical testing, the tendon midsubstance (a, b) and insertion (c, d) modulus was measured for 300 d and 570 d tendons, respectively (n = 10–14/genotype/age). A stress-relaxation test was applied to the tendons at 3% (e, f), 4% (g, h), and 5% (i, j) strain to determine the viscoelastic response of the tendons at 300 d and 570 d (mean ± SD, n = 13–16). Data shown as mean ± standard deviation. Bars indicate significance of $p < 0.05/12$ between genotypes at 300 d or 570 d. * indicates significance of $p < 0.05/12$ between 300 d and 570 d within a genotype. Comparisons were made with two-way ANOVAs based on genotype and age with Bonferroni post-hoc comparisons.

20 A) compared to WT and I-*Dcn*$^{-/-}$*/Bgn*$^{-/-}$. Decorin knockdown did not produce the same increase in midsubstance modulus at 570d, where no changes across the genotypes were observed (Fig. 20 B). Additionally, no changes in the insertion modulus were found at 300d or 570d (Fig. 20 C, D). Stress-relaxation tests performed at 3% strain found decreased relaxation in I-*Dcn*$^{-/-}$ tendons compared to WT and I-*Dcn*$^{-/-}$*/Bgn*$^{-/-}$ at 300d (Fig. 20 E), and I-*Dcn*$^{-/-}$*/Bgn*$^{-/-}$ had increased relaxation compared to WT at 570d (Fig. 20 F). Additionally, relaxation increased between 300d and 570d for I-*Dcn*$^{-/-}$ tendons (Fig. 20 E, F). However, there was a significant interaction between genotype and age during the stress-relaxation tests performed at 3% strain. At 4% strain, I-*Dcn*$^{-/-}$*/Bgn*$^{-/-}$ showed increased relaxation compared to I-*Dcn*$^{-/-}$ at 300d (Fig. 20 G) and increased relaxation

compared to WT, I-*Dcn*$^{-/-}$, and I-*Bgn*$^{-/-}$ at 570d (Fig. 20 H). Stress relaxation at 5% strain did not change between groups (Fig. 20 I, J).

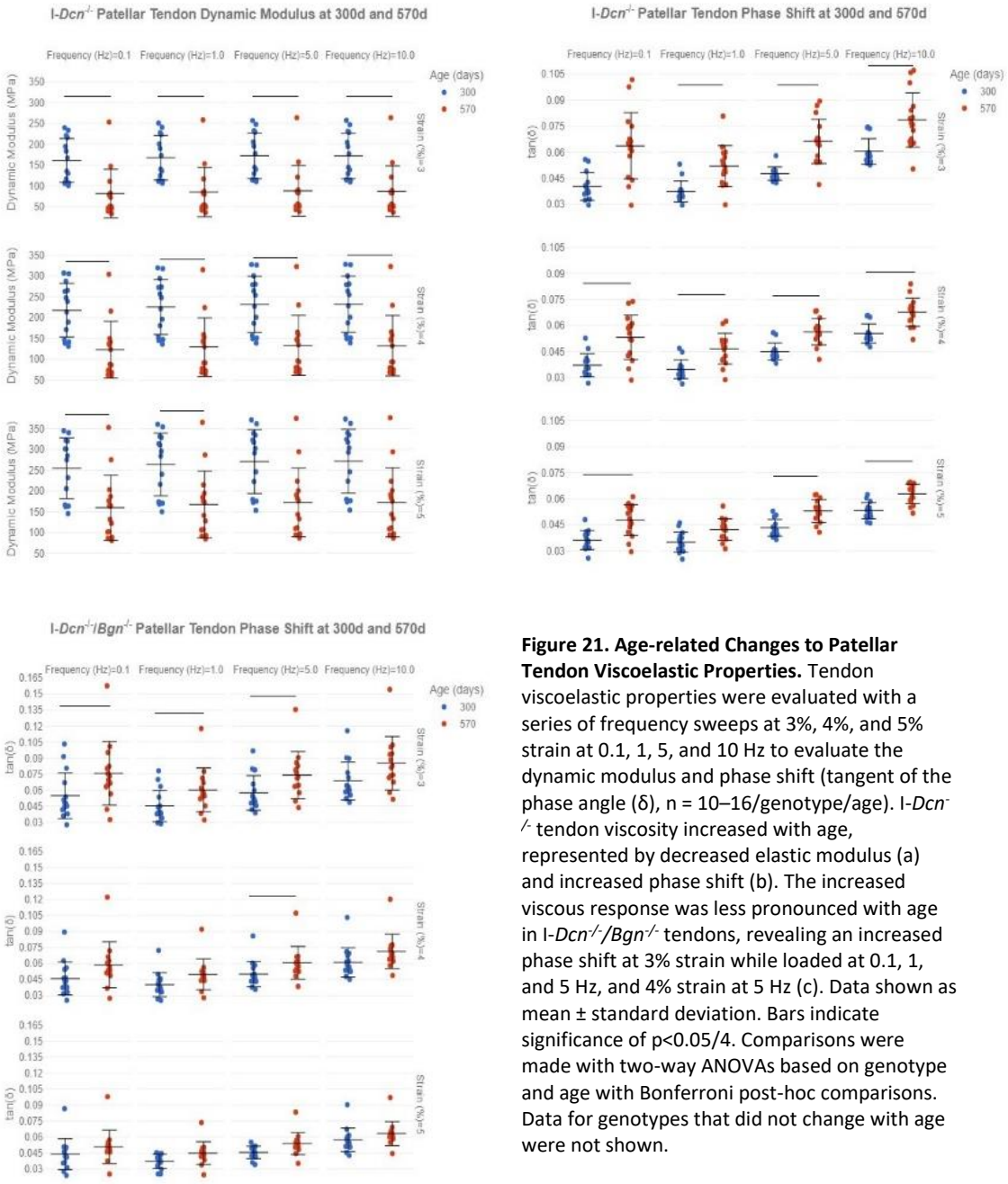

Figure 21. Age-related Changes to Patellar Tendon Viscoelastic Properties. Tendon viscoelastic properties were evaluated with a series of frequency sweeps at 3%, 4%, and 5% strain at 0.1, 1, 5, and 10 Hz to evaluate the dynamic modulus and phase shift (tangent of the phase angle (δ), n = 10–16/genotype/age). I-*Dcn*$^{-/-}$ tendon viscosity increased with age, represented by decreased elastic modulus (a) and increased phase shift (b). The increased viscous response was less pronounced with age in I-*Dcn*$^{-/-}$/*Bgn*$^{-/-}$ tendons, revealing an increased phase shift at 3% strain while loaded at 0.1, 1, and 5 Hz, and 4% strain at 5 Hz (c). Data shown as mean ± standard deviation. Bars indicate significance of $p<0.05/4$. Comparisons were made with two-way ANOVAs based on genotype and age with Bonferroni post-hoc comparisons. Data for genotypes that did not change with age were not shown.

To further determine the roles of decorin and biglycan in aging tendon viscoelastic mechanics, we measured the dynamic modulus (E*) and phase shift (tangent of loss angle, tan (δ)) during dynamic loading. E* and phase shift showed no

changes between genotypes at 300d or 570d, but changes were found within genotypes between ages. Specifically, I-*Dcn*$^{-/-}$ reduced dynamic modulus at 3% and 4% strain across all loading frequencies, and at 5% strain at 0.1 and 1 Hz (Fig 21A). Changes in phase angle shift were also found between 300d and 570d for both I-*Dcn*$^{-/-}$ (Fig. 21B) and I-*Dcn*$^{-/-}$*/Bgn*$^{-/-}$ (Fig. 21C) tendons. Reductions in I-*Dcn*$^{-/-}$ phase shift were observed at 3% strain at 1, 5, and 10 Hz, 4% strain at 0.1, 1, 5, and 10 Hz, and 5% strain at 0.1, 5, and 5 Hz. I-*Dcn*$^{-/-}$/Bgn$^{-/-}$ reductions in phase shift were found at 3% strain at 0.1, 1, and 5 Hz and 4% strain at 5 Hz.

4.3.3 Small Leucine-Rich Proteoglycan Knockdown Produced Minimal Changes to Collagen Fiber Realignment

Decreased circular variance ratio, which correlates with increased collagen fiber realignment, was found for WT and I-*Dcn*$^{-/-}$ tendons at 300d (Fig. 22A) and I-*Dcn*$^{-/-}$/*Bgn*$^{-/-}$ tendons at 570d between 1% and 3% strain (Fig. 22B). Analysis of the midsubstance revealed increased realignment for WT, I-*Dcn*$^{-/-}$, I-*Bgn*$^{-/-}$, and I-*Dcn*$^{-/-}$/*Bgn*$^{-/-}$ tendons at 300d (Fig. 22C) and 570d (Fig. 22D) between 1% and 3% strain, and no further

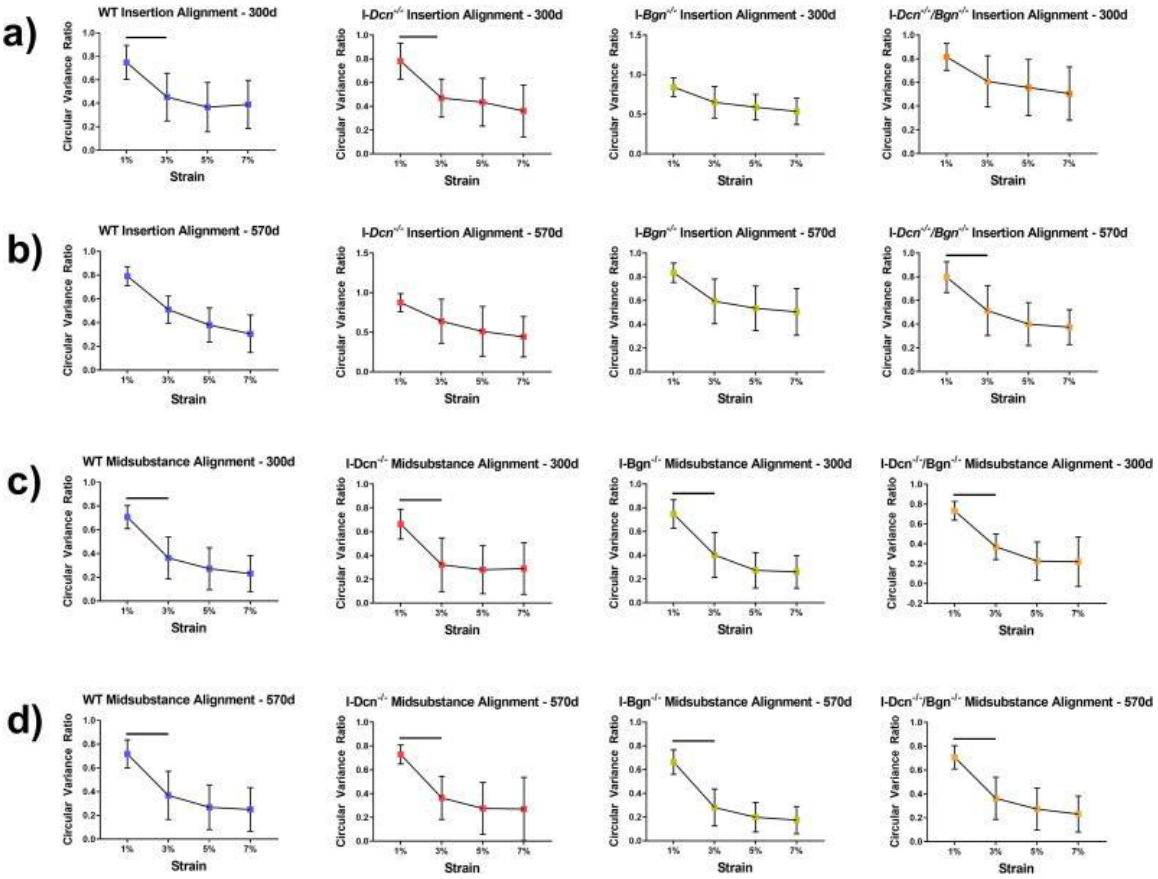

Figure 22. Collagen Fiber Realignment in the Patellar Tendon Insertion and Midsubstance. Collagen fiber realignment was measured during the ramp to failure by analyzing the circular variance of the collagen fiber distribution angles at 1%, 3%, 5%, and 7% strain, then normalizing those values by the circular variance at 0% strain to obtain the circular variance ratio (n = 10–14/genotype/age). Differential responses were observed in the insertion, with realignment occurring in 300 d WT and I-*Dcn*$^{-/-}$ tendons between 1–3% strain (a), while only I-*Dcn*$^{-/-}$/*Bgn*$^{-/-}$ tendon realignment increased between 1–3% strain at 570 d. All groups demonstrated similar realignment mechanics in the midsubstance, with realignment occurring between 1–3% strain (c, d). Data shown as mean ± standard deviation. Bars indicate significance of $p < 0.05/36$. Comparisons were made with a three-way ANOVA based on genotype, age, and strain with Bonferroni post-hoc comparisons. Strain was the only significant factor.

realignment occurred at 5% or 7% strain. No differences in realignment were found in either the insertion or midsubstance between genotypes or ages.

4.3.4 Alterations to Collagen Fibril Diameter Were Consistently Present After Knockdown of Decorin and Biglycan

After TEM imaging no gross changes to fibril shape were apparent after SLRP knockdown in aged or geriatric tendon (Fig. 23A). 300d the I-*Dcn*$^{-/-}$, I-*Bgn*$^{-/-}$, and I-*Dcn*$^{-/-}$*/Bgn*$^{-/-}$ tendons revealed altered fibril diameter distributions compared to WT tendons (Fig. 23B, C). Additionally, at 300d, the I-*Dcn*$^{-/-}$ tendon collagen fibrils showed increased diameter heterogeneity and decreased minimum fibril diameter. At 570d, only I-*Dcn*$^{-/-}$ and I-*Bgn*$^{-/-}$ tendons exhibited altered collagen fibril diameter distributions compared to

WT. The I-*Dcn*$^{-/-}$ tendons also displayed reduced fibril diameter in quartiles 2-4 of the fibril diameter distribution compared to WT (Fig. 23B, D).

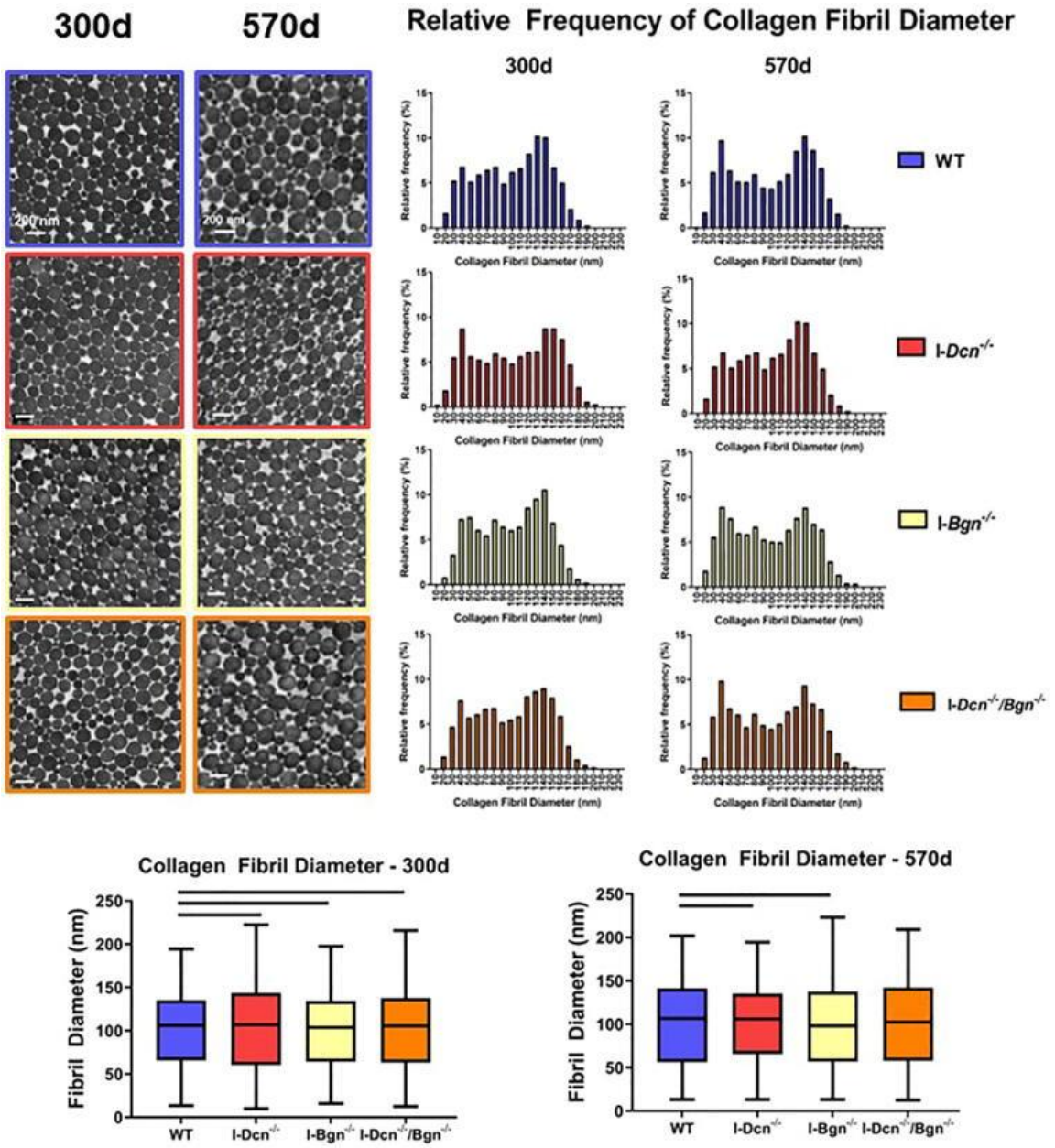

Figure 23. Effect of Decorin and Biglycan Knockdown on Patellar Tendon Collagen Fibril Diameter. Tendon microstructure was examined using transmission electron microscopy to measure collagen fibril diameter (a, n = 4/genotype/age). After obtaining the fibril diameter values, relative frequency distributions were created for each genotype at 370 d and 570 d for comparisons (b). Alterations were consistently present after SLRP knockdown at 300d relative to WT (c), however I-*Dcn*$^{-/-}$/*Bgn*$^{-/-}$ tendons were the only group with no alterations to the collagen fibril distribution compared to WT at 570 d (d). Data shown as median with the box containing quartiles 1–3 and the range spanning the minimum to maximum collagen fibril diameter. Bars indicate significance of $p < 0.05/3$. Kolmogorov-Smirnov tests were used to compare the WT fibril diameter distribution to each experimental group.

4.3.5 Biglycan Knockdown Resulted in Minimal Changes to Nuclear Shape in Aged Tendons

Tendons were stained with hematoxylin and eosin to visualize the macroscopic tendon structure and cellular population to measure cellularity and nuclear aspect ratio. No abnormalities were present in the overall tendon structure at 300d or 570d (Fig. 24A, B). Cells present in the I-*Bgn*$^{-/-}$ tendons exhibited an increased nuclear aspect ratio, indicating a more rounded nuclear shape, compared to WT and I-*Dcn*$^{-/-}$/*Bgn*$^{-/-}$ tendon cells at the 300d timepoint (Fig. 24C), while no changes were present between the genotypes at 570d (Fig. 24D). No changes were found in cellularity between genotypes at 300d or 570d (data not shown).

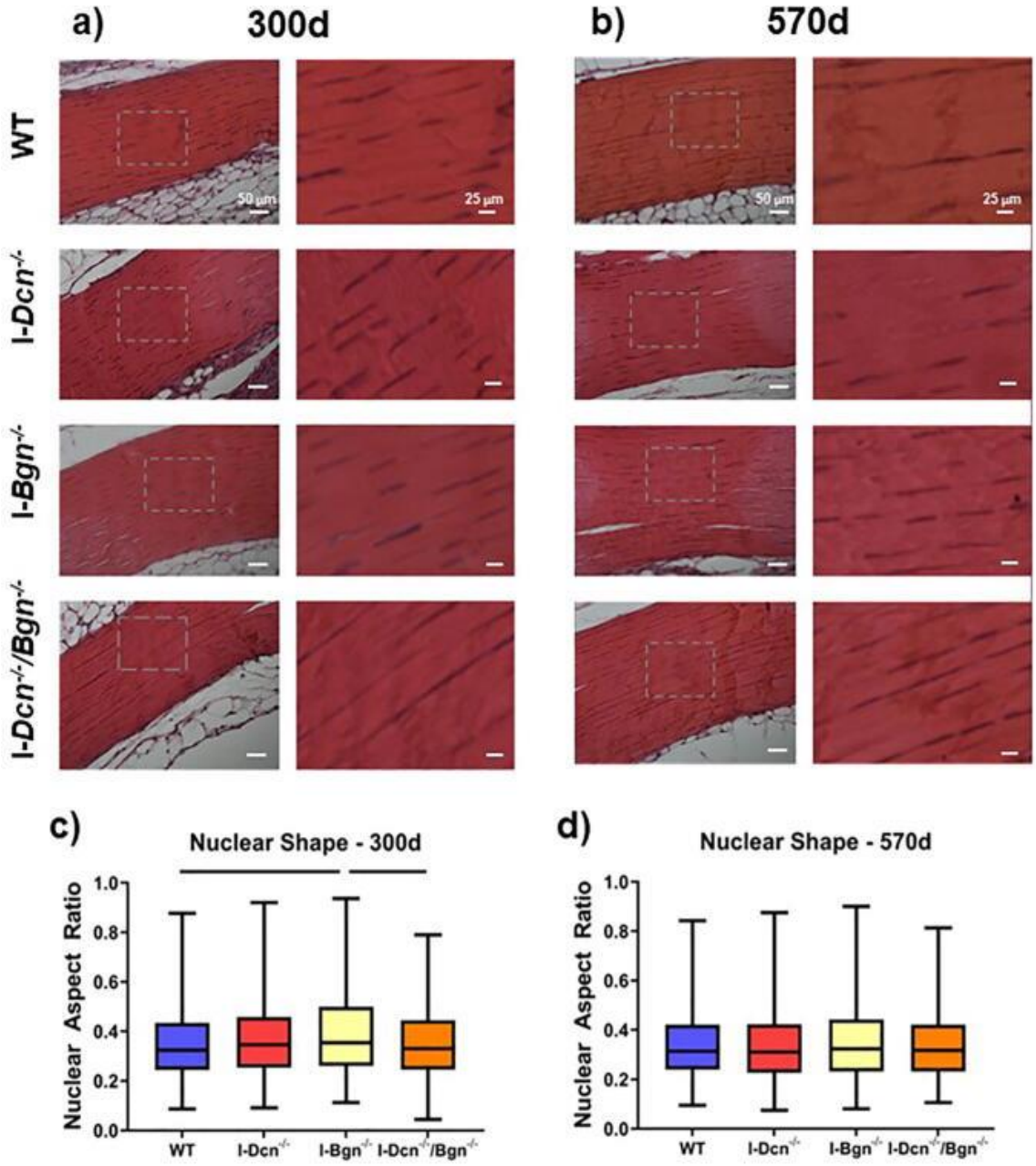

Figure 24. Patellar Tendon Cellular Nuclear Aspect Ratio After SLRP Knockdown. Tendons were stained with hematoxylin and eosin to visualize the macroscopic collagen structure, cellularity, and nuclear aspect ratio at 300 d (a) and 500 d (b, n = 4/genotype/age). Gray boxes denote areas of higher magnification to show greater detail. No irregularities were noted in the tendon structure, and no changes to cellularity were observed (data not shown). Nuclear aspect ratio was increased in I-*Bgn*$^{-/-}$ tendons at 300 d (c), but no changes were present between genotypes at 570 d (d). Data shown as median with the box containing quartiles 1–3 and the range spanning the minimum to maximum nuclear aspect ratio. Bars indicate significance of $p < 0.05/6$. Kolmogorov-Smirnov tests were used to compare the nuclear aspect ratio distributions between groups.

4.4 Discussion

Though the roles of decorin and biglycan in aged and geriatric tendons have been previously considered, this is the first study to examine the differential and combined roles of decorin and biglycan at these ages in tendon without the confounding effects of abnormal tendon development. This was achieved using TM-inducible SLRP knockdown mouse models that allowed decorin and biglycan knockdown after musculoskeletal maturity. We hypothesized that the knockdown of decorin and compound decorin/biglycan knockdown in aged and geriatric mice would result in improved tendon mechanical properties compared to the biglycan knockdown and WT tendons. Additionally, we expected alterations to the tendon fibril structure after decorin or biglycan knockdown, while the compound decorin/biglycan knockdown tendon fibril structure would resemble the structure of the decorin knockdown tendons. Furthermore, we hypothesized that the changes found in the aged tendons would be exacerbated in the geriatric tendons. A multidisciplinary approach was utilized to determine that decorin and biglycan play important differential roles in the regulation of tendon mechanics and structure during aging. In support of our hypotheses, the knockdown of decorin resulted in an improved tendon aging phenotype while knockdown of biglycan had no impact on mechanics. We also found that the knockdown of decorin or biglycan resulted in alterations to tendon structure. Contrary to our hypothesis, the compound decorin/biglycan knockdown model did not mimic the decorin knockdown model and resulted in increased viscoelastic mechanics with age.

TM-inducible knockdown models were utilized in this study to allow for normal development with the targeted genes activated, avoiding the confounding effects of abnormal development associated with traditional knockout models.[12,13] TM-inducible models require TM treatment for Cre activation and subsequent excision of the target

genes. This process occurs after TM metabolizes into 4-hydroxytamoxifen, which binds to an estrogen receptor and enables translocation of the CreERT2 complex into the nucleus.[14] The ability for 4-hydroxytamoxifen to bind to estrogen receptors may interfere with the estrogen pathway and result in unintended side effects during tendon homeostasis.[15] While TM treatment may result in temporary disruption of the estrogen pathway, the long timeline and treatment of control groups with TM in this study mitigates any impact of unintended side effects that TM may cause during tendon homeostasis.

To elucidate the regulatory roles of decorin and biglycan throughout tendon aging two timepoints were used that correlate with aged and geriatric mice. 300-day old mice were selected as the aged group because of the decline in mechanical properties of the tendons compared to mature (150-day) mouse tendons combined with the similarities between the survival curves of mice at this age and 60–65-year-old women, where both survival curves fall below an 85% survival rate.[16,17] The 60–65-year-old population is still active, less sedentary than older populations, but also represent a population where tendon injuries are common.[18] 570-day old mice were used to represent an extremely aged group (termed geriatric) to further define the effects of SLRP knockdown on geriatric tendon because intermediate timepoints did not show additional age-related declines in tendon mechanics compared to 300d, and later time points were not viable due to low survival rates in our SLRP knockdown models at this timepoint.

The improved tendon aging phenotype associated with decorin knockdown has been previously shown using a traditional mouse knockout model, where knockout of decorin resulted in minor decreases in viscoelastic and quasi-static mechanics with age relative to the changes associated with biglycan knockout and WT tendons.[7] It was

speculated that decorin knockout improved tendon aging due to its role in fibrillogenesis, where continued decorin-fibril interactions facilitated lateral growth of mature fibrils, resulting in changes to the tendon ultrastructure and mechanical properties. Overall, these results are supported in the current study, where decorin knockdown during homoeostasis in skeletally mature mice resulted in improved quasi-static and viscoelastic mechanics at 300d, although these improvements were no longer present at the 570d time point. Interestingly, we found that knockdown of decorin resulted in a broadening of the collagen fibril diameter distribution at 300d where improved mechanics were present, and a decrease in the fibril diameter at 570d where these improvements were no longer present. This supports the idea that decorin is a mediator of fibrillogenesis whose role is highly context dependent,[19] but a repeatable pattern in how decorin facilitates an improved tendon aging phenotype has not been discovered.

Our dynamic mechanical loading data revealed differences with age within individual genotypes that were not apparent from the quasi-static mechanics. While the quasi-static data did not show differences between 300d and 570d mechanics, dynamic modulus and phase angle shift were sensitive to the changes between 300d and 570d after decorin and compound decorin/biglycan knockdown. This may be due to the proposed role of proteoglycans in maintaining hydrostatic pressure within the tendon by interacting with the fluid phase to support viscoelastic mechanics. However, multiple studies have produced evidence rejecting this hypothesis using various methods to reduce proteoglycan content and deplete the GAG content from SLRPs and the surrounding tissue.[20–22] Alternatively, these differences found may reveal that dynamic loading is more sensitive to changes to tendon structure and function associated with

SLRP knockdown since dynamic loading is more representative of the *in vivo* loading environment.

The observation that reduced decorin expression has a greater impact than biglycan expression in tissues rich in collagenous fibers is not new. Previous data suggests that greater impact of decorin deficiency compared to biglycan deficiency on skin integrity is consistent with greater abundance of decorin in the dermis.[23] Additionally, the similarity in ultrastructural changes produced by decorin or biglycan deficiency is consistent with the similar roles that each SLRP plays in interactions with dermal collagen. Similarly, the current study revealed a greater impact from decorin knockdown relative to biglycan knockdown on tendon mechanics, however the ultrastructural changes to tendon fibril diameter were similar. While the relative abundance of decorin and biglycan likely plays a major role in the effects of knockdown on tendon aging, an additional study examining the effects of decorin and biglycan knockdown during tendon aging noted the roles of biglycan in tendon stem cell regulation, and that stem cell regulation will likely have less of an impact during tendon aging due to senescence.[24]

Contrary to our hypothesis, the compound knockdown of decorin and biglycan did not mimic the I-Dcn$^{-/-}$ tendons but produced tendons with increased viscoelastic properties. The role of SLRPs in tendon viscoelastic mechanics is controversial. The altered viscoelastic mechanics observed in the 570d I-*Dcn*$^{-/-}$/*Bgn*$^{-/-}$ group cannot be explained by alterations to collagen fibril structure since this group showed no changes in these measures relative to WT. Previous work has suggested that the decorin and biglycan GAG chains play a direct role in the regulation of tendon mechanics.[25,26] However, subsequent studies digested the SLRP GAG chains did not observe any

changes to mechanics.[22,27,28] The mechanisms driving the alterations observed in the compound decorin and biglycan knockdown viscoelastic mechanics in our present study are unclear. Knockdown of decorin and biglycan could produce alterations to viscoelastic mechanics due to the wide range of biological functions of these proteins, including regulation of various collagens[19,29–31], innate immune receptors[32], and multiple signaling pathways including TGF-β[33], Wnt[34], and VEGFA[35]. Additionally, the altered viscoelastic properties could be due to the upregulation of class II SLRPs observed at 570d. The upregulation of fibromodulin and keratocan could disrupt additional pathways that are prevalent during tendon aging, such as LOX mediated collagen crosslinking.[36–38] While this study focused on measuring the expression of class I and II fibril-associated SLRPs to determine any compensatory upregulation that may have occurred, a multiomic-based approach can be applied to our I-*Dcn*$^{-/-}$/*Bgn*$^{-/-}$ model at 570d to determine the signaling changes that may be driving the alterations to viscoelastic mechanics.

This study has several limitations. We focused our studies on the patellar tendon, while additional tendons, such as the Achilles, may alter the impact that SLRP knockdown has on tendon mechanics and structure throughout aging. Future work will include additional tendons to broaden the context of our current study. Additionally, this study did not explore functional changes alongside the mechanical and structural analyses. However, our mechanical testing protocol and multi-faceted structural analysis is more sensitive to detecting changes within tendon than functional measurements, such as gait or running analyses. Since no changes in gait were noted among our animals, we chose to not include any of these functional measures. Finally, this study used gene expression to validate knockdown in our models and did not include protein measures. We have previously validated that knockdown of decorin and biglycan gene

expression was accompanied by a substantial reduction in decorin and biglycan protein levels in tendon 30 days after Cre induction.[11] Our current study showed similar levels of gene expression after knockdown with a timeline that was 6 to 15 times longer between Cre induction and sacrifice, allowing a greater degree of protein turnover to occur.

This study identified insights into the differential roles of decorin and biglycan during tendon aging without the confounding factor of abnormal tendon development associated with knockout models. Knockdown of decorin resulted in increased midsubstance modulus and decreased stress relaxation at 300d. However, these changes did not persist at 570d. Knockdown of biglycan resulted in minimal changes to the tendon throughout aging. Interestingly, the compound knockdown of decorin and biglycan resulted in a unique phenotype that was detrimental to overall tendon mechanics and structure.

4.5 References

1. Zhang G, Young BB, Ezura Y, Favata M, Soslowsky LJ, Chakravarti S, Birk DE. Development of tendon structure and function: Regulation of collagen fibrillogenesis. Journal of Musculoskeletal Neuronal Interactions. 2005 [accessed 2017 Aug 10];5(1):5–21. https://pubmed.ncbi.nlm.nih.gov/15788867/. doi:10.1016/j.biomaterials.2010.02.062

2. Chen S, Birk DE. The regulatory roles of small leucine-rich proteoglycans in extracellular matrix assembly. FEBS Journal. 2013 [accessed 2018 Feb 6];280(10):2120–2137. http://www.ncbi.nlm.nih.gov/pubmed/23331954. doi:10.1111/febs.12136

3. Schonherr E, Witsch-Prehm P, Harrach B, Robenek H, Rauterberg J, Kresse H. Interaction of biglycan with type I collagen. Journal of Biological Chemistry. 1995;270(6):2776–2783. doi:10.1074/jbc.270.6.2776

4. Dourte LM, Pathmanathan L, Mienaltowski MJ, Jawad AF, Birk DE, Soslowsky LJ. Mechanical, compositional, and structural properties of the mouse patellar tendon with changes in biglycan gene expression. Journal of Orthopaedic Research. 2013 [accessed 2017 Aug 10];31(9):1430–1437. http://www.ncbi.nlm.nih.gov/pubmed/23592048. doi:10.1002/jor.22372

5. Dourte LM, Pathmanathan L, Jawad AF, Iozzo R V, Mienaltowski MJ, Birk DE, Soslowsky LJ. Influence of decorin on the mechanical, compositional, and structural properties of the mouse patellar tendon. Journal of biomechanical engineering. 2012 [accessed 2016 Jul 18];134(3):031005. http://www.ncbi.nlm.nih.gov/pubmed/22482685. doi:10.1115/1.4006200

6. Dunkman AA, Buckley MR, Mienaltowski MJ, Adams SM, Thomas SJ, Satchell L,

Kumar A, Pathmanathan L, Beason DP, Iozzo R V, et al. The tendon injury response is influenced by decorin and biglycan. Annals of Biomedical Engineering. 2014 [accessed 2016 Jul 13];42(3):619–630. http://www.ncbi.nlm.nih.gov/pubmed/24072490. doi:10.1007/s10439-013-0915-2

7. Dunkman AA, Buckley MR, Mienaltowski MJ, Adams SM, Thomas SJ, Satchell L, Kumar A, Pathmanathan L, Beason DP, Iozzo R V, et al. Decorin expression is important for age-related changes in tendon structure and mechanical properties. Matrix Biology. 2013 [accessed 2016 Aug 26];32(1):3–13. http://www.ncbi.nlm.nih.gov/pubmed/23178232. doi:10.1016/j.matbio.2012.11.005

8. Dunkman AA, Buckley MR, Mienaltowski MJ, Adams SM, Thomas SJ, Kumar A, Beason DP, Iozzo R V, Birk DE, Soslowsky LJ. The injury response of aged tendons in the absence of biglycan and decorin. Matrix Biology. 2014 [accessed 2016 Jul 13];35:232–238. http://www.ncbi.nlm.nih.gov/pubmed/24157578. doi:10.1016/j.matbio.2013.10.008

9. Buckwalter JA, Heckman J. An AOA critical issue: aging of the North American population: new challenges for orthopaedics. The Journal of bone and joint surgery. American volume. 2003 [accessed 2017 Aug 10];85-A(4):748–758. http://www.ncbi.nlm.nih.gov/pubmed/12672854

10. Lindemann I, Coombes BK, Tucker K, Hug F, Dick TJM. Age-related differences in gastrocnemii muscles and Achilles tendon mechanical properties in vivo. Journal of Biomechanics. 2020;112:110067. doi:10.1016/J.JBIOMECH.2020.110067

11. Robinson KA, Sun M, Barnum CE, Weiss SN, Huegel J, Shetye SS, Lin L, Saez D, Adams SM, Iozzo R V., et al. Decorin and biglycan are necessary for maintaining

collagen fibril structure, fiber realignment, and mechanical properties of mature tendons. Matrix Biology. 2017 Sep 5 [accessed 2017 Sep 25]. http://www.sciencedirect.com/science/article/pii/S0945053X17301063?via%3Dihub. doi:10.1016/j.matbio.2017.08.004

12. Metzger D, Clifford J, Chiba H, Chambon P. Conditional site-specific recombination in mammalian cells using a ligand- dependent chimeric Cre recombinase. Proceedings of the National Academy of Sciences of the United States of America. 1995 [accessed 2020 Nov 10];92(15):6991–6995. /pmc/articles/PMC41457/?report=abstract. doi:10.1073/pnas.92.15.6991

13. Schwenk F, Kühn R, Angrand PO, Rajewsky K, Stewart AF. Temporally and spatially regulated somatic mutagenesis in mice. Nucleic Acids Research. 1998 [accessed 2020 Nov 10];26(6):1427–1432. /pmc/articles/PMC147429/?report=abstract. doi:10.1093/nar/26.6.1427

14. Barbieri RL. The Breast. In: Yen & Jaffe's Reproductive Endocrinology. Elsevier; 2009. p. 235–248. https://www.sciencedirect.com/topics/medicine-and-dentistry/1-1-2-triphenylethylene-derivative. doi:10.1016/B978-1-4160-4907-4.00010-3

15. Best KT, Studentsova V, Ackerman JE, Nichols AEC, Myers M, Cobb J, Knapp E, Awad HA, Loiselle AE. Effects of tamoxifen on tendon homeostasis and healing: Considerations for the use of tamoxifen-inducible mouse models. Journal of Orthopaedic Research. 2021;39(7):1572–1580. doi:10.1002/jor.24767

16. Arias E. National Vital Statistics Reports, Volume 61, Number 3, 09/24/2012... for 2008. 2008;61(3):20-21,26-27. https://www.cdc.gov/nchs/data/nvsr/nvsr61/nvsr61_03.pdf

17. Yuan R, Tsaih S-W, Petkova SB, Evsikova CM de, Xing S, Marion MA, Bogue MA, Mills KD, Peters LL, Bult CJ, et al. Aging in inbred strains of mice: study design and interim report on median lifespans and circulating IGF1 levels. Aging cell. 2009 [accessed 2021 Jul 27];8(3):277. /pmc/articles/PMC2768517/. doi:10.1111/J.1474-9726.2009.00478.X

18. Matthews CE, Chen KY, Freedson PS, Buchowski MS, Beech BM, Pate RR, Troiano RP. Amount of time spent in sedentary behaviors in the United States, 2003-2004. American Journal of Epidemiology. 2008;167(7):875–881. doi:10.1093/aje/kwm390

19. Reed CC, Iozzo R V. The role of decorin in collagen fibrillogenesis and skin homeostasis. Glycoconjugate Journal. 2002 [accessed 2018 Dec 2];19(4/5):249–255. http://link.springer.com/10.1023/A:1025383913444. doi:10.1023/A:1025383913444

20. Robinson PS, Huang T-F, Kazam E, Iozzo R V., Birk DE, Soslowsky LJ. Influence of Decorin and Biglycan on Mechanical Properties of Multiple Tendons in Knockout Mice. Journal of Biomechanical Engineering. 2005;127(1):181. http://biomechanical.asmedigitalcollection.asme.org/article.aspx?articleid=1413750. doi:10.1115/1.1835363

21. Fessel G, Snedeker JG. Evidence against proteoglycan mediated collagen fibril load transmission and dynamic viscoelasticity in tendon. Matrix Biology. 2009 [accessed 2018 Dec 6];28(8):503–510. https://www.sciencedirect.com/science/article/pii/S0945053X09001061?via%3Dihub. doi:10.1016/j.matbio.2009.08.002

22. Lujan TJ, Underwood CJ, Jacobs NT, Weiss JA. Contribution of glycosaminoglycans to viscoelastic tensile behavior of human ligament. Journal of Applied Physiology. 2009

[accessed 2021 Aug 6];106(2):423. /pmc/articles/PMC2644241/. doi:10.1152/JAPPLPHYSIOL.90748.2008

23. Corsi A, Xu T, Chen XD, Boyde A, Liang J, Mankani M, Sommer B, Iozzo R V., Eichstetter I, Robey PG, et al. Phenotypic effects of biglycan deficiency are linked to collagen fibril abnormalities, are synergized by decorin deficiency, and mimic Ehlers-Danlos-like changes in bone and other connective tissues. Journal of Bone and Mineral Research. 2002;17(7):1180–1189. doi:10.1359/jbmr.2002.17.7.1180

24. Leiphart RJ, Shetye SS, Weiss SN, Dyment NA, Soslowsky LJ. Induced Knockdown of Decorin, Alone and in Tandem With Biglycan Knockdown, Directly Increases Aged Murine Patellar Tendon Viscoelastic Properties. Journal of Biomechanical Engineering. 2020;142(11). https://asmedigitalcollection.asme.org/biomechanical/article/doi/10.1115/1.4048030/1086080/Induced-Knockdown-of-Decorin-Alone-and-in-Tandem. doi:10.1115/1.4048030

25. Cribb AM, Scott JE. Tendon response to tensile stress: an ultrastructural investigation of collagen:proteoglycan interactions in stressed tendon. Journal of Anatomy. 1995 [accessed 2022 May 5];187(Pt 2):423. /pmc/articles/PMC1167437/?report=abstract

26. Liao J, Vesely I. Skewness angle of interfibrillar proteoglycans increases with applied load on mitral valve chordae tendineae. Journal of Biomechanics. 2007 [accessed 2022 May 5];40(2):390–398. www.elsevier.com/locate/jbiomech. doi:10.1016/J.JBIOMECH.2005.12.011

27. Lujan TJ, Underwood CJ, Henninger HB, Thompson BM, Weiss JA. Effect of dermatan sulfate glycosaminoglycans on the quasi-static material properties of the

human medial collateral ligament. Journal of Orthopaedic Research. 2007 [accessed 2019 Feb 13];25(7):894–903. http://doi.wiley.com/10.1002/jor.20351. doi:10.1002/jor.20351

28. Fessel G, Snedeker JG. Evidence against proteoglycan mediated collagen fibril load transmission and dynamic viscoelasticity in tendon. Matrix Biology. 2009 [accessed 2019 Feb 13];28(8):503–510. https://www.sciencedirect.com/science/article/pii/S0945053X09001061?via%3Dihub. doi:10.1016/J.MATBIO.2009.08.002

29. Reese SP, Underwood CJ, Weiss JA. Effects of decorin proteoglycan on fibrillogenesis, ultrastructure, and mechanics of type I collagen gels. Matrix Biology. 2013 [accessed 2018 Dec 2];32(7–8):414–423. https://www.sciencedirect.com/science/article/pii/S0945053X13000681. doi:10.1016/J.MATBIO.2013.04.004

30. Chen S, Young MF, Chakravarti S, Birk DE. Interclass small leucine-rich repeat proteoglycan interactions regulate collagen fibrillogenesis and corneal stromal assembly. Matrix Biology. 2014 [accessed 2018 Dec 2];35:103–111. https://www.sciencedirect.com/science/article/pii/S0945053X14000055. doi:10.1016/J.MATBIO.2014.01.004

31. Iozzo R V., Schaefer L. Proteoglycan form and function: A comprehensive nomenclature of proteoglycans. Matrix Biology. 2015 [accessed 2017 Aug 24];42:11–55. http://linkinghub.elsevier.com/retrieve/pii/S0945053X15000402. doi:10.1016/j.matbio.2015.02.003

32. Merline R, Moreth K, Beckmann J, Nastase M V., Zeng-Brouwers J, Tralhão JG,

Lemarchand P, Pfeilschifter J, Schaefer RM, Iozzo R V., et al. Signaling by the matrix proteoglycan decorin controls inflammation and cancer through PDCD4 and microRNA-21. Science Signaling. 2011;4(199):1–15. doi:10.1126/scisignal.2001868

33. Melchior-Becker A, Dai G, Ding Z, Schäfer L, Schrader J, Young MF, Fischer JW. Deficiency of Biglycan Causes Cardiac Fibroblasts to Differentiate into a Myofibroblast Phenotype. Journal of Biological Chemistry. 2011;286(19):17365–17375. doi:10.1074/JBC.M110.192682

34. Berendsen AD, Fisher LW, Kilts TM, Owens RT, Robey PG, Gutkind JS, Young MF. Modulation of canonical Wnt signaling by the extracellular matrix component biglycan. Proceedings of the National Academy of Sciences. 2011;108(41):17022–17027. http://www.pnas.org/cgi/doi/10.1073/pnas.1110629108. doi:10.1073/pnas.1110629108

35. Berendsen AD, Pinnow EL, Maeda A, Brown AC, McCartney-Francis N, Kram V, Owens RT, Robey PG, Holmbeck K, de Castro LF, et al. Biglycan modulates angiogenesis and bone formation during fracture healing. Matrix Biology. 2014;35:223–231. doi:10.1016/J.MATBIO.2013.12.004

36. Ezura Y, Chakravarti S, Oldberg A, Chervoneva I, Birk DE. Differential Expression of Lumican and Fibromodulin Regulate Collagen Fibrillogenesis in Developing Mouse Tendons. The Journal of Cell Biology. 2000 [accessed 2022 May 5];151(4):779. /pmc/articles/PMC2169450/. doi:10.1083/JCB.151.4.779

37. Kalamajski S, Bihan D, Bonna A, Rubin K, Farndale RW. Fibromodulin Interacts with Collagen Cross-linking Sites and Activates Lysyl Oxidase. The Journal of Biological Chemistry. 2016 [accessed 2022 May 5];291(15):7951. /pmc/articles/PMC4825002/. doi:10.1074/JBC.M115.693408

38. Kalamajski S, Liu C, Tillgren V, Rubin K, Oldberg Å, Rai J, Weis MA, Eyre DR. Increased C-telopeptide Cross-linking of Tendon Type I Collagen in Fibromodulin-deficient Mice. The Journal of Biological Chemistry. 2014 [accessed 2022 May 5];289(27):18873. /pmc/articles/PMC4081928/. doi:10.1074/JBC.M114.572941

39. Favata M. Scarless Healing in the Fetus: Implications and Strategies for Postnatal Tendon Repair. University of Pennsylvania; 2006.

40. Lake SP, Miller KS, Elliott DM, Soslowsky LJ. Effect of fiber distribution and realignment on the nonlinear and inhomogeneous mechanical properties of human supraspinatus tendon under longitudinal tensile loading. Journal of Orthopaedic Research. 2009 [accessed 2016 May 31];27(12):1596–1602. http://www.ncbi.nlm.nih.gov/pubmed/19544524. doi:10.1002/jor.20938

41. Miller KS, Connizzo BK, Feeney E, Soslowsky LJ. Characterizing local collagen fiber re-alignment and crimp behavior throughout mechanical testing in a mature mouse supraspinatus tendon model. Journal of Biomechanics. 2012 [accessed 2019 May 30];45(12):2061–2065. https://www.sciencedirect.com/science/article/abs/pii/S0021929012003387. doi:10.1016/J.JBIOMECH.2012.06.006

42. Birk DE, Trelstad RL. Extracellular compartments in tendon morphogenesis: Collagen fibril, bundle, and macroaggregate formation. Journal of Cell Biology. 1986 [accessed 2017 Aug 10];103(1):231–240. http://www.ncbi.nlm.nih.gov/pubmed/3722266. doi:10.1083/jcb.103.1.231

43. Birk DE, Zycband EI, Woodruff S, Winkelmann DA, Trelstad RL. Collagen fibrillogenesis in situ: Fibril segments become long fibrils as the developing tendon

matures. Developmental Dynamics. 1997 [accessed 2016 May 31];208(3):291–298. http://doi.wiley.com/10.1002/%28SICI%291097-0177%28199703%29208%3A3%3C291%3A%3AAID-AJA1%3E3.0.CO%3B2-D. doi:10.1002/(SICI)1097-0177(199703)208:3<291::AID-AJA1>3.0.CO;2-D

44. Vallat R. Pingouin: statistics in Python. Journal of Open Source Software. 2018 [accessed 2020 May 27];3(31):1026. http://joss.theoj.org/papers/10.21105/joss.01026. doi:10.21105/joss.01026

CHAPTER 5: THE NEONATAL ACHILLES TENDON COLLAGEN MICROSTRUCTURE IS NEGATIVELY IMPACTED BY DECORIN AND BIGLYCAN KNOCKDOWN AFTER INJURY AND DURING DEVELOPMENT

5.1 Introduction

Tendons are a highly aligned and hierarchically organized collagen I-rich tissue that provide joint stability and transmit forces from muscle to bone. Tendon injuries present challenges to the individual by limiting daily activities and are increasingly common, resulting in a significant clinical burden.[1–3] Unfortunately, current therapeutics for tendon injury remain controversial with weak or inconclusive evidence for improving outcomes after injury.[4] Recently, neonatal mouse injury models have demonstrated an improved healing response in tendon, offering a new model to study for the development of therapeutics. Unfortunately, little is known about neonatal tendon development and the mechanisms that drive neonatal tendon healing.

Tendon development in the neonate mainly consists of collagen fibril growth and maturation, as the majority of collagen fibril assembly occurs during embryonic development.[5] Fibrillogenesis facilitates tendon growth and maturation, which is a multi-step process consisting of the production of collagen molecules to form fibril intermediates, linear growth of the fibril intermediates to produce longer fibrils, and finally lateral fusion of the fibrils to increase fibril diameter.[5] Early in development tendons have a narrow distribution of small diameter collagen fibrils.[6] As growth and maturation progresses this distribution broadens as large diameter fibrils are accumulated. Modulation of fibrillogenesis during this phase of development is vital to ensure that the

proper hierarchical structure of tendon is achieved since this process coincides with increases in ambulation, mechanical loading, and tendon mechanics.[6–8]

The changes in tendon structure, mechanics, and composition that are observed in the neonate are paralleled by the changes that occur after tendon injury. For example, after injury new collagen molecules are produced, which will lead to the production of larger diameter collagen fibrils via fibrillogenesis to establish the post-injury tendon structure. Due to this growth, similar changes to the collagen fibril diameter distribution are observed over time. Regulators of fibrillogenesis during tendon development, such as decorin and biglycan, are also upregulated after injury to prevent lateral fusion between immature collagen fibrils.[5,9] Ultimately, the healing response does not replicate the original developmental processes that created the native tendon; healing produces scar tissue that is mechanically and structurally inferior. However, multiple neonatal Achilles injury model have demonstrated that when tendon injury occurs during neonatal development a healing response that rapidly improves tendon structure and mechanics emerges.[10,11] Using a neonatal Achilles tendon injury model to study the processes that regulate fibrillogenesis during tendon development and healing can provide insights that lead to improvements in therapeutics and clinical outcomes after injury.

Decorin and biglycan are two class I SLRPs that are key regulators of collagen fibrillogenesis and highly expressed in tendon. Decorin and biglycan share a similar structure, consisting of leucine-rich repeats connected to one or two glycosaminoglycan chains, respectively.[12] Expression of decorin and biglycan is high during neonatal development, but expression patterns vary with decorin being steadily expressed while biglycan peaks early and tapers off around postnatal day 7.[6,9] Both SLRPs have shown to be key regulators of collagen fibrillogenesis during tendon development and healing,

with deficiency of decorin and biglycan producing alterations to collagen fibril diameter and the presence of abnormally shaped fibrils.[5,9,13,14] These changes to tendon structure impact tendon mechanics, producing changes in structural and material properties and viscoelastic mechanics depending on the model system that is employed.[15–23] Decorin and biglycan also have roles in various signaling pathways including regulation of TGF-β activity, immune signaling through toll-like receptors, and the formation and maintenance of the tendon stem/progenitor cell (TSPC) niche.[24–30] These previous studies demonstrate the importance of decorin and biglycan in the development and maintenance of tendon structure and mechanics through direct regulation of fibrillogenesis and signaling across vital pathways. However, little work has been done to explore the impact of these SLRPs on early neonatal tendon development when expression of decorin and biglycan is high, tendon growth and maturation is beginning, and the potential for an improved healing response is present.

Therefore, the objectives of this study were to determine the effects of decorin and biglycan knockdown on **(1)** the development of the neonatal Achilles tendon structure and mechanics and **(2)** the ability for the neonatal Achilles tendon to rapidly heal and recover biomechanical properties after injury. To achieve this, we used an inducible compound decorin/biglycan mouse model to knock down expression at two timepoints: on the day of birth (postnatal day 0) and at the time of injury (postnatal day 7). We hypothesized that knockdown of decorin and biglycan would **(1)** disrupt the neonatal development of tendon, resulting in decreased quasi-static and viscoelastic mechanical properties, altered collagen fiber realignment during loading, and altered collagen fibril diameter. We also hypothesized that **(2)** decorin and biglycan deficiency would impair the neonatal healing response by disrupting collagen fibril formation,

producing injured tendons with impaired mechanics, reduced collagen fiber realignment, and altered collagen fibril diameter distributions with a large population of small diameter fibrils. Mechanical properties, collagen fibril diameter, gene expression, and histology were defined in the Achilles tendon to test our hypotheses.

5.2 Methods

5.2.1 Animals

All methods utilized in this study were approved by the University of Pennsylvania Institutional Animal Care and Use Committee. The mice used in this study had a C57BL/6 background (Charles River, Wilmington, MA). *Dcn*$^{+/+}$/*Bgn*$^{+/+}$ (WT) were used as controls and compound *Dcn*$^{flox/flox}$/*Bgn*$^{flox/flox}$ (I-*Dcn* $^{-/-}$/*Bgn*$^{-/-}$) mice with a tamoxifen (TM)-inducible Cre, (B6.129-Gt(ROSA)26Sortm1(cre/ERT2)Tyj/J, Jackson Labs, Bar Harbor, ME) were used as the experimental group. WT and I-*Dcn* $^{-/-}$/*Bgn*$^{-/-}$ mice were randomized into two groups: (1) uninjured mice with TM treatment on the day of birth (P0) that were sacrificed at postnatal day 7 (P7) (WT-P7 and I-*Dcn* $^{-/-}$/*Bgn*$^{-/-}$-P7, n=16/group) and (2) mice that received TM treatment prior to unilateral Achilles tendon injury at P7 before sacrifice at P17 (WT-P17 and I-*Dcn* $^{-/-}$/*Bgn*$^{-/-}$-P17, n=20/group). All pups were administered 0.1 mg TM / 1 g body weight (T5648, Sigma, St. Louis, MO) suspended in corn oil (C8267, Sigma). Pups that received TM at P0 were administered TM via intragastric injection, while pups treated at P7 were administered TM via intraperitoneal injection before surgery; a 29G needle was used for all pups. Prior to injury, each WT-P17 and I-*Dcn* $^{-/-}$/*Bgn*$^{-/-}$-P17 animal was randomly assigned to an assay to ensure that both limbs from each mouse (injured and uninjured) were not allocated to the same

assay. Before tamoxifen treatment, the litter and the dam were placed in a separate cage, away from other mice in the colony, to avoid unintentional Cre activation.

5.2.2 Neonatal Achilles Tendon Surgery

After TM injection at P7, WT-P17 and I-*Dcn* $^{-/-}$/*Bgn* $^{-/-}$-P17 mice underwent surgery for a unilateral, full thickness, partial width Achilles tendon injury. Prior to surgery, pain management was provided with a subcutaneous injection of Buprenorphine Sustained-Release. The animals were initially anesthetized using 3% isoflurane; isoflurane was maintained at 1.5% throughout surgery with a constant oxygen flow rate of 1L/min. A 3mm incision was made in the skin medial to the right Achilles tendon, then a rubber backing was placed beneath the center of the tendon to provide support. A 0.3mm biopsy punch (RBP-03, Robbins Instruments, Houston, TX) was used to create a full thickness, partial width central defect in the Achilles tendon, then the skin was closed using a 6.0 prolene suture. Mice returned to normal cage activity and postoperative Buprenorphine Sustained-Release was given 3 days after surgery.

5.2.3 Gene Expression Analysis

Immediately after sacrifice, mouse Achilles tendons were dissected and stored in RNAlater (Thermo-Fisher, Waltham, MA) at -20°C to stabilize the RNA (n=3-5/group). Gene expression was measured using a Fluidigm 96.96 Dynamic Array™ IFC (Fluidigm, San Francisco, CA) after samples underwent preparation consisting of RNA isolation, reverse transcription, and pre-amplification as previously described.[31] The Achilles tendons were prepared for RNA isolation by transferring the tissue to TRIzol (ThermoFisher) followed by disruption using a pestle and mortar and vortexing. Direct-zol RNA Microprep kits (Zymo Research, Irvine, CA) were used to isolate the RNA, then the RNA was reverse-transcribed using a High-Capacity cDNA RT kit (ThermoFisher).

After reverse transcription, the cDNA for all targets, except for *Col1a1*, was pre-amplified for 15 cycles using Taqman Gene Expression Assays (Fluidigm), then loaded into a Fluidigm 96.96 Dynamic Array™ IFC (Fluidigm) at the University of Pennsylvania Molecular Profiling Facility. Expression was measured across 92 genes; 18S, Rps17, and Abl1 were used as housekeeper genes. ΔCt values were determined by subtracting each Ct from the average Ct value of the housekeeper genes. ΔΔCt values were calculated by subtracting ΔCt values from the average WT ΔCt value.

5.2.4 Viscoelastic Biomechanical Testing

Prior to biomechanical testing, Achilles tendons (n=8-12/group) were prepared as previously described.[6] Each sample was prepared under a dissection microscope to isolate the Achilles tendon and calcaneus and remove any excess tissue. After dissection, the cross-sectional area of the tendon was measured with a custom device using a laser and translational stages.[32] Cross-sectional area was measured every 0.5 mm along the length of the tendon to obtain 6-8 measurements per sample, then the average cross-sectional area was obtained from these measurements using custom Matlab software (Matlab2021a, Mathworks, Inc., Natick, MA). Verhoeff's stain was used to apply stain lines at 1 mm intervals, beginning at the calcaneal insertion, for optical strain tracking. Sandpaper was glued to the calcaneal and myotendinous ends of the Achilles tendon, then secured using custom grips, to set a gauge length of 2.5 mm for mice sacrificed at P7 or 3 mm for mice sacrificed at P17. Next, the grips were secured using a custom grip holder to ensure that the sample would remain unloaded until it was mounted for mechanical testing.[6]

The Achilles tendon was mounted in 1x phosphate-buffered saline bath at 37°C within a tensile testing system (Instron 5848, Instron Corp., Norwood, MA) integrated

with a custom cross-polarized light setup.[33] After the tendon was secured, it was preloaded to 0.01 N and an image was taken for gauge length measurements, then the viscoelastic mechanical testing protocol was initiated. The mechanical testing protocol consisted of a stress relaxation followed by a series of frequency sweeps and finished with a ramp to failure. During the ramp to failure a series of image maps were taken for optical strain tracking and collagen fiber realignment analysis; each image map consisted of 18 images obtained over 5 seconds, with 10 seconds separating each image map.[33] Collagen fiber realignment analysis was determined at 1%, 5%, 10%, 15%, and 20% strain using custom MatLab software (Matlab2021a) and outputted as circular variance ratio. Circular variance describes the distribution of collagen fiber realignment along the surface of the tendon and has an inverse relationship with collagen fiber realignment. The circular variance ratio is defined as the circular variance at a discrete strain level normalized by the circular variance of the tendon at gauge length. Optical tracking was used to determine the tendon modulus and was calculated using custom MatLab software (Matlab2021a).

5.2.5 Transmission Electron Microscopy

Achilles tendons (n=4/group) were analyzed using transmission electron microscopy (TEM). Samples were fixed *in situ* as previously described.[22,34,35] Post-staining with uranyless followed by 1% phosphotungstic acid, pH 3.2, was utilized for contrast enhancement. Cross sectional images within the midsubstance of the Achilles tendons were examined at 80 kV using a JEOL 1010 transmission electron microscope. Images were digitally captured at an instrument magnification of 60,000x using an 2k x 2k AMT CCD camera. Collagen fibril diameter was measured along the minor axis of the fibril using a custom program (Matlab2021a). Fibril diameter analyses were completed

using images from the center of the tendon. All fibrils within a predetermined region of interest (ROI) on the digitized image were analyzed. Non-overlapping ROIs were selected based on fibril orientation (i.e., cross section) and absence of cells.

5.2.6 Histology Preparation and Staining

Mouse hindlimbs were disarticulated at the hip, and the Achilles tendon was positioned perpendicular to the foot and placed in 4% paraformaldehyde at 4°C for 2 days. After fixation, the limbs were transferred to a 30% sucrose solution at 4°C for 24 hours for cryopreservation then embedded in OCT media. 8 µm sagittal sections were collected throughout the tendon using Cryofilm Type IIC (Section Lab, Inc., Japan)[36], affixed to glass slides with 1.5% chitosan in 0.25% acetic acid, then sections were dried at 4°C. Sections were stained with either hematoxylin and eosin or toluidine blue. P17 uninjured and injured sections were mounted with Hoechst 333424 (ThermoFisher) as a nuclear marker. Toluidine blue staining was quantified by determining the percentage of the tissue positive for metachromatic staining. Image analysis was performed using Fiji.[37]

5.2.7 Statistics

Mechanical properties and histological parameters were compared using Student t-tests. A two-way repeated measures ANOVA w/ Bonferroni post-hoc analysis was used to compare fiber realignment data using genotype and strain as factors. Collagen fibril diameter distributions were compared using the Kolmogorov-Smirnov test, and F tests were used to compare collagen fibril diameter variance. Principal component analysis (PCA) was performed on ΔΔCt values via scikit-learn[38]. Data preprocessing for PCA and gene expression analysis was conducted using NumPy and pandas.[39,40] Matplotlib was used for PCA data visualization.[41] Principal component (PC) scores and ΔCt values

were compared using Student t-tests. Significance was set at $p \leq 0.05$, and trends were set at $p \leq 0.1$.

5.3 Results

5.3.1 Decorin and biglycan were effectively knocked down in P7 and P17 mice

P7 I-*Dcn*$^{-/-}$/*Bgn*$^{-/-}$ Achilles tendons had a 4.25-fold decrease in decorin expression and a 4.54-fold decrease in biglycan expression relative to WT (Fig. 25 A, B). Uninjured P17 I-*Dcn*$^{-/-}$/*Bgn*$^{-/-}$ decorin expression decreased by 2.40-fold and biglycan expression decreased by 2.44-fold, while injured P17 I-*Dcn*$^{-/-}$/*Bgn*$^{-/-}$ tendon expression decreased by 2.54-fold and 3.53-fold for decorin and biglycan, respectively, compared to P17 WT tendons (Fig. 25 C, D).

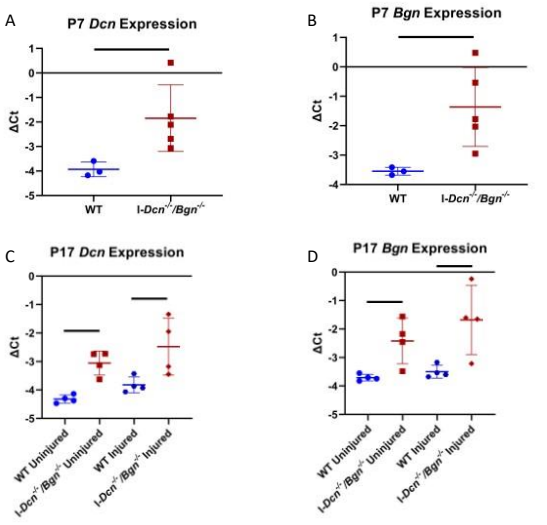

Figure 25. Decorin and biglycan expression in P7 and P17 Achilles Tendons. *Dcn* and *Bgn* expression was measured in P7 (A, B) and P17 (C, D) tendons after tamoxifen treatment. Knockdown of *Dcn* and *Bgn* was confirmed in P7 I-*Dcn*$^{-/-}$/*Bgn*$^{-/-}$ tendons and in P17 I-*Dcn*$^{-/-}$/*Bgn*$^{-/-}$ tendons that were injured and uninjured. Data shown as average with standard deviation.

5.3.2 Variance from *Dcn* and *Bgn* expression was highly correlated with variance contributed by differentially expressed genes in P7 I-*Dcn*$^{-/-}$/*Bgn*$^{-/-}$ tendons

95% of the variance from P7 ΔΔCt values was captured in 6 principal components (PC1: 35.0%, PC2: 24.9%, PC3: 15.0%, PC4: 11.6%, PC5: 6.4%, PC6: 5.1%). PC3 scores were significantly reduced in I-*Dcn*$^{-/-}$/*Bgn*$^{-/-}$ tendons (Fig. 26 A, B); *Bgn* and *Dcn* ΔΔCt values were among the top variables (second and third, respectively)

that contributed to PC3. Expression of three additional genes, *Axin2*, *Col12a1*, and *Prg4*, was altered after *Dcn* and *Bgn* knockdown (Table 2). *Axin2* expression was increased in I-*Dcn*$^{-/-}$/*Bgn*$^{-/-}$ tendons (Fig. 26 C) and was the largest contributor to PC3. *Col12a1* (fourth largest contributor to PC3) and *Prg4* (fifteenth largest contributor to PC3) expression decreased in I-*Dcn*$^{-/-}$/*Bgn*$^{-/-}$ tendons (Fig. 26 D, E).

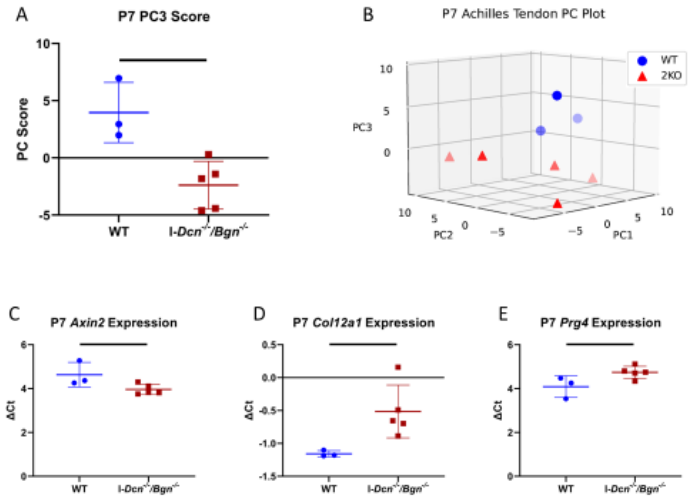

Figure 26. P7 Achilles Tendon Gene Expression. Gene expression in P7 tendons was analyzed with principal component analysis, and the score of principal component 3 was reduced in I-*Dcn*$^{-/-}$/*Bgn*$^{-/-}$ tendons relative to WT (A, B). Alterations to expression of individual genes were also present after knockdown of *Dcn* and *Bgn*, with increased *Axin2* (C) expression and decreased expression of *Col12a1* and *Prg4* (D, E). Data shown as average with standard deviation.

Table 2. P7 Achilles tendon gene expression. Genes were listed in descending order according to the magnitude of the contribution of the gene to PC3. ΔCt data displayed as mean ± standard deviation and * denotes significance ($p<0.05$).

Gene	PC3 Contribution	WT ΔCt	I-*Dcn*$^{-/-}$/*Bgn*$^{-/-}$ ΔCt
AXIN2	0.2380	4.635 ± 0.561	3.963 ± 0.235 *
BGN	-0.2237	-3.548 ± 0.132	-1.364 ± 1.342 *
DCN	-0.2217	-3.934 ± 0.305	-1.845 ± 1.36 *
COL12a1	-0.2212	-1.157 ± 0.047	-0.514 ± 0.401 *
LTBP4	0.2159	1.942 ± 0.28	1.534 ± 0.293
KERA	-0.2112	-1.682 ± 0.099	-1.002 ± 0.476
TAZ	0.1933	2.409 ± 0.315	2.209 ± 0.168
TIMP1	-0.1901	0.876 ± 0.246	1.484 ± 0.452
CD3e	0.1751	11.43 ± 0.58	10.032 ± 1.792
GJA1	-0.1686	-0.4 ± 0.11	-0.01 ± 0.417
MMP14	0.1627	-0.4 ± 0.154	-0.993 ± 0.426
YAP1	0.1615	0.911 ± 0.326	0.461 ± 0.448
BMP4	0.1609	4.04 ± 0.327	3.685 ± 0.345
IL1B	0.1586	11.129 ± 1.084	10.698 ± 0.591
PRG4	-0.1570	4.089 ± 0.491	4.744 ± 0.275 *
LOXL1	0.1464	1.824 ± 0.32	1.67 ± 0.559
SCX	-0.1445	1.018 ± 0.283	1.413 ± 0.49

HSPG2	0.1352	-0.097 ± 0.014	-0.459 ± 0.333
TGFBR2	0.1342	0.99 ± 0.521	0.937 ± 0.536
PLOD3	0.1313	1.606 ± 0.383	1.536 ± 0.257
SOX9	0.1293	3.652 ± 0.603	3.306 ± 0.261
IL6	0.1282	9.482 ± 0.425	9.436 ± 0.492
ITGB5	-0.1240	3.235 ± 0.183	4.018 ± 0.89
TLR2	-0.1234	3.743 ± 0.167	4.122 ± 0.539
TNMD	-0.1216	-2.583 ± 0.14	-2.327 ± 0.535
ACTA2	-0.1213	-1.848 ± 0.309	-0.717 ± 0.796
H2AFX	-0.1191	4.678 ± 0.411	8.877 ± 3.731
MKX	-0.1168	0.636 ± 0.108	0.794 ± 0.926
COL14a1	-0.1163	-0.387 ± 0.06	-0.315 ± 0.39
COL1a2	-0.1106	-4.24 ± 0.583	-4.148 ± 0.378
ADAMTS1	0.1102	2.716 ± 0.61	2.709 ± 0.555
TGFB2	0.1101	3.15 ± 0.509	2.787 ± 0.495
EGR1	-0.1084	6.469 ± 0.591	10.872 ± 3.768
IL33	-0.1074	2.136 ± 0.347	2.901 ± 0.561
THBS4	0.1021	-0.167 ± 0.195	-0.646 ± 0.457
MMP13	-0.1012	3.496 ± 2.561	4.467 ± 2.316
ITGA11	0.0959	2.749 ± 0.248	2.524 ± 0.421
ADAMTS15	0.0953	3.412 ± 0.554	3.447 ± 0.334
MMP9	-0.0907	3.766 ± 3.582	4.719 ± 2.94
SPARC	-0.0891	-3.664 ± 0.536	-3.271 ± 0.641
ITGA5	0.0875	2.476 ± 0.13	2.364 ± 0.375
TGFB1	0.0839	3.252 ± 0.408	2.973 ± 0.447
VCAN	-0.0836	-0.035 ± 0.257	0.311 ± 0.383
ITGA1	-0.0796	2.058 ± 0.354	2.608 ± 0.482
MMP2	0.0787	-0.636 ± 0.415	-0.689 ± 0.489
COL2a1	-0.0745	-1.811 ± 0.123	-1.562 ± 0.631
CDH11	-0.0675	0.945 ± 0.305	1.22 ± 0.401
ADGRE1	0.0637	2.289 ± 0.467	2.586 ± 0.75
THBS2	-0.0628	-0.447 ± 0.344	-0.177 ± 0.363
VIM	-0.0558	-2.883 ± 0.231	-2.423 ± 0.48
CD38	-0.0546	4.874 ± 0.464	5.372 ± 0.445
PLOD2	-0.0532	1.06 ± 0.41	1.326 ± 0.769
COL1a1	-0.0514	7.676 ± 0.152	7.589 ± 0.656
MSTN	0.0493	2.17 ± 0.891	2.239 ± 0.779
MMP8	0.0485	10.795 ± 0.813	11.131 ± 0.584
ITGB1	-0.0463	-1.566 ± 0.254	-1.324 ± 0.444
TNC	0.0456	-0.095 ± 0.424	-0.335 ± 0.557
LTBP1	0.0454	1.504 ± 0.1	1.37 ± 0.464
CASP3	0.0441	2.186 ± 0.282	2.227 ± 0.461
ASPN	-0.0435	-0.75 ± 0.387	-0.381 ± 0.377
FAP	-0.0433	0.805 ± 0.382	1.081 ± 0.509
COL3a1	-0.0422	-4.066 ± 0.455	-3.723 ± 0.684
TLR4	-0.0410	2.322 ± 0.222	2.724 ± 0.407
ITGA2	-0.0387	1.834 ± 0.289	1.852 ± 0.591
TIMP3	-0.0377	-0.323 ± 0.303	0.072 ± 0.483
COL6a2	0.0372	-1.815 ± 0.019	-1.838 ± 0.376
IL12	0.0370	13.531 ± 1.184	13.911 ± 1.602
FMOD	-0.0355	-1.287 ± 0.397	-1.328 ± 0.391
LUM	-0.0326	-0.099 ± 0.368	0.34 ± 0.479
IL13	-0.0300	9.926 ± 0.448	10.642 ± 0.681

TNFa	-0.0277	7.045 ± 0.268	7.489 ± 0.517
ACAN	-0.0217	-0.607 ± 0.477	-0.57 ± 0.762
LOXL2	-0.0206	-0.936 ± 0.229	-0.933 ± 0.481
CTGF	0.0206	2.657 ± 0.552	2.989 ± 0.956
POSTN	0.0200	-2.901 ± 0.247	-2.813 ± 0.5
IL10	-0.0195	11.917 ± 1.041	12.749 ± 0.822
CD31	0.0185	2.222 ± 0.794	2.704 ± 0.739
CD163	0.0177	2.799 ± 0.571	3.412 ± 0.917
FBN1	0.0142	-1.624 ± 0.133	-1.359 ± 0.708
FN1	-0.0137	-1.74 ± 0.077	-1.521 ± 0.499
COL11a1	-0.0130	-0.881 ± 0.343	-1.026 ± 0.694
COL5a1	0.0121	-0.984 ± 0.07	-0.933 ± 0.287
COL6a1	-0.0118	-0.717 ± 0.341	-0.858 ± 0.276
MMP3	0.0116	5.996 ± 0.495	6.777 ± 1.627
CD68	-0.0114	2.037 ± 0.564	2.422 ± 0.332
ITGAv	-0.0081	2.217 ± 0.33	2.452 ± 0.881
PCNA	0.0061	1.283 ± 0.398	1.586 ± 0.349
TGFB3	0.0053	1.241 ± 0.268	1.316 ± 0.346
COMP	0.0050	0.471 ± 0.535	0.311 ± 0.642

5.3.3 Variance of P17 expression data was driven by differentially expressed genes after *Dcn* and *Bgn* knockdown

PCA revealed that 95% of the variance of P17 ΔΔCt values was captured in 6 PCs for uninjured tendons (PC1: 48.2%, PC2: 17.4%, PC3: 11.3%, PC4: 10.9%, PC5: 5.7%, PC6: 3.9%) and 5 PCs for injured tendons (PC1: 55.8%, PC2: 17.3%, PC3: 10.6%, PC4: 6.2%, PC5: 5.2%). P17 I-*Dcn*$^{-/-}$/*Bgn*$^{-/-}$ tendons had increased PC1 scores compared to WT for uninjured (Fig. 27 A, B) and injured samples had

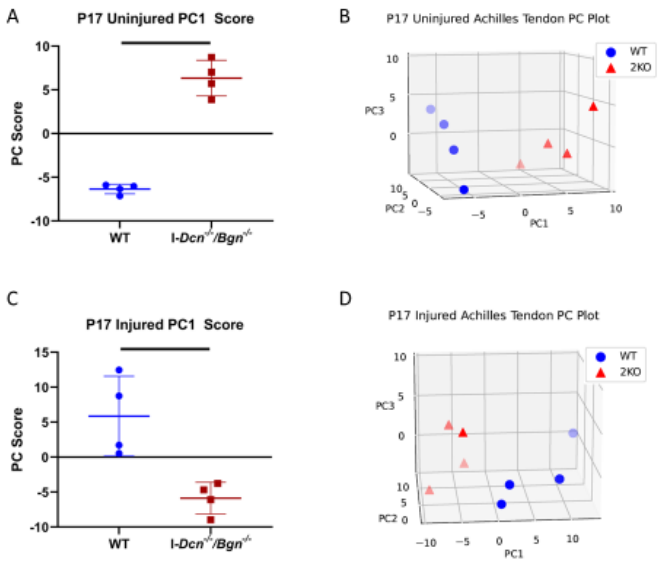

Figure 27. P17 Uninjured and Injured Achilles Principal Component Analysis of Gene Expression Data. Principal component analysis was used to analyze uninjured and injured gene expression data from P17 tendons. PC1 was increased in uninjured (A, B) I-*Dcn*$^{-/-}$/*Bgn*$^{-/-}$ tendons, while PC1 was decreased in injured tendons (C, D). Data shown as average with standard deviation.

decreased PC1 scores (Fig. 27 C, D). PC1 scores were correlated with genes that were differentially expressed in I-*Dcn*$^{-/-}$/*Bgn*$^{-/-}$ tendons relative to WT (Tables 3, 4). Analysis of individual gene expression found that 42 genes were differentially expressed in uninjured I-*Dcn*$^{-/-}$/*Bgn*$^{-/-}$ tendons compared to WT (Table 3), while injured I-*Dcn*$^{-/-}$/*Bgn*$^{-/-}$ tendons revealed changes to expression in 46 genes (Table 4). 19 of the 42 genes that were significantly altered were unique to the uninjured group and 23 of the 46 genes were unique to injured I-*Dcn*$^{-/-}$/*Bgn*$^{-/-}$ tendons.

Table 3. P17 uninjured Achilles tendon gene expression. Genes were listed in descending order according to the magnitude of the contribution of the gene to PC1. ΔCt data displayed as mean ± standard deviation and * denotes significance ($p<0.05$). Δ denotes significance for P17 uninjured tendons, but not for P17 injured tendons.

Gene	PC1 Contribution	WT ΔCt	I-*Dcn*$^{-/-}$/*Bgn*$^{-/-}$ ΔCt
IL33	-0.1531	6.109 ± 0.192	2.871 ± 0.38 *
LOXL2	-0.1525	0.893 ± 0.13	-1.338 ± 0.526 *
BMP4	0.1523	2.99 ± 0.101	4.011 ± 0.121 *
MMP3	-0.1519	7.866 ± 0.272	5.866 ± 0.423 * Δ
MSTN	-0.1517	6.463 ± 0.492	3.48 ± 0.302 * Δ
SCX	-0.1516	3.718 ± 0.275	1.241 ± 0.435 *
COL6a2	-0.1507	-0.068 ± 0.167	-1.499 ± 0.33 *
MMP2	0.1479	-1.201 ± 0.059	-0.469 ± 0.097 * Δ
TLR2	0.1476	3.299 ± 0.121	4.301 ± 0.257 * Δ
LTBP1	-0.1459	1.77 ± 0.03	1.3 ± 0.167 *
TNFa	-0.1442	9.973 ± 0.427	8.469 ± 0.503 *
TLR4	0.1440	1.921 ± 0.228	3.114 ± 0.169 * Δ
KERA	-0.1428	0.924 ± 0.273	-0.219 ± 0.463 * Δ
ACTA2	-0.1417	2.719 ± 0.562	0.932 ± 0.609 *
DCN	0.1401	-4.319 ± 0.142	-3.055 ± 0.424 *
VCAN	-0.1392	2.423 ± 0.391	1.272 ± 0.315 *
FBN1	-0.1385	0.378 ± 0.345	-0.742 ± 0.39 *
BGN	0.1376	-3.704 ± 0.115	-2.418 ± 0.803 *
PRG4	0.1375	0.516 ± 0.177	1.933 ± 0.521 * Δ
CD163	0.1367	1.945 ± 0.445	3.338 ± 0.336 *
COL11a1	-0.1350	-0.23 ± 0.447	-1.67 ± 0.331 * Δ
COL12a1	-0.1337	-0.11 ± 0.281	-0.883 ± 0.328 *
TIMP3	0.1332	-1.312 ± 0.193	-0.555 ± 0.269 *
TNMD	-0.1316	-1.378 ± 0.232	-2.146 ± 0.232 * Δ
SPARC	0.1301	-4.885 ± 0.225	-4.07 ± 0.554 *
TIMP1	-0.1292	1.72 ± 0.516	0.781 ± 0.436 *
COMP	-0.1265	-0.267 ± 0.239	-1.274 ± 0.429 * Δ
GJA1	-0.1252	0.226 ± 0.275	-0.369 ± 0.27 *
VIM	0.1243	-2.683 ± 0.218	-2.316 ± 0.112 * Δ
COL1a1	-0.1220	6.909 ± 0.352	6.309 ± 0.169 *
ITGB1	-0.1208	-0.478 ± 0.173	-0.845 ± 0.278
LTBP4	0.1208	0.804 ± 0.102	1.592 ± 0.329 * Δ

PLOD2	-0.1207	1.284 ± 0.093	0.57 ± 0.398 *
IL10	0.1200	9.158 ± 0.917	11.377 ± 0.794 * Δ
ADAMTS15	-0.1192	4.667 ± 0.526	3.821 ± 0.282 * Δ
ASPN	-0.1187	1.011 ± 0.333	0.451 ± 0.318 * Δ
ITGA5	0.1180	2.225 ± 0.229	3.015 ± 0.323 * Δ
TGFB3	0.1170	0.65 ± 0.254	0.999 ± 0.151
COL3a1	-0.1161	-2.991 ± 0.217	-3.354 ± 0.152 * Δ
SOX9	-0.1145	4.288 ± 1.186	2.232 ± 0.681 * Δ
ITGA11	0.1142	1.978 ± 0.241	2.374 ± 0.082 *
FMOD	0.1093	-3.134 ± 0.276	-2.683 ± 0.296
THBS2	-0.1093	-0.337 ± 0.11	-0.75 ± 0.426
IL1B	-0.1081	11.131 ± 0.614	9.628 ± 0.884 *
COL1a2	0.1056	-5.198 ± 0.284	-4.836 ± 0.25
AXIN2	0.1038	3.912 ± 0.114	4.236 ± 0.215 * Δ
ADAMTS1	-0.1029	3.41 ± 0.311	2.97 ± 0.419
ITGA2	-0.1024	2.424 ± 0.403	1.952 ± 0.178
MMP14	0.1009	-0.819 ± 0.168	-0.324 ± 0.271 *
COL2a1	-0.0947	-0.902 ± 1.658	-2.81 ± 0.685
FAP	-0.0943	2.006 ± 0.698	1.428 ± 0.241
EGR1	-0.0932	9.757 ± 4.534	5.704 ± 0.742
LUM	-0.0926	1.761 ± 0.607	1.231 ± 0.422
TGFB2	-0.0923	3.562 ± 0.142	3.315 ± 0.362
LOXL1	-0.0919	2.73 ± 0.143	2.466 ± 0.376
TAZ	0.0895	2.283 ± 0.206	2.499 ± 0.11
CTGF	0.0875	0.02 ± 0.71	0.749 ± 0.579
TNC	-0.0868	0.363 ± 0.601	-0.096 ± 0.448
MMP8	0.0828	8.975 ± 0.189	10.828 ± 1.972
COL5a1	-0.0810	-0.461 ± 0.354	-0.826 ± 0.182
ADGRE1	-0.0798	4.423 ± 0.236	4.159 ± 0.404
PLOD3	-0.0796	2.246 ± 0.078	2.147 ± 0.21
CD68	0.0788	1.975 ± 0.419	2.529 ± 0.395
H2AFX	-0.0741	7.894 ± 3.105	5.981 ± 0.166
ACAN	-0.0739	-0.617 ± 1.002	-1.491 ± 0.79
CD3e	0.0728	11.103 ± 0.788	11.732 ± 0.353
ITGA1	0.0704	2.535 ± 0.169	2.763 ± 0.212
COL6a1	0.0661	-1.032 ± 0.441	-0.826 ± 0.241
IL6	-0.0661	11.2 ± 1.223	10.613 ± 0.302
PCNA	-0.0657	2.904 ± 0.19	2.767 ± 0.376
CD31	0.0619	3.355 ± 0.145	3.944 ± 0.686
COL14a1	-0.0597	2.081 ± 0.258	1.86 ± 0.291
ITGAv	-0.0548	2.469 ± 0.456	2.316 ± 0.325
CD38	-0.0531	6.631 ± 0.559	6.42 ± 0.669
MMP13	0.0464	-0.931 ± 0.878	-0.531 ± 0.192
POSTN	-0.0427	-1.434 ± 0.26	-1.546 ± 0.353
ITGB5	0.0398	2.937 ± 0.392	3.157 ± 0.304
CDH11	-0.0397	2.127 ± 0.629	1.993 ± 0.432
MKX	0.0396	0.262 ± 0.302	0.392 ± 0.161
TGFBR2	0.0374	0.981 ± 0.375	1.275 ± 0.429
HSPG2	-0.0328	-0.28 ± 0.301	-0.382 ± 0.146
CASP3	-0.0251	3.06 ± 0.244	3.067 ± 0.324
MMP9	0.0163	-1.22 ± 1.241	-0.951 ± 0.286
YAP1	0.0135	1.223 ± 0.098	1.346 ± 0.327
FN1	-0.0088	-1.712 ± 0.138	-1.731 ± 0.097

THBS4	0.0049	-1.95 ± 0.144	-1.895 ± 0.298
TGFB1	-0.0035	2.702 ± 0.185	2.775 ± 0.337

Table 4. P17 uninjured Achilles tendon gene expression. Genes were listed in descending order according to the magnitude of the contribution of the gene to PC1. ΔCt data displayed as mean ± standard deviation and * denotes significance ($p<0.05$). Δ denotes significance for P17 injured tendons, but not for P17 uninjured tendons.

Gene	PC1 Contribution	WT ΔCt	I-*Dcn*$^{-/-}$/*Bgn*$^{-/-}$ ΔCt
COL6a2	0.1423	-0.567 ± 0.574	-1.88 ± 0.121 *
CDH11	0.1407	1.18 ± 0.57	0.115 ± 0.325 * Δ
TGFBR2	0.1406	0.76 ± 0.491	-0.056 ± 0.203 * Δ
IL33	0.1406	4.165 ± 1.106	2.546 ± 0.297 *
FN1	0.1400	-1.954 ± 0.199	-2.553 ± 0.069 *
LOXL2	0.1390	0.754 ± 0.68	-1.263 ± 0.145 *
LTBP1	0.1387	2.403 ± 0.504	1.252 ± 0.153 *
MMP14	0.1382	-0.891 ± 0.388	-1.724 ± 0.168 *
PLOD3	0.1379	2.176 ± 0.283	1.291 ± 0.212 * Δ
GJA1	0.1375	0.154 ± 0.459	-0.887 ± 0.338 *
ADAMTS1	0.1372	3.262 ± 0.556	2.403 ± 0.158 * Δ
COL14a1	0.1364	2.016 ± 0.536	1.101 ± 0.32 * Δ
CD3e	0.1363	10.272 ± 1.074	8.271 ± 0.484 * Δ
TNC	0.1363	0.288 ± 0.429	-1.453 ± 0.296 * Δ
COL12a1	0.1361	-0.443 ± 0.398	-1.442 ± 0.415 *
TGFB2	0.1357	3.439 ± 0.421	2.813 ± 0.103 * Δ
SCX	0.1357	2.999 ± 0.638	1.393 ± 0.433 *
ITGAv	0.1345	2.449 ± 0.257	1.403 ± 0.208 * Δ
ITGB1	0.1343	-1.109 ± 0.398	-1.548 ± 0.186
LOXL1	0.1331	2.218 ± 0.629	0.989 ± 0.397 * Δ
TIMP1	0.1327	0.584 ± 0.709	-0.538 ± 0.49 *
TGFB1	0.1325	2.806 ± 0.176	1.936 ± 0.188 * Δ
ACTA2	0.1321	0.995 ± 0.92	-0.591 ± 0.394 *
THBS2	0.1320	-0.353 ± 0.838	-1.388 ± 0.179 * Δ
TNFa	0.1308	8.01 ± 0.918	6.143 ± 0.762 *
FBN1	0.1308	-0.351 ± 0.748	-1.672 ± 0.328 * Δ
FAP	0.1308	1.582 ± 0.145	0.646 ± 0.326 * Δ
ITGA11	0.1298	1.847 ± 0.428	0.911 ± 0.552 *
COL5a1	0.1287	-0.441 ± 0.424	-1.396 ± 0.108 * Δ
ADGRE1	0.1280	2.843 ± 1.064	1.787 ± 0.329
VCAN	0.1267	1.932 ± 0.8	0.785 ± 0.276 *
IL1B	0.1264	10.06 ± 1.093	7.025 ± 0.783 *
PCNA	0.1262	2.587 ± 0.302	1.677 ± 0.359 * Δ
MMP2	0.1237	-1.487 ± 0.734	-2.076 ± 0.275
ITGB5	0.1236	2.943 ± 0.367	2.622 ± 0.213
ADAMTS15	0.1225	3.66 ± 0.617	3.025 ± 0.304
TGFB3	0.1221	1.001 ± 0.242	0.442 ± 0.246 * Δ
THBS4	0.1204	-1.415 ± 0.475	-1.92 ± 0.312
ITGA5	0.1193	2.458 ± 0.408	2.076 ± 0.204
SPARC	-0.1191	-3.788 ± 0.237	-3.157 ± 0.348 *
CTGF	-0.1177	0.049 ± 0.388	1.327 ± 0.718 * Δ
CASP3	0.1170	2.538 ± 0.295	1.915 ± 0.383 * Δ
PLOD2	0.1166	1.502 ± 0.173	0.611 ± 0.405 *

MMP3	0.1163	4.653 ± 1.642	3.721 ± 0.514
ITGA2	0.1159	3.924 ± 0.419	2.758 ± 0.666 * Δ
LUM	0.1159	-0.025 ± 1.022	-0.918 ± 0.483
CD38	0.1133	5.262 ± 0.563	4.799 ± 0.374
BMP4	-0.1121	3.806 ± 0.124	4.323 ± 0.145 *
CD68	0.1112	1.0 ± 0.763	0.552 ± 0.335
YAP1	0.1111	1.407 ± 0.141	0.986 ± 0.192 * Δ
ASPN	0.1024	-1.351 ± 0.845	-1.766 ± 0.184
COL3a1	0.0999	-3.354 ± 0.667	-3.705 ± 0.316
IL6	0.0990	9.416 ± 0.949	7.932 ± 0.74 * Δ
KERA	0.0969	-0.833 ± 0.784	-1.277 ± 0.524
CD31	0.0960	2.458 ± 0.616	2.28 ± 0.375
COL1a1	0.0954	7.573 ± 0.438	6.428 ± 0.489 *
POSTN	0.0901	-2.673 ± 0.618	-2.916 ± 0.156
BGN	-0.0898	-3.497 ± 0.225	-1.678 ± 1.216 *
COL6a1	0.0883	-0.318 ± 0.225	-0.574 ± 0.223
COL2a1	-0.0883	-1.101 ± 1.705	0.49 ± 1.835
CD163	-0.0873	2.566 ± 0.295	3.323 ± 0.362 *
TIMP3	-0.0848	-0.709 ± 0.044	-0.326 ± 0.245 *
MSTN	0.0815	2.69 ± 1.336	2.224 ± 0.85
DCN	-0.0791	-3.821 ± 0.276	-2.479 ± 1.0 *
VIM	0.0786	-2.645 ± 0.393	-2.804 ± 0.254
MKX	0.0777	0.824 ± 0.317	0.599 ± 0.53
COL11a1	0.0754	-0.296 ± 0.221	-0.969 ± 0.65
HSPG2	0.0749	0.044 ± 0.263	-0.435 ± 0.296 * Δ
ITGA1	0.0670	3.001 ± 0.212	2.808 ± 0.353
COMP	0.0600	0.268 ± 0.239	-0.247 ± 0.922
MMP9	0.0547	-0.935 ± 0.346	-1.472 ± 0.394
TNMD	0.0531	-2.304 ± 0.677	-2.374 ± 0.436
MMP8	0.0503	8.506 ± 0.182	8.18 ± 1.27
TLR2	0.0452	3.501 ± 0.482	3.591 ± 0.263
ACAN	-0.0406	-0.403 ± 1.357	-0.402 ± 0.909
FMOD	0.0389	-1.36 ± 0.114	-1.613 ± 0.808
SOX9	-0.0357	3.793 ± 1.135	3.645 ± 0.699
COL1a2	0.0328	-3.984 ± 0.185	-4.25 ± 0.256
LTBP4	0.0292	1.545 ± 0.433	1.385 ± 0.23
MMP13	-0.0227	-1.73 ± 0.384	-1.479 ± 0.443
EGR1	-0.0164	7.998 ± 3.228	7.05 ± 1.257
TLR4	0.0154	2.072 ± 0.372	2.26 ± 0.251
AXIN2	-0.0127	4.305 ± 0.418	4.348 ± 0.533
TAZ	0.0109	2.471 ± 0.169	2.466 ± 0.191
IL10	0.0100	8.582 ± 0.484	8.979 ± 0.722
PRG4	-0.0082	2.24 ± 0.482	2.509 ± 0.524
H2AFX	0.0027	7.121 ± 1.946	6.1 ± 0.41

5.3.4 Individual gene expression was altered in P17 I-*Dcn*$^{-/-}$/*Bgn*$^{-/-}$ tendons

Uninjured P17 tendons increased expression of two SLRPs, *Kera* and *Aspn*, in response to *Dcn* and *Bgn* knockdown relative to WT tendons (Fig. 28 A, B). Collagen expression was altered in uninjured and injured I-*Dcn*$^{-/-}$/*Bgn*$^{-/-}$ tendons; *Col1a1*, *Col6a2*, and *Col12a1* expression was upregulated in uninjured and injured tendons (Fig. 28 C, F, H). Additionally, *Dcn* and *Bgn* deficiency resulted in increased expression of *Col3a1* and *Col11a1* in uninjured tendons (Fig. 28 D, G), while *Col5a1* and *Col14a1* were upregulated after injury (Fig. 28 E, I). *Dcn* and *Bgn* knockdown also increased *TGFB1, TGFB2, TGFB3 and TGFBR2* expression after injury (Fig. 28 J-M). *TLR2* and *TLR4*

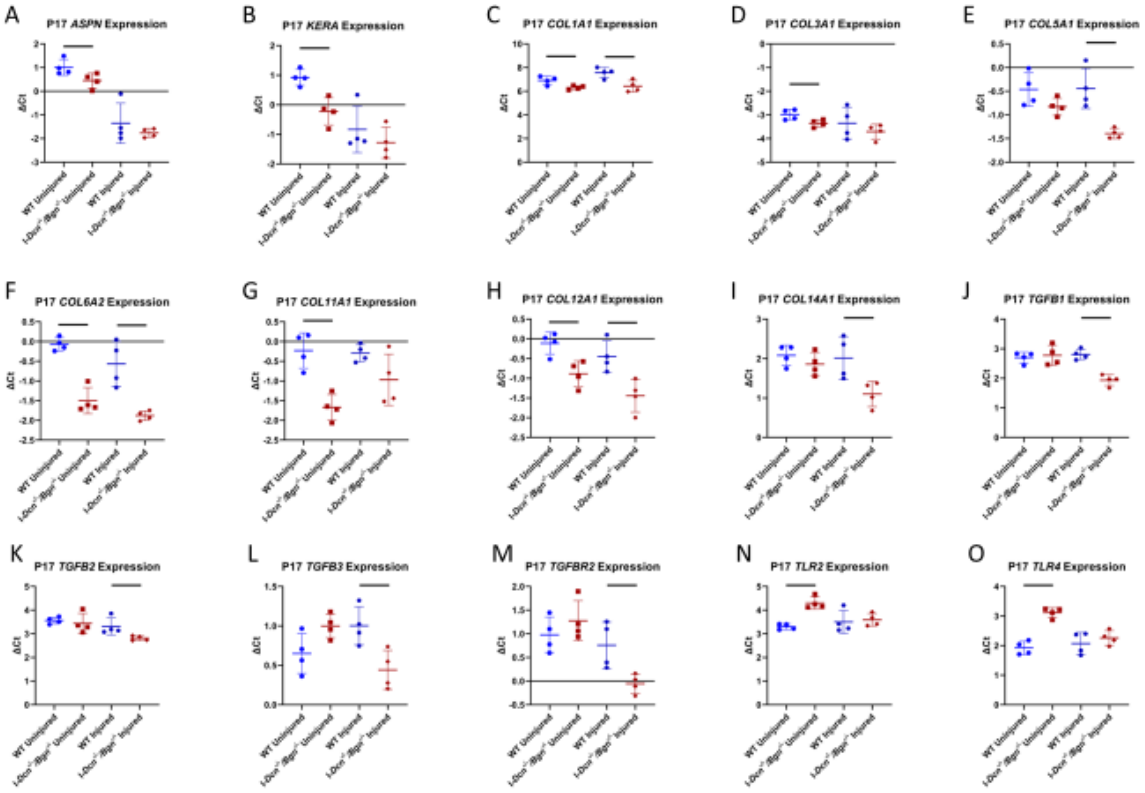

Figure 28. Differential Gene Expression of P17 Achilles Tendons. Analysis of Fluidigm data revealed alterations to gene expression in uninjured and injured P17 tendons. Increased expression of *Aspn* (A) and *Kera* (B) was observed in uninjured I-*Dcn*$^{-/-}$/*Bgn*$^{-/-}$ tendons. *Col1a1* (A), *Col6a2* (F), and *Col12a1* (H) expression increased in uninjured and injured tendons after decorin and biglycan knockdown. Uninjured I-*Dcn*$^{-/-}$/*Bgn*$^{-/-}$ tendons also had increased *Col3a1* (D) and *Col11a1* (G), while *TLR2* (N) and *TLR4* (O) expression was increased. *Col5a1* (E), *Col14a1* (I), *TGFB1* (J), *TGFB2* (K), *TGFB3* (L), and *TGFBR2* (M) expression was increased in the P17 injured I-*Dcn*$^{-/-}$/*Bgn*$^{-/-}$ tendons. Data shown as average with standard deviation.

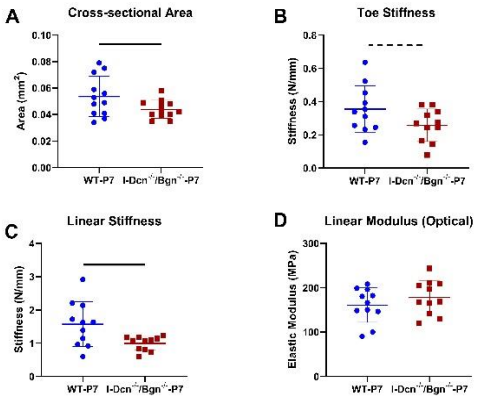

Figure 29. P7 Achilles Tendon Quasi-static Mechanics. Achilles tendon Quasi-static mechanics were measured during the ramp-to-failure in the mechanical testing protocol. I-*Dcn*$^{-/-}$/*Bgn*$^{-/-}$-P7 cross-sectional area (A) was reduced compared to WT-P7. A trending decrease was observed in toe stiffness (B) while linear stiffness was decreased (C). Linear modulus was not affected after knockdown (D). Data shown as average with standard deviation.

expression was downregulated in uninjured I-*Dcn*$^{-/-}$/*Bgn*$^{-/-}$ tendons, but there were no changes to *TLR2* or *TLR4* in injured I-*Dcn*$^{-/-}$/*Bgn*$^{-/-}$ tendons compared to WT (Fig. 28 N, O).

5.3.5 Decorin and biglycan deficiency produced neonatal tendons with decreased cross-sectional area and decreased stiffness

Knockdown of decorin and biglycan produced tendons with decreased cross-sectional area at P7, which was also accompanied by reduced linear stiffness and a trending decrease in toe stiffness compared to WT (Fig. 29 A-C). There were no changes to transition strain or linear modulus (Fig. 29 D), and no changes to tendon relaxation, dynamic modulus, or phase shift (Fig. 30 A-G).

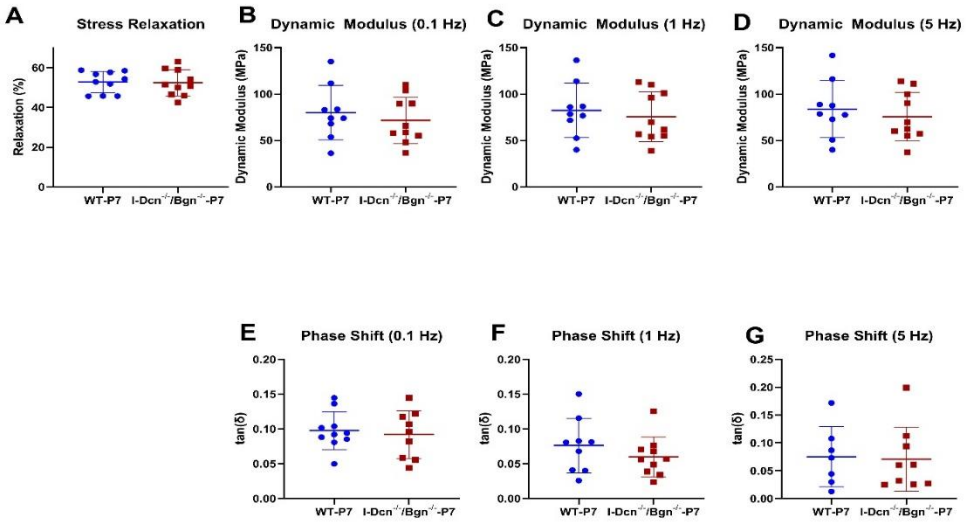

Figure 30. Viscoelastic Mechanics in P7 Achilles Tendons. Viscoelastic mechanics were obtained by performing a stress relaxation followed by a series of frequency sweeps. Knockdown of decorin and biglycan did affect stress relaxation (A), dynamic modulus (B-D), or phase shift (E-G) at 0.1, 1, or 5 Hz. Data shown as average with standard deviation.

5.3.6 Collagen Fiber Realignment Ended Prematurely In I-*Dcn*$^{-/-}$/*Bgn*$^{-/-}$-P7 Tendons

WT-P7 and I-*Dcn*$^{-/-}$/*Bgn*$^{-/-}$-P7 Achilles tendon collagen fiber realignment increased from 1% to 5%, 5% to 10%, and 10% to 15% strain (Fig. 31). However, only WT-P7 realignment increased between 15% to 20% strain, whereas collagen fiber realignment in Achilles tendons deficient in decorin and biglycan did not continue to realign at these higher strain levels.

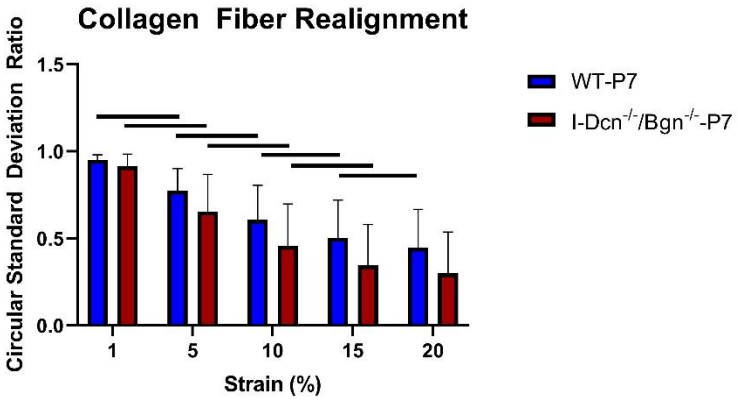

Figure 31. P7 Achilles Tendon Collagen Fiber Realignment. Collagen fiber realignment was measured during the ramp-to-failure and calculated at 1%, 5%, 10%, 15%, and 20% strain. WT-P7 collagen fiber realignment increased between 1%-5%, 5%-10%, 10%-15%, and 15%-20% strain. I-*Dcn*$^{-/-}$/*Bgn*$^{-/-}$-P7 fiber realignment increased between 1%-5%, 5%-10%, and 10%-15% strain. Data shown as average with standard deviation.

5.3.7 I-*Dcn*$^{-/-}$/*Bgn*$^{-/-}$-P7 Tendons Displayed a Substantial Decrease in Collagen Fibril Diameter

I-*Dcn*$^{-/-}$/*Bgn*$^{-/-}$-P7 Achilles tendon collagen fibril distributions displayed notable changes in diameter compared to the WT-P7 tendons. Both groups exhibited unimodal

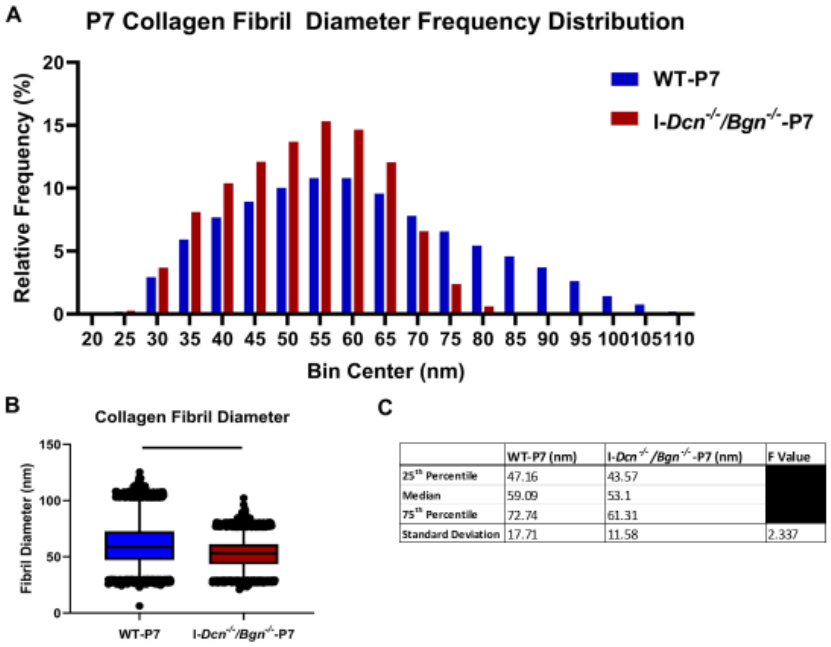

	WT-P7 (nm)	I-*Dcn*$^{-/-}$/*Bgn*$^{-/-}$-P7 (nm)	F Value
25th Percentile	47.16	43.57	
Median	59.09	53.1	
75th Percentile	72.74	61.31	
Standard Deviation	17.71	11.58	2.337

Figure 32. P7 Achilles Tendon Collagen Fibril Diameter. Collagen fibril diameter was measured using transmission electron microscopy from the tendon midsubstance. The collagen fibril diameter frequency distribution binned fibrils into 5 nm bins. The WT-P7 distribution shows an accumulation of large diameter fibrils, while I-*Dcn*$^{-/-}$/*Bgn*$^{-/-}$ tendons show a large population of small diameter fibrils with an absence of larger diameter fibrils (A). Comparisons between the groups confirmed a decrease in fibril diameter in the I-*Dcn*$^{-/-}$/*Bgn*$^{-/-}$ tendons (B). Breakdown of each group by quartile showed that I-*Dcn*$^{-/-}$/*Bgn*$^{-/-}$ collagen fibril diameter was lower at the first, second, and third quartiles (C).

collagen fibril diameter distributions (Fig. 32 A). Tendons deficient in decorin and biglycan revealed smaller diameter collagen fibrils (Fig. 32 B), decreased collagen fibril diameter variance, and a negatively skewed distribution relative to WT tendons (Figure 32 C). I-*Dcn*$^{-/-}$/*Bgn*$^{-/-}$-P7 collagen fibril diameter was reduced at the 25th (43.66 nm versus 46.85 nm), 50th (53.23 nm versus 58.58 nm), and 75th (61.41 nm versus 72.03 nm) percentiles compared to WT-P7 (Fig. 32 C).

5.3.8 Post-Injury Mechanics Were Impaired in Decorin and Biglycan Deficient Achilles

No changes in cross-sectional area (Fig. 33 A, B) or maximum stress (Fig. 33 I, J) were observed after knockdown of decorin and biglycan, while maximum force

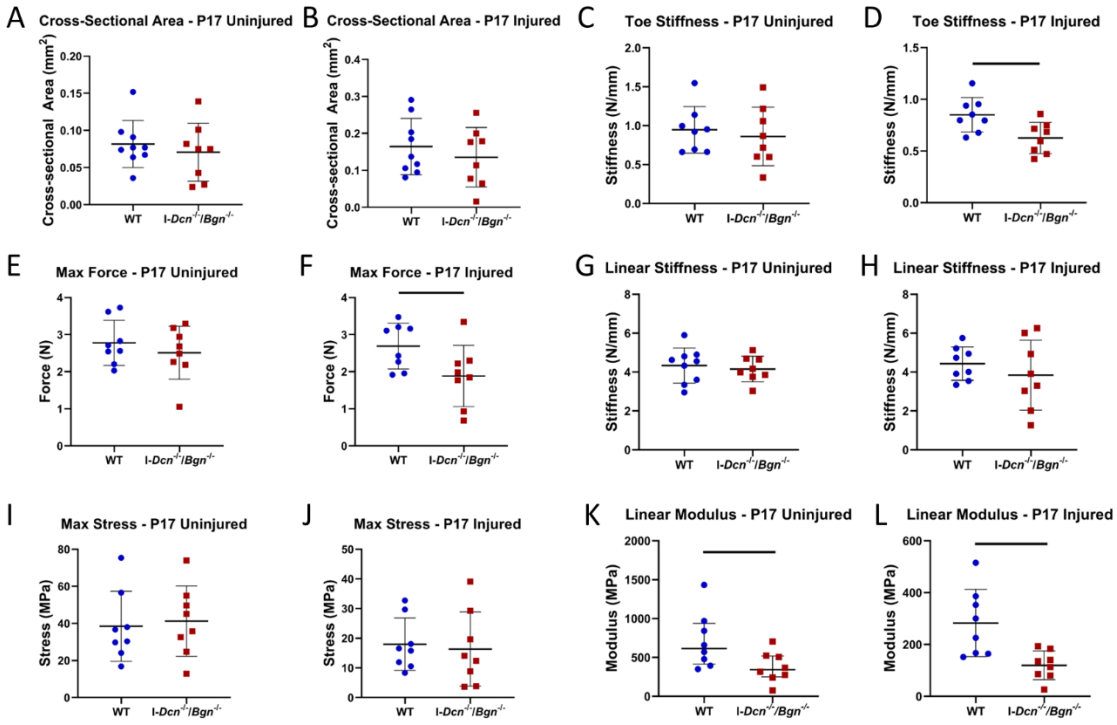

Figure 33. Quasi-static Mechanics of P17 Achilles Tendons. Quasi-static mechanics were obtained at the end of the mechanical testing protocol during the ramp-to-failure. Linear modulus decreased in the uninjured I-*Dcn*$^{-/-}$/*Bgn*$^{-/-}$-P17 tendons (K) with no changes to cross-sectional area (A), toe (C) or linear stiffness (G), maximum force (E) or maximum stress (I). Injured I-*Dcn*$^{-/-}$/*Bgn*$^{-/-}$-P17 tendons had a decreased toe stiffness (D), maximum force (F), and linear modulus (L). Data shown as average with standard deviation.

decreased in the injured I-*Dcn*$^{-/-}$/*Bgn*$^{-/-}$-P17 tendons (Fig. 33 F). Additionally, injury after decorin and biglycan knockdown decreased toe stiffness (Fig. 33 D) and linear modulus (Fig. 33 L), with linear modulus also decreasing in uninjured I-*Dcn*$^{-/-}$/*Bgn*$^{-/-}$-P17 tendons (Fig. 33 K). No changes in linear stiffness, stress relaxation, dynamic modulus, or phase shift were present between I-*Dcn*$^{-/-}$/*Bgn*$^{-/-}$-P17 and WT-17 tendons (Fig. 34).

5.3.9 Minimal Collagen Realignment Occurred in Injured I-*Dcn*$^{-/-}$/*Bgn*$^{-/-}$-P17 Achilles

Uninjured WT-17 and I-*Dcn*$^{-/-}$/*Bgn*$^{-/-}$-P17 tendon collagen realignment occurred from 1% to 5% strain and 5% to 10% strain. WT-17 tendon realignment peaked between 10% and 15% strain, with no additional realignment occurring between 15% and 20% strain (Fig. 35). In contrast, I-*Dcn*$^{-/-}$/*Bgn*$^{-/-}$-P17 tendon realignment did not increase

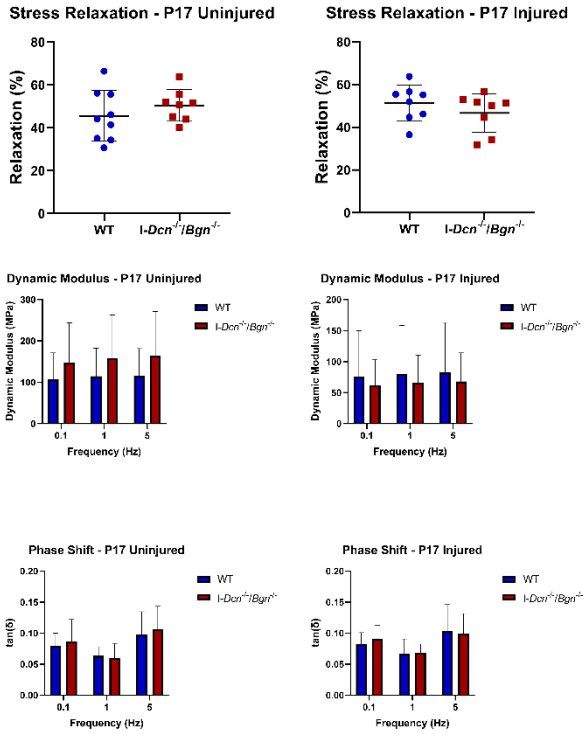

Figure 34. P17 Achilles Viscoelastic Mechanics.
Viscoelastic mechanics were obtained by performing a stress relaxation followed by a series of frequency sweeps. No changes in viscoelastic mechanics were found in uninjured or injured I-*Dcn*$^{-/-}$/*Bgn*$^{-/-}$-P17 tendons. Data shown as average with standard deviation.

between 10% to 15% strain, with increased realignment observed between 15% and 20% strain. Collagen fiber realignment of injured WT-17 and I-*Dcn*$^{-/-}$/*Bgn*$^{-/-}$-P17 tendons increased between 1% and 5% strain. The WT-17 group displayed continued realignment between 5% and 10% strain and 10% and 15% strain, whereas I-*Dcn*$^{-/-}$/*Bgn*$^{-/-}$-P17 realignment slowed considerably with no changes detected beyond 5% strain (Fig. 35).

5.3.10 I-*Dcn*$^{-/-}$/*Bgn*$^{-/-}$-P17 Achilles Tendons had a Large Population of Small Diameter Fibrils Post-Injury

Overall, the uninjured WT-P17 and I-*Dcn*$^{-/-}$/*Bgn*$^{-/-}$-P17 collagen fibril diameter distributions were broadly dispersed and with similar symmetry and skewness (Fig. 36). Collagen fibril diameter variance was reduced in decorin and biglycan deficient uninjured

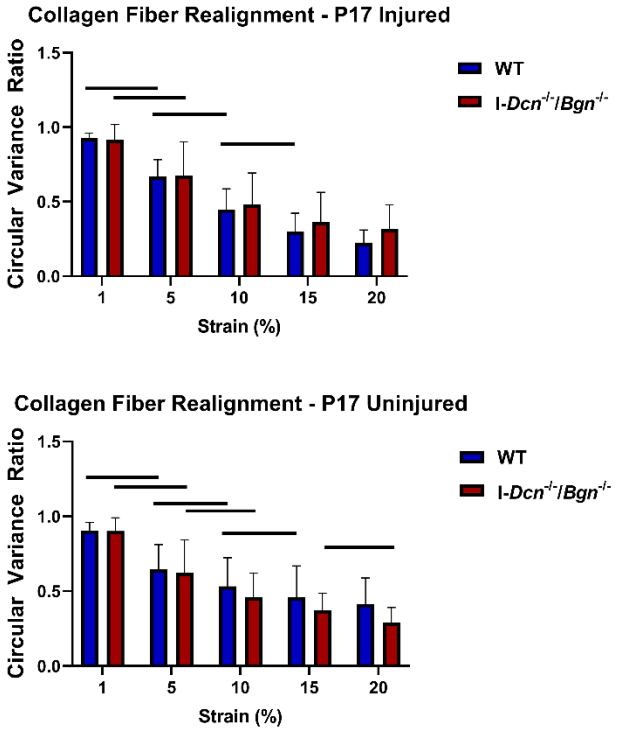

Figure 35. P17 Achilles Tendon Collagen Fiber Realignment. The P17 tendon collagen fiber realignment was observed during the ramp-to-failure and calculated at 1%, 5%, 10%, 15%, and 20% strains. Injured WT-P17 tendons between 1-5%, 5-10%, and 10-15% strains, while injured I-*Dcn*$^{-/-}$/*Bgn*$^{-/-}$-P17 tendons realigned between 1-5% strain. Realignment occurred in uninjured WT-P17 tendons between 1-5%, 5-10%, and 10-15% strains. Uninjured I-*Dcn*$^{-/-}$/*Bgn*$^{-/-}$-P17 tendon realignment occurred between 1-5%, 5-10%, and 15-20% strains. Data shown as average with standard deviation.

(Fig. 36 C) and injured tendons (Fig. 37 C). Uninjured I-*Dcn*$^{-/-}$/*Bgn*$^{-/-}$-P17 tendons revealed a lack of large diameter fibrils and collagen fibril diameter was decreased relative to WT-17. This was demonstrated by smaller diameters at the 25th (53.17 nm vs 55.55 nm), 50th (71.76 nm vs 75.77 nm) and 75th (88.73 nm vs 94.64 nm) percentiles (Fig. 36). Injured tendons revealed that knockdown of decorin and biglycan had a large impact on the re-establishment of tendon microstructure post-injury. The WT-17 and I-*Dcn*$^{-/-}$/*Bgn*$^{-/-}$-P17 fibril diameter distributions were both unimodal and right skewed, consisting of a large population of small diameter fibrils. However, the I-*Dcn*$^{-/-}$/*Bgn*$^{-/-}$-P17

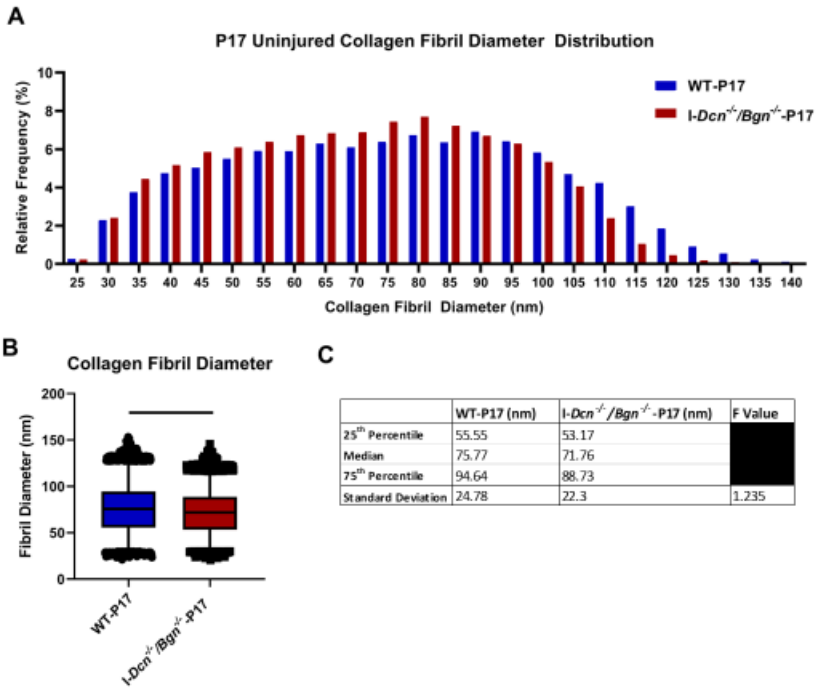

Figure 36. Uninjured P17 Tendon Collagen Fibril Diameter. Collagen fibril diameter was measured using transmission electron microscopy from the tendon midsubstance. The uninjured collagen fibril diameter frequency distributions showed similarly broad distributions (A) with a shift towards smaller diameter fibrils in the I-*Dcn*$^{-/-}$/*Bgn*$^{-/-}$-P17 group (B). Breakdown of the distributions by quartile revealed differences between the two groups are primarily among the large diameter fibrils (C). Data shown as average with standard deviation.

fibril population was highly concentrated, with greater than 50% possessing diameters between 30 and 45 nm, resulting in a reduction in fibril diameter compared to WT-P17 tendons. These reductions after decorin and biglycan knockdown were observed across the 25th, 50th, and 75th percentiles (Fig 37).

5.3.11 Histological analyses revealed no changes after knockdown of decorin and biglycan

No differences in cellularity or nuclear aspect ratio were observed in P7 (Fig. 38 A, B) or P17 I-*Dcn*$^{-/-}$/*Bgn*$^{-/-}$ tendons (Fig. 38 D, E, G, H). Toluidine blue staining was also unchanged in decorin and biglycan deficient tendons at P7 and P17 timepoints (Fig 38 C, F, I).

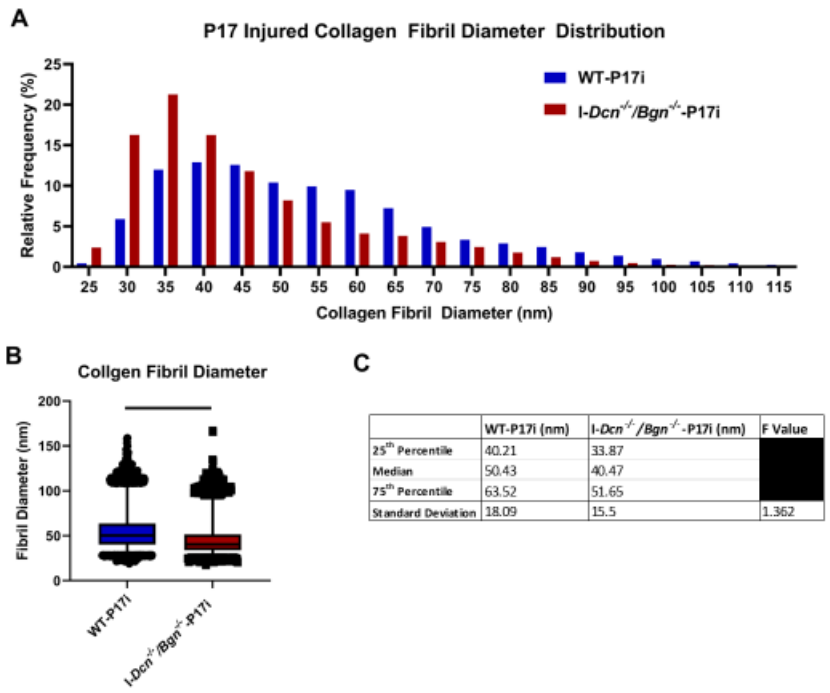

Figure 37. Injured P17 Tendon Collagen Fibril Diameter. Collagen fibril diameter was measured using transmission electron microscopy from the tendon midsubstance. The uninjured collagen fibril diameter frequency distributions showed similarly broad distributions (A) with a shift towards smaller diameter fibrils in the I-*Dcn*$^{-/-}$/*Bgn*$^{-/-}$-P17 group (B). Breakdown of the distributions by quartile revealed differences between the two groups are primarily among the large diameter fibrils (C). Data shown as average with standard deviation.

5.4 Discussion

The objectives of this study were to explore the effects of decorin and biglycan deficiency on (1) neonatal development of tendon structural and mechanical properties and (2) the healing response of Achilles tendon in the neonate. To achieve these objectives, we used a TM-inducible compound *Dcn/Bgn* mouse knockdown model. This model allows the mice to undergo normal development up until TM treatment, isolating the effects of decorin and biglycan knockdown to the desired experimental timeline. We hypothesized (1) that knockdown of decorin and biglycan at postnatal day 0 would disrupt neonatal tendon development and produce tendons with decreased quasi-static and viscoelastic mechanical properties, altered collagen fiber realignment, and an

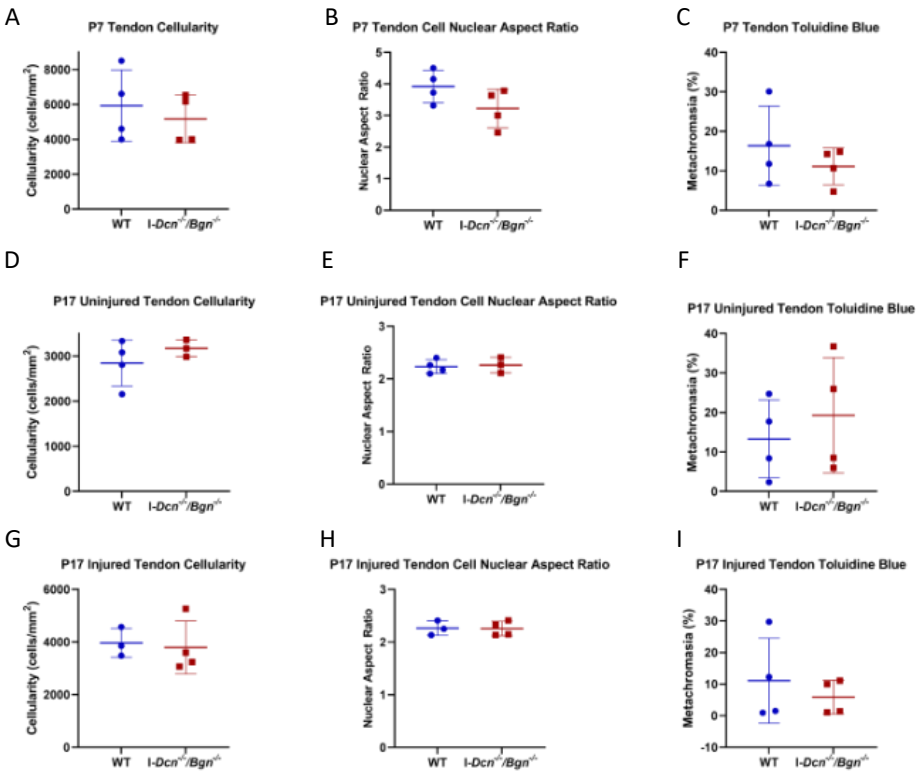

Figure 38. Histological Analysis of Neonatal Achilles Tendon. No changes were observed in cellularity or nuclear aspect ratio after knockdown of decorin and biglycan at P7 (A, B) or P17 in uninjured (D, E) or injured (G, H) tendons. Likewise, toluidine blue staining was unchanged in I-*Dcn*$^{-/-}$/*Bgn*$^{-/-}$ tendons at P7 (C) and in both P17 group comparisons (F, I). Data shown as average with standard deviation.

altered tendon collagen fibril diameter distribution compared to WT Achilles tendons. Additionally, we hypothesized (2) that knockdown of decorin and biglycan at postnatal day 7, at the time of Achilles tendon injury, would impair the neonatal healing response by disrupting collagen fibril formation, leading to tendons with impaired mechanics, reduced collagen fiber realignment, and altered collagen fibril diameter distributions with a high population of small diameter fibrils. In support of our first hypothesis, I-*Dcn*$^{-/-}$/*Bgn*$^{-/-}$ -P7 Achilles tendons revealed reduced CSA and stiffness, early cessation of collagen fiber realignment during tensile loading, and a unimodal collagen fibril distribution consisting of small to medium diameter fibrils. The results indicated that the second hypothesis was also supported; knockdown of decorin and biglycan disrupted the

neonatal healing response. I-*Dcn*$^{-/-}$/*Bgn*$^{-/-}$-P17 injured Achilles tendons had a decreased maximum force, toe stiffness, and linear modulus, altered collagen fiber realignment dynamics, and a collagen fibril distribution with a disproportionately large number of small fibrils compared to WT-P17 tendons.

Effective knockdown of *Dcn* and *Bgn* was demonstrated for all three I-*Dcn*$^{flox/flox}$/*Bgn*$^{flox/flox}$ experimental groups. PCA revealed that the greatest separation between P7 WT and I-*Dcn*$^{-/-}$/*Bgn*$^{-/-}$ Achilles tendons occurred in PC3, where *Dcn* and *Bgn* were 2 of the top 3 variables that contributed to this PC. While P7 I-*Dcn*$^{-/-}$/*Bgn*$^{-/-}$ tendons only had changes to 3 individual genes, *Axin2*, *Prg4*, *and Col12a1*, these genes were also among the top contributors to PC3.

Axin2 was the top variable that contributed to PC3 in P7 tendons, and expression was increased after knockdown of *Dcn* and *Bgn*. *Axin2* is a Wnt target gene, and previous work indicates that Wnt signaling may play a role in tendon cell proliferation and differentiation, with evidence also suggesting that Axin2-lineage cells are one of the sources of cells that contribute to the neonatal regenerative repair response in tendon.[42] Biglycan has demonstrated the ability to modulate Wnt signaling via binding of the biglycan proteoglycan and core protein to Wnt3a, resulting in enhanced Wnt-induced transcriptional activity.[43] Given the ability for biglycan to modulate Wnt signaling and the suggested role of biglycan as a regulator of tendon stem/progenitor cell fate[44], additional work should examine the interactions between biglycan and Wnt signaling during neonatal tendon development and the subsequent effects on cells that contribute to neonatal tendon development and regeneration, such as TSPCs and Axin2-lineage cells.

After confirmation of *Dcn* and *Bgn* knockdown, expression of *Fmod, Lum, Kera,* and *Aspn* was measured due to the structural and functional similarities of these SLRPs with *Dcn* and *Bgn*.[45–47] No changes to SLRP expression were found in P7 or injured P17 tendons after knockdown of *Dcn* and *Bgn*. Upregulation of *Kera* and *Aspn* was present in uninjured P17 I-$Dcn^{-/-}/Bgn^{-/-}$ tendons, indicating that the effects from the knockdown model may be partially masked in this group due to the ability of *Kera* and *Aspn* to regulate fibrillogenesis via collagen binding and the overlap in signaling pathways.[48–50] Overall, the neonatal I-$Dcn^{flox/flox}/Bgn^{flox/flox}$ mouse model demonstrated knockdown of the target genes with minimal upregulation of class I and II SLRPs.

Dcn and *Bgn* deficient tendons showed extensive alterations to collagen expression at P17 with relatively minor changes present at P7. *Col1a1* and *Col6a2* expression increased after knockdown of *Dcn* and *Bgn* in uninjured and injured P17 tendons, with upregulation of *Col1a1* indicating an increase in overall ECM production, and upregulation of *Col6a2* potentially indicating disruption of the neonatal developmental and healing responses. Evidence suggests type VI collagen plays a vital role in neonatal tendon growth, demonstrated by continued expression during neonatal development and an increased number of small diameter collagen fibrils in collagen VI knockout mice.[51,52] Collagen VI is also co-expressed and co-localized with biglycan, and evidence suggests that both of these molecules are necessary for the formation of the pericellular matrix, which facilitates mechanotransduction and proper cell function.[14] Elevated expression of *Col6a2* in the presence of an increased number of small diameter collagen fibrils may indicate that the role of collagen VI in tendon growth and healing may be dependent on the co-localization of biglycan for regulation of fibrillogenesis.

Changes to *Col12a1* were present across all groups; *Col12a1* was downregulated at P7 and upregulated in both P17 groups. Additionally, *Col14a1* was upregulated in injured P17 tendons. Collagen types XII and XIV act as bridging molecules between type I collagen fibrils or between type I collagen and additional ECM components.[53–55] Type XII collagen has been suggested to play an important role in tendon formation by organizing and maintaining tendon tissue architecture, while type XIV collagen is thought to modulate collagen fibrillogenesis. Thus, changes to *Col12a1* and *Col14a1* expression offer a potential mechanism for structural and mechanical changes observed in this study.

Decorin- and biglycan-mediated regulation of inflammatory processes were also impacted in P17 I-*Dcn*$^{-/-}$/*Bgn*$^{-/-}$ mice. Decorin and biglycan are able to act as damage-associated molecular patterns (DAMPs) following release from the ECM after injury, modulating activation of pro-inflammatory receptors such as toll-like receptor (TLRs) and transforming growth factor beta (TGF-β) receptors.[30] TLR2 and TLR4 expression was reduced in uninjured P17 I-*Dcn*$^{-/-}$/*Bgn*$^{-/-}$ tendons, but no change was found in P17 injured tendons. This suggests that decorin and biglycan may not be necessary for activation of TLR2 and TLR4 after injury. Injured P17 I-*Dcn*$^{-/-}$/*Bgn*$^{-/-}$ tendon expression of TGF-β1/2/3 and TGF-β receptor 2 (TGFBR2) was increased, indicating vital roles for decorin and biglycan in the modulation of TGF-β activity after injury in the neonate.

The changes in collagen fibril diameter at P7 were striking, with decorin and biglycan deficiency producing many small diameter fibrils and an absence of larger diameter fibrils, which should be accumulating by P7.[56] I-*Dcn*$^{-/-}$/*Bgn*$^{-/-}$-P17 tendons revealed similar outcomes, although the deviation from WT-P17 was most striking in the injured tendons. Knockdown of decorin and biglycan also reduced collagen fibril diameter variance

across all groups, which is indicative of a reduction in fibril diameter heterogeneity and supports previous observations that decorin and biglycan are regulators of lateral growth of collagen fibrils. The impact of decorin and biglycan knockdown on tendon microstructure were reflected in the tendon mechanics. WT-P7 tendons showed a steady increase in collagen realignment throughout the toe and linear regions, while I-*Dcn*$^{-/-}$/*Bgn*$^{-/-}$-P7 realignment occurred rapidly in the toe region, before peaking in the linear region at 15% strain. Injured I-*Dcn*$^{-/-}$/*Bgn*$^{-/-}$-P17 tendon realignment also showed an early peak at 5% strain before slowing at higher strains while having a high population of small collagen fibrils present. The immature collagen fibril structures observed in the I-*Dcn*$^{-/-}$/*Bgn*$^{-/-}$-P7 and injured I-*Dcn*$^{-/-}$/*Bgn*$^{-/-}$-P17 tendons are the likely early peaks in collagen fiber realignment compared to their respective WT controls, since developmental age and underlying ECM fibril structure is thought to influence tendon realignment.[57]

Additionally, the effect of decorin and biglycan knockdown on the underlying collagen fibril structure impacted tendon mechanics, which were negatively influenced in regardless of age or state of injury. I-*Dcn*$^{-/-}$/*Bgn*$^{-/-}$-P7 tendon cross-sectional area was reduced when the neonate is undergoing rapid growth and increasing ambulation.[6,58] Linear stiffness and toe stiffness were also reduced, while linear modulus was unchanged. While neonates are growing rapidly at P7, ambulation is still relatively low, so the effect of the immature collagen fibril structure may have a larger impact on material properties with increased mechanical loading and a longer developmental timeline. I-*Dcn*$^{-/-}$/*Bgn*$^{-/-}$-P17 linear modulus was decreased in both injured and uninjured tendons, indicating that the reduced modulus in the injured tendon is partially due to knockdown of decorin and biglycan and not necessarily indicative of an impaired healing

response. Interestingly, viscoelastic mechanics were unaffected by decorin and biglycan knockdown regardless of age or injury. Previous studies using SLRP knockdown models commonly reported viscoelastic mechanics being more sensitive to the impact of SLRP deficiency on tendon mechanics than quasi-static mechanics.[17,20,59] Previous studies using the I-*Dcn*$^{-/-}$/*Bgn*$^{-/-}$ model in mature and aged mice showed few changes to tendon quasi-static mechanics and, especially in aged mice, drastically altered viscoelastic mechanics, making the lack of changes to viscoelastic mechanics in this study particularly surprising.[22,49]

This study is not without limitations. Gene expression was measured 7 and 10 days after knockdown. While expression data suggests sufficient knockdown of *Dcn* and *Bgn* occurred, no protein measurements were used to further validate the expression results. Additionally, both *Dcn* and *Bgn* were knocked down in the experimental group, thus this study is unable to differentiate between the roles of decorin and biglycan during neonatal development. Future studies will utilize single knockdown models to explore the individual roles of decorin and biglycan during neonatal tendon development. No data was collected measuring gait or ground reaction forces throughout neonatal development. Measuring these outcomes would help inform if changes to tendon structure and mechanics manifest in joint function and will be included in future work. Finally, additional timepoints to study the effects on development and healing on a longer timeline would provide greater insight on the impacts of decorin and biglycan knockdown in the neonate.

Overall, this study demonstrated that decorin and biglycan deficiency negatively impacted neonatal development and the neonatal healing response. P7 and injured neonatal tendons had large populations of small diameter fibrils, indicating that decorin

and biglycan are vital to fibrillogenesis in these contexts. The small diameter fibrils likely caused the negatively impacted collagen fiber realignment and quasi-static mechanics. This study provided a better understanding of the roles of decorin and biglycan in the Achilles tendon after injury and during neonatal development. Establishing a better understanding of these processes can help inform future therapeutics for tendon injury and aging.

5.5 References

1. Lantto I, Heikkinen J, Flinkkilä T, et al. 2015. Epidemiology of Achilles tendon ruptures: Increasing incidence over a 33-year period. Scand. J. Med. Sci. Sport. 25(1):e133–e138 [cited 2020 Nov 10] Available from: https://pubmed.ncbi.nlm.nih.gov/24862178/.

2. Clayton RAE, Court-Brown CM. 2008. The epidemiology of musculoskeletal tendinous and ligamentous injuries. Injury 39(12):1338–1344.

3. BMUS. 2014. United States Bone and Joint Initiative: The Burden of Musculoskeletal Diseases in the United States, Third Edit. Rosemont, IL.

4. AAOS. 2009. The Diagnosis and Treatment of Achilles Tendon Rupture: Guideline and evidence report.

5. Zhang G, Young BB, Ezura Y, et al. 2005. Development of tendon structure and function: Regulation of collagen fibrillogenesis. J. Musculoskelet. Neuronal Interact. 5(1):5–21 [cited 2017 Aug 10] Available from: https://pubmed.ncbi.nlm.nih.gov/15788867/.

6. Ansorge HL, Adams SM, Birk DE, Soslowsky LJ. 2011. Mechanical, compositional and structural properties of the post-natal mouse Achilles tendon. Ann. Biomed. Eng. 39(7):1904–1913 [cited 2016 May 17] Available from: http://www.ncbi.nlm.nih.gov/pubmed/21431455.

7. Parry DAD, Barnes GRG, Craig AS. 1978. A comparison of the size distribution of collagen fibrils in connective tissues as a function of age and a possible relation between fibril size distribution and mechanical properties. Proc. R. Soc. London -

Biol. Sci. 203(1152):305–321 [cited 2020 Dec 17] Available from: https://pubmed.ncbi.nlm.nih.gov/33395/.

8. Moore MJ, De Beaux A. 1987. A quantitative ultrastructural study of rat tendon from birth to maturity. J. Anat. 153:163–9 [cited 2020 Dec 20] Available from: http://www.ncbi.nlm.nih.gov/pubmed/3429315.

9. Zhang G, Ezura Y, Chervoneva I, et al. 2006. Decorin regulates assembly of collagen fibrils and acquisition of biomechanical properties during tendon development. J. Cell. Biochem. 98(6):1436–1449 [cited 2017 Aug 10] Available from: http://doi.wiley.com/10.1002/jcb.20776.

10. Ansorge HL, Hsu JE, Edelstein L, et al. 2012. Recapitulation of the achilles tendon mechanical properties during neonatal development: A study of differential healing during two stages of development in a mouse model. J. Orthop. Res. 30(3):448–56 [cited 2016 May 17] Available from: http://www.ncbi.nlm.nih.gov/pubmed/22267191.

11. Howell K, Chien C, Bell R, et al. 2017. Novel Model of Tendon Regeneration Reveals Distinct Cell Mechanisms Underlying Regenerative and Fibrotic Tendon Healing. Sci. Rep. 7:45238 [cited 2017 Apr 27] Available from: http://www.nature.com/articles/srep45238.

12. Iozzo R V. 1999. The biology of the small leucine-rich proteoglycans. Functional network of interactive proteins. J. Biol. Chem. 274(27):18843–18846 [cited 2016 Aug 31] Available from: http://www.jbc.org/cgi/doi/10.1074/jbc.274.27.18843.

13. Corsi A, Xu T, Chen XD, et al. 2002. Phenotypic effects of biglycan deficiency are

linked to collagen fibril abnormalities, are synergized by decorin deficiency, and mimic Ehlers-Danlos-like changes in bone and other connective tissues. J. Bone Miner. Res. 17(7):1180–1189.

14. Leiphart RJ, Pham H, Harvey T, et al. 2022. Coordinate roles for collagen VI and biglycan in regulating tendon collagen fibril structure and function. Matrix Biol. Plus 13(11):100099 Available from: https://doi.org/10.1016/j.mbplus.2021.100099.

15. Robinson PS, Huang T-F, Kazam E, et al. 2005. Influence of Decorin and Biglycan on Mechanical Properties of Multiple Tendons in Knockout Mice. J. Biomech. Eng. 127(1):181 Available from: http://biomechanical.asmedigitalcollection.asme.org/article.aspx?articleid=1413750.

16. Robinson PS, Lin TW, Reynolds PR, et al. 2004. Strain-rate sensitive mechanical properties of tendon fascicles from mice with genetically engineered alterations in collagen and decorin. J. Biomech. Eng. 126(2):252–257 [cited 2016 Nov 23] Available from: http://biomechanical.asmedigitalcollection.asme.org/article.aspx?articleid=1411613.

17. Dourte LM, Pathmanathan L, Jawad AF, et al. 2012. Influence of decorin on the mechanical, compositional, and structural properties of the mouse patellar tendon. J. Biomech. Eng. 134(3):031005 [cited 2016 Jul 18] Available from: http://www.ncbi.nlm.nih.gov/pubmed/22482685.

18. Dourte LM, Pathmanathan L, Mienaltowski MJ, et al. 2013. Mechanical, compositional, and structural properties of the mouse patellar tendon with

changes in biglycan gene expression. J. Orthop. Res. 31(9):1430–1437 [cited 2017 Aug 10] Available from: http://www.ncbi.nlm.nih.gov/pubmed/23592048.

19. Dunkman AA, Buckley MR, Mienaltowski MJ, et al. 2014. The injury response of aged tendons in the absence of biglycan and decorin. Matrix Biol. 35:232–238 [cited 2016 Jul 13] Available from: http://www.ncbi.nlm.nih.gov/pubmed/24157578.

20. Dunkman AA, Buckley MR, Mienaltowski MJ, et al. 2013. Decorin expression is important for age-related changes in tendon structure and mechanical properties. Matrix Biol. 32(1):3–13 [cited 2016 Aug 26] Available from: http://www.ncbi.nlm.nih.gov/pubmed/23178232.

21. Connizzo BK, Sarver JJ, Birk DE, et al. 2013. Effect of age and proteoglycan deficiency on collagen fiber re-alignment and mechanical properties in mouse supraspinatus tendon. J. Biomech. Eng. 135(2):021019 [cited 2017 May 30] Available from: http://www.ncbi.nlm.nih.gov/pubmed/23445064.

22. Robinson KA, Sun M, Barnum CE, et al. 2017. Decorin and biglycan are necessary for maintaining collagen fibril structure, fiber realignment, and mechanical properties of mature tendons. Matrix Biol. [cited 2017 Sep 25] Available from: http://www.sciencedirect.com/science/article/pii/S0945053X17301063?via%3Dihub.

23. Beach ZM, Bonilla KA, Dekhne MS, et al. 2022. Biglycan has a major role in maintenance of mature tendon mechanics. J. Orthop. Res. (September 2021):1–11.

24. Anders H-J, Schaefer L. 2014. Beyond tissue injury-damage-associated molecular patterns, toll-like receptors, and inflammasomes also drive regeneration and fibrosis. J. Am. Soc. Nephrol. 25(7):1387–400 [cited 2018 Jun 5] Available from: http://www.ncbi.nlm.nih.gov/pubmed/24762401.

25. Babelova A, Moreth K, Tsalastra-Greul W, et al. 2009. Biglycan, a danger signal that activates the NLRP3 inflammasome via toll-like and P2X receptors. J. Biol. Chem. 284(36):24035–24048.

26. Nastase M V., Young MF, Schaefer L. 2012. Biglycan: A Multivalent Proteoglycan Providing Structure and Signals. J. Histochem. Cytochem. 60(12):963–975.

27. Bi Y, Ehirchiou D, Kilts TM, et al. 2007. Identification of tendon stem/progenitor cells and the role of the extracellular matrix in their niche. Nat. Med. 13(10):1219–1227.

28. Hildebrand A, Romaris M, Rasmussen LM, et al. 1994. Interaction of the small interstitial proteoglycans biglycan, decorin and fibromodulin with transforming growth factor β. Biochem. J. 302(2):527–534 [cited 2021 Dec 11] Available from: /pmc/articles/PMC1137259/?report=abstract.

29. Abbah SA, Thomas D, Browne S, et al. 2016. Co-transfection of decorin and interleukin-10 modulates pro- fibrotic extracellular matrix gene expression in human tenocyte culture. Nat. Publ. Gr. 6(November 2015):1–9 [cited 2018 Jun 14] Available from: http://www.ncbi.nlm.nih.gov/pubmed/26860065.

30. Moreth K, Iozzo R V., Schaefer L. 2012. Small leucine-rich proteoglycans orchestrate receptor crosstalk during inflammation. Cell Cycle 11(11):2084–2091.

31. Leiphart RJ, Shetye SS, Weiss SN, et al. 2020. Induced Knockdown of Decorin, Alone and in Tandem With Biglycan Knockdown, Directly Increases Aged Murine Patellar Tendon Viscoelastic Properties. J. Biomech. Eng. 142(11) Available from: https://asmedigitalcollection.asme.org/biomechanical/article/doi/10.1115/1.4048030/1086080/Induced-Knockdown-of-Decorin-Alone-and-in-Tandem.

32. Peltz CD, Perry SM, Getz CL, Soslowsky LJ. 2009. Mechanical properties of the long-head of the biceps tendon are altered in the presence of rotator cuff tears in a rat model. J. Orthop. Res. 27(3):416–420 [cited 2016 May 18] Available from: http://www.ncbi.nlm.nih.gov/pubmed/18924143.

33. Lake SP, Miller KS, Elliott DM, Soslowsky LJ. 2009. Effect of fiber distribution and realignment on the nonlinear and inhomogeneous mechanical properties of human supraspinatus tendon under longitudinal tensile loading. J. Orthop. Res. 27(12):1596–1602 [cited 2016 May 31] Available from: http://www.ncbi.nlm.nih.gov/pubmed/19544524.

34. Birk DE, Trelstad RL. 1986. Extracellular compartments in tendon morphogenesis: Collagen fibril, bundle, and macroaggregate formation. J. Cell Biol. 103(1):231–240 [cited 2017 Aug 10] Available from: http://www.ncbi.nlm.nih.gov/pubmed/3722266.

35. Birk DE, Zycband EI, Woodruff S, et al. 1997. Collagen fibrillogenesis in situ: Fibril segments become long fibrils as the developing tendon matures. Dev. Dyn. 208(3):291–298 [cited 2016 May 31] Available from: http://doi.wiley.com/10.1002/%28SICI%291097-0177%28199703%29208%3A3%3C291%3A%3AAID-AJA1%3E3.0.CO%3B2-D.

36. Ushiku C, Adams DJ, Jiang X, et al. 2010. Long bone fracture repair in mice harboring GFP reporters for cells within the osteoblastic lineage. J. Orthop. Res. 28(10):1338–1347 [cited 2022 May 31] Available from: https://onlinelibrary.wiley.com/doi/full/10.1002/jor.21105.

37. Schindelin J, Arganda-Carreras I, Frise E, et al. 2012. Fiji: an open-source platform for biological-image analysis. Nat. Methods 9(7):676–682 Available from: http://www.nature.com/articles/nmeth.2019.

38. Pedregosa F, Varoquaux G, Gramfort A, et al. 2011. Scikit-learn: Machine Learning in {P}ython. J. Mach. Learn. Res. 12:2825–2830 Available from: http://www.jmlr.org/papers/volume12/pedregosa11a/pedregosa11a.pdf.

39. Harris CR, Millman KJ, van der Walt SJ, et al. 2020. Array programming with NumPy. Nature 585(7825):357–362 Available from: https://www.nature.com/articles/s41586-020-2649-2.

40. McKinney W. 2010. Data Structures for Statistical Computing in Python. p 56–61 Available from: https://conference.scipy.org/proceedings/scipy2010/mckinney.html.

41. Hunter JD. 2007. Matplotlib: A 2D graphics environment. Comput. Sci. \& Eng. 9(3):90–95.

42. Walia B, Li TM, Crosio G, et al. 2022. Axin2-lineage cells contribute to neonatal tendon regeneration. Connect. Tissue Res. :1–14 [cited 2022 Mar 6] Available from: https://pubmed.ncbi.nlm.nih.gov/35180018/.

43. Berendsen AD, Fisher LW, Kilts TM, et al. 2011. Modulation of canonical Wnt

signaling by the extracellular matrix component biglycan. Proc. Natl. Acad. Sci. 108(41):17022–17027 Available from: http://www.pnas.org/cgi/doi/10.1073/pnas.1110629108.

44. Bi Y, Ehirchiou D, Kilts TM, et al. 2007. Identification of tendon stem/progenitor cells and the role of the extracellular matrix in their niche. Nat. Med. 13(10):1219–1227 [cited 2017 Oct 4] Available from: http://www.nature.com/doifinder/10.1038/nm1630.

45. Heinegård D. 2009. Proteoglycans and more - From molecules to biology. Int. J. Exp. Pathol. 90(6):575–586.

46. Lorenzo P, Aspberg A, Önnerfjord P, et al. 2001. Identification and Characterization of Asporin: A NOVEL MEMBER OF THE LEUCINE-RICH REPEAT PROTEIN FAMILY CLOSELY RELATED TO DECORIN AND BIGLYCAN. J. Biol. Chem. 276(15):12201–12211.

47. Iozzo R V., Schaefer L. 2015. Proteoglycan form and function: A comprehensive nomenclature of proteoglycans. Matrix Biol. 42:11–55 [cited 2017 Aug 24] Available from: http://linkinghub.elsevier.com/retrieve/pii/S0945053X15000402.

48. Kalamajski S, Aspberg A, Lindblom K, et al. 2009. Asporin competes with decorin for collagen binding, binds calcium and promotes osteoblast collagen mineralization. Biochem. J. 423(1):53–59 [cited 2018 Apr 25] Available from: http://www.ncbi.nlm.nih.gov/pubmed/19589127.

49. Beach ZM, Dekhne MS, Rodriguez AB, et al. 2022. Decorin knockdown is beneficial for aged tendons in the presence of biglycan expression. Matrix Biol.

Plus 15:100114 Available from: https://doi.org/10.1016/j.mbplus.2022.100114.

50. Rees SG, Waggett AD, Kerr BC, et al. 2009. Immunolocalisation and expression of keratocan in tendon. Osteoarthr. Cartil. 17(2):276–279 Available from: http://dx.doi.org/10.1016/j.joca.2008.07.007.

51. Izu Y, Ansorge HL, Zhang G, et al. 2011. Dysfunctional tendon collagen fibrillogenesis in collagen VI null mice. Matrix Biol. 30(1):53–61 [cited 2017 Oct 20] Available from: http://dx.doi.org/10.1016/j.matbio.2010.10.001.

52. Banos CC, Thomas AH, Kuo CK. 2008. Collagen fibrillogenesis in tendon development: current models and regulation of fibril assembly. Birth Defects Res. C. Embryo Today 84(3):228–244 [cited 2023 Jan 14] Available from: https://pubmed.ncbi.nlm.nih.gov/18773462/.

53. Young BB, Zhang G, Koch M, Birk DE. 2002. The roles of types XII and XIV collagen in fibrillogenesis and matrix assembly in the developing cornea. J. Cell. Biochem. 87(2):208–220.

54. Zhang G, Young BB, Birk DE. 2003. Differential expression of type XII collagen in developing chicken metatarsal tendons. J. Anat. 202(5):411–420 [cited 2020 Dec 16] Available from: https://pubmed.ncbi.nlm.nih.gov/12739618/.

55. Young BB, Gordon MK, Birk DE. 2000. Expression of type XIV collagen in developing chicken tendons: Association with assembly and growth of collagen fibrils. Dev. Dyn. 217(4):430–439 [cited 2020 Dec 16] Available from: https://pubmed.ncbi.nlm.nih.gov/10767087/.

56. Ansorge HL, Adams S, Jawad AF, et al. 2012. Mechanical property changes

during neonatal development and healing using a multiple regression model. J. Biomech. 45(7):1288–1292 [cited 2016 May 17] Available from: http://www.ncbi.nlm.nih.gov/pubmed/22381737.

57. Miller KS, Connizzo BK, Soslowsky LJ. [date unknown]. Collagen Fiber Re-Alignment in a Neonatal Developmental Mouse Supraspinatus Tendon Model.

58. McBride DJ, Trelstad RL, Silver FH. 1988. Structural and mechanical assessment of developing chick tendon. Int. J. Biol. Macromol. 10(4):194–200.

59. Dunkman AA, Buckley MR, Mienaltowski MJ, et al. 2014. The tendon injury response is influenced by decorin and biglycan. Ann. Biomed. Eng. 42(3):619–630 [cited 2016 Jul 13] Available from: http://www.ncbi.nlm.nih.gov/pubmed/24072490.

CHAPTER 6: CONCLUSIONS AND FUTURE DIRECTIONS

6.1 Introduction

This dissertation explored the regulatory roles of decorin and biglycan in tendon throughout multiple stages of life: establishment and recovery of tendon properties during neonatal development and healing, maintenance of tendon biomechanics in mature adults, and modulation of age-related decline in tendon mechanics. These studies were done using tamoxifen-inducible mouse models that give temporal control over decorin and biglycan expression, allowing the impact of knockdown to be isolated to the desired experimental timeline. The impact of the use of tamoxifen on tendon healing was also determined to provide important context to researchers who want to apply this model to studies involving injured tissue. This chapter will discuss conclusions from each study and future directions for this work.

6.2 Chapter II Conclusions

A growing interest in the mechanisms that govern tendon healing has resulted in the increased use of the tamoxifen-inducible mouse knockdown model to address these questions. However, tamoxifen is a selective estrogen receptor modulator and may interfere with the tendon healing process. The objective of this study was to evaluate the effects of tamoxifen on post-injury tendon mechanics in wild-type mice.

The mice received treatment just before surgery, which would induce an acute patellar tendon injury before the tendons were evaluated three weeks post-injury. Three experimental groups were established based on the treatment they received: tamoxifen suspended in corn oil, corn oil, and no treatment.

Mechanical testing of the tendons post-injury revealed no changes to viscoelastic mechanics, quasi-static mechanics, or collagen realignment after tamoxifen treatment. Additionally, histological analysis revealed no changes to cellularity or nuclear shape. Overall, this study revealed that tamoxifen treatment at the time of tendon injury did not result in changes to tendon mechanics at three weeks post-injury.

6.3 Chapter III Conclusions

Decorin and biglycan are two small leucine-rich proteoglycans (SLRPs) that regulate collagen fibrillogenesis and extracellular matrix assembly in tendon. Previous studies have explored the roles of decorin and biglycan in the maintenance of mature tendon structure and mechanics, but utilized conventional knockout models, thus a confounding variable was present due to irregular tendon development. The objective of this study was to determine the individual roles of these molecules in maintaining the structural and mechanical properties of tendon during homeostasis in mature mice using inducible knockdown models. We hypothesized that knockdown of decorin in mature tendons would result in detrimental changes to tendon structure and mechanics while knockdown of biglycan would have a minor effect on these parameters

Contrary to our hypothesis, knockdown of decorin resulted in minor alterations to tendon structure and no changes to mechanics while knockdown of biglycan resulted in broad changes to tendon structure and mechanics. Specifically, knockdown of biglycan resulted in reduced insertion modulus, maximum stress, dynamic modulus, stress relaxation, and increased collagen fiber realignment during loading. Knockdown of decorin and biglycan produced similar changes to tendon microstructure by increasing the collagen fibril diameter relative to wild-type controls. Biglycan knockdown also decreased the cell nuclear aspect ratio, indicating a more spindle-like nuclear shape.

Overall, the extensive changes to tendon structure and mechanics after knockout of biglycan, but not decorin, provides evidence that biglycan plays a major role in the maintenance of tendon structure and mechanics in skeletally mature mice during homeostasis.

6.4 Chapter IV Conclusions

Previously, knockout models were used to demonstrate that decorin prevented the age-related decline of tendon mechanics. However, abnormal development using conventional knockout models introduces a confounding variable which was potentially compounded due to the long timeline required for aging studies. Additionally, a compound *Dcn/*Bgn knockdown model was used to determine the effects of decorin and biglycan knockdown on tendon aging. The objective of this study was to determine the effects of decorin and biglycan knockdown on tendon structure and mechanics in aged tendons using tamoxifen-inducible knockdown models. We hypothesized that the knockdown of decorin and compound knockdown of decorin and biglycan would prevent age-related declines in tendon mechanics and structure compared to biglycan knockdown and wild-type controls, and that these changes would be exacerbated at geriatric ages.

Knockdown of decorin led to increased midsubstance modulus and decreased stress relaxation in aged tendons. However, these changes were not sustained in the geriatric tendons. Knockdown in biglycan led to no changes in mechanics in the aged or geriatric tendons. Contrary to our hypothesis, the compound *Dcn/*Bgn knockdown did not parallel the decorin knockdown model but had a unique genotype with increased viscoelastic properties in the aged and geriatric tendons. Structurally, knockdown of SLRPs, except for the geriatric *Dcn/Bgn* knockdown group, resulted in alterations to the

collagen fibril diameter relative to wild-type controls. Overall, this study identified the differential roles of decorin and biglycan throughout tendon aging in the maintenance of tendon structural and mechanical properties and revealed that the compound decorin and biglycan knockdown phenotype did not resemble the single gene decorin or biglycan models and was detrimental to tendon properties throughout aging.

6.5 Chapter V Conclusions

Tendon injuries result in lifelong burdens due to the fibrotic healing response that produces low quality tissue that is unable to recover pre-injury structure and mechanics, resulting in functional impairment. Increased interest in studying neonatal development and the improved healing response observed in neonates is increasing, with the goal of using this approach to create better therapeutics for tendon injury. Decorin and biglycan are two small leucine-rich proteoglycans that play important roles in collagen fibrillogenesis to develop, maintain, and repair tendon structure. However, little is known about the roles of decorin and biglycan in early neonatal development, when the potential for the improved healing response observed in neonates is high. The goal of this study was to determine the effects of decorin and biglycan knockdown during neonatal tendon development and after injury in the neonate. We hypothesized that knockdown of decorin and biglycan would disrupt the neonatal tendon developmental and healing processes and produce tendons with impaired mechanical and structural properties.

Knockdown of decorin and biglycan immediately after birth produced tendons with an immature collagen fibril phenotype that had many small diameter fibrils. Similar results were seen in the injured group, where >50% of the collagen fibrils were between 30-45 nm in diameter and few large fibrils were present. For both groups, the small

collagen fibrils manifested in the tendon response to load, where collagen fiber realignment peaked at low strain levels before the rate of alignment decreased. Quasistatic mechanics were also impaired, however there were no changes in viscoelastic mechanics. The mechanics results were unusual because many studies using SLRP knockdown models report changes to viscoelastic mechanics, not quasistatic mechanics. Overall, this study demonstrated the importance of decorin and biglycan in tendon fibrillogenesis and the impact that small diameter collagen fibrils can have on tendon mechanical properties, with an immature microstructure being detrimental to the tendon response to load.

6.6 Future Directions

6.6.1 Additional analysis of the effects of tamoxifen on tendon injury

In our recent study, we observed that tamoxifen treatment did not affect post-injury tendon mechanics, cellularity, or nuclear aspect ratio at 3 weeks post-injury. However, the heavy emphasis on biomechanical testing methods in this study was a limitation; structural and biological analyses would provide a more complete examination of the effects of tamoxifen on tendon healing. Future studies should be conducted to determine the effects of tamoxifen on additional parameters of tendon healing, such as tendon structure, collagen organization, and cell populations. Specific methods that should be included to examine the impact on tendon structure include TEM for collagen microstructure and polarized light microscopy combined with picrosirius red staining for collagen organization. Gene expression analysis can help determine the impact of TM treatment on regulation of the post-injury tendon healing response, expression of ECM components, and ECM assembly by measuring the expression of collagens, proteoglycans, and growth factors (e.g., TGF-β, IGF-1, and VEGF). Additionally, the

analysis of key cell markers should be analyzed, particularly for myofibroblasts (*Acta2*) due to their critical role in wound healing. Future work examining the impact of TM on tendon healing should also include additional post-injury time points and study sex differences between male and female mice. These studies will provide valuable insight into the potential interactions between tamoxifen and the tendon healing response and will enhance our understanding of the reliability and limitations of using tamoxifen inducible Cre recombinase models to study tendon injury.

6.6.2 Further investigation into effects of decorin on tendon aging

This work demonstrated that knockdown of decorin counteracted the typical age-related decline in tendon mechanics. However, the mechanisms driving this process remain unclear. Previous work using a decorin knockout model to study tendon aging made similar observations of a distinct aging process with less pronounced changes to mechanics relative to WT aged tendons. The authors speculated that the natural decline in mechanical properties throughout aging could be due to (1) continued decorin-fibril interactions facilitating lateral growth throughout aging or (2) decorin-induced signaling pathways, such as crosslinking. Our recent study used tamoxifen inducible models for temporal control of decorin expression, facilitating normal tendon development and isolating the knockdown to mature mice undergoing the aging process. The aged I-*Dcn*$^{-/-}$ tendons revealed an increased fibril diameter compared to WT, which does not support the previous speculation that the tendon aging process is due to decorin-fibril interactions driving lateral growth. Due to the lack of investigation of the role of decorin signaling on tendon aging, additional studies exploring aging signaling pathways should be conducted.

While previous work has measured aged tendon mechanics and structure, cellular and compositional changes should be further explored to test the hypothesis that decorin knockdown is beneficial to tendon aging. Tenocyte senescence is associated with age-related tendon disorders and impaired healing and is correlated with an upregulation of p16, p53, p15, and p21. Reduced tenocyte proliferation and metabolic activity is also associated with tendon aging. Tendon aging is also associated with a reduced ability to modulate inflammation and alterations to enzymatic activity, with increases in pro-inflammatory cytokines IL-6, IL-1β, and TNF-α, increased expression and activity of MMP-2 and MMP-9, and reductions in TIMP-1 and TIMP-2. Additionally, lysyl oxidase expression and the presence of advanced glycation end-products are correlated with tendon aging and ECM stiffness via collagen crosslinking and could provide insight into the improved mechanics observed after knockdown of decorin. A better understanding of the molecular mechanisms driving the improvements in tendon mechanics that have been observed after decorin knockdown may inform therapeutics that can reduce age-related injuries and declines in tendon function.

Alterations to enzymatic activity have also been observed with age, with aged rats showing increased expression and activity of matrix metalloproteinase-2 (MMP-2) and MMP-9 while tissue inhibitor of metalloproteinase-1 (TIMP-1) and TIMP-2 were reduced.

6.6.3 Differential effects of (single) decorin and biglycan knockdown on neonatal tendon development and healing

This study demonstrated that knockdown of decorin and biglycan significantly impacted neonatal tendon development and the neonatal tendon wound healing response. The negative impact of *Dcn* and *Bgn* knockdown on neonatal tendon

development and healing was demonstrated by decreased quasistatic mechanics, altered collagen fiber realignment, and an increase in small diameter collagen fibrils. However, the use of the compound knockdown model did not allow for the exploration of the individual roles of decorin and biglycan in neonatal development and healing. Previous work has observed unexpected outcomes when comparing the individual effects of *Dcn* or *Bgn* knockdown on tendon mechanics and structure to compound knockdown of *Dcn* and *Bgn*, making the inclusion of the single knockdown models imperative when attempting to define the roles of these proteins in tendon studies. Therefore, future work should use I-*Dcn*$^{-/-}$ and I-*Bgn*$^{-/-}$ knockdown models to define the differential roles of decorin and biglycan on neonatal tendon development and healing.

6.6.4 Additional post-injury time points after neonatal mouse injury

The original study that established the neonatal tendon injury model found that healing is accelerated and capable of recovering baseline mechanics when injury occurs at P7, but the healing response resembled adult healing when the injury occurred at P21. These conclusions were based on a 10-day post-injury timeline, which was used in this dissertation when exploring the roles of decorin and biglycan in neonatal tendon healing. The long-term outcomes of early and late neonatal tendon healing remain unknown and should be included in future studies with the addition of 3-week, 6-week, and 12-week post-injury timepoints. This would align with timepoints commonly used in adult models for tendon healing, which would normally correlate with the proliferative and early remodeling (3 weeks) and late remodeling phases (6 week) in adults. These longer timepoints would test the hypothesis that neonatal healing is accelerated compared to the adult. The 12-week post-injury timepoint would put the mice past sexual

maturity, to test whether neonatal healing is regenerative or if structural and mechanical deficits remain into adulthood.

A limitation of the work presented in this dissertation was also the lack of a short-term timepoint, which would've informed the impact of *Dcn* and *Bgn* knockdown on the early inflammatory phase of tendon healing. Future studies using knockdown models should include this timepoint, with proper care that the study design results in proper knockdown of the target molecules shortly after injury.

6.6.5 Exploring the differences between neonatal and adult tendon healing

The neonatal tendon developmental model has demonstrated potential as a paradigm that can provide insights to improve clinical outcomes for tendon injuries. This is due to the distinct characteristics of the injury response that include rapid healing capable of recovering baseline tendon mechanics, a reduced inflammatory response, and decreased scar tissue formation. However, little is known about the differential processes that give the neonatal tendon healing response improved capabilities compared to adults. To explore these differences, future work should conduct a transcriptome-wide analysis on neonatal and adult tendons in uninjured and injured states using RNA sequencing (RNA-seq). This analysis would provide additional context to previous work that has examined the roles of various biological pathways during neonatal tendon healing and potentially provide novel pathways for future studies.

Specifically, the uninjured tendon analysis would provide an understanding of the baseline gene expression that facilitates an improved healing response. Transcriptomic analysis shortly after injury during the early inflammatory response can further explore the hypothesis that the immune system is a key regulator of regenerative versus reparative tendon healing. Single cell RNA-seq can be combined with lineage tracing to

determine the differential signaling pathways between the intrinsic and extrinsic cell populations that have been hypothesized to be responsible for driving a regenerative or fibrotic healing response. Furthermore, tendon extracellular matrix composition and related signaling molecules can be observed throughout the remodeling process to determine long-term outcomes after neonatal injury, which has been understudied thus far.

Combining RNA-seq with mass spectrometry can provide additional understanding of the molecular changes that occur in a biological system with insights into regulation at the translational level and post-translational modification of proteins. Mass spectrometry can also be used to identify and quantify small molecules, such as metabolites, which can provide further insight into the molecular changes occurring in a biological system. This could be used to investigate the fragmentation of extracellular matrix molecules, such as SLRPs, throughout healing, which has been hypothesized to be a biomarker of disease and have consequences for tissue integrity. Combining RNA-seq with mass spectrometry can provide a more comprehensive understanding of the molecular changes that occur as a result of tendon injury, which can help researchers gain a better understanding of the underlying mechanisms driving neonatal and adult tendon healing. Ultimately, these efforts could provide additional context for previous and ongoing studies while potentially offering insights into possible targets for future therapies for tendon injuries.

6.6.6 Role of decorin and biglycan in the post-injury immune response

While developmental models have demonstrated an improved ability to recover after tendon injury, the mechanisms that drive this response are not well understood. The inflammatory phase is the first phase of wound healing, which is governed by

immune cell populations that infiltrate the injury site. Modulation of the inflammatory response has been used as a strategy for therapeutics seeking to improve clinical outcomes after tissue injury due to the inverse correlation between the capacity to regenerate tissue and the advancement of the immune system that has been observed throughout evolution and during development. Differences in the inflammatory response have similarly been noted between neonatal and adult tendon injury models, with additional work needed to define the cells and signals that drive the wound healing response in each model.

Decorin and biglycan have primarily been studied as structural elements in tendon due to their roles in the regulation of collagen fibrillogenesis. Increasingly, the function of decorin and biglycan as signaling molecules within tendon is being studied. When studying the regulatory roles of decorin and biglycan in tendon healing, it is often from the perspective of ECM derived molecules that will modulate fibrillogenesis to restore structure and mechanics. After injury decorin and biglycan are released due to proteolytic degradation of the ECM and act as damage-associated molecular patterns (DAMPs) capable of interacting with pathogen recognition receptors (PRRs).[1,2] Neutrophils, macrophages, and dendritic cells are capable of recognizing DAMPs via two types of PRRs: Toll-like receptors (TLRs) and NOD-like receptors (NLRs) through their leucine-rich repeat (LRR)-motifs, allowing them to interact with other LRR-proteins.[3,4] Biglycan can also activate the adaptive immune system, acting as a bridge between innate and adaptive immunity.[5] Defining the relationships between decorin, biglycan, and various immune receptors could elucidate the mechanisms that drive the healing response or chronic inflammatory conditions. Studying this relationship within the context of the neonatal injury model or other regenerative model systems could be

particularly useful to inform therapeutics.[6,7] One potential cellular population that could be explored within this context is the tenophage, a macrophage-like tendon cell population.[8] Given the importance of inflammation and the immune response after injury, the ability for decorin and biglycan to act as DAMPs opens new avenues of research when considering their roles after injury.

6.6.7 Additional ideas for future studies

This section will address a series of additional ideas for future studies, which will be focused on exploring the regional effects of decorin and biglycan knockdown on neonatal tendon, the modulation of mechanical stimuli during tendon development, and the use of decorin and biglycan as therapeutics for tendon injury and aging.

This dissertation observed the importance of decorin and biglycan in the development and post-injury recovery of tendon structure and mechanics. However, the analyses were focused on the whole tendon, without taking the heterogeneous or anisotropic nature of tendon into account. To improve upon this limitation, regional analysis of tendon composition, structure, and mechanics should be employed. This can be achieved with the use of atomic force microscopy (AFM) to correlate the mechanical and structural properties that emerge alongside the compositional changes that occur throughout development and after injury. AFM can be used to measure similar viscoelastic parameters that are used at the macroscale, including stress-relaxation, dynamic modulus, and measurement of the phase shift during loading. Additionally, structural analyses can be conducted, including collagen fibril alignment and the quantification of crimp. These methods may also be used to test the recent hypothesis that the reduction in healing capabilities observed in the neonate is due to the increased deposition of ECM that occurs throughout development.[9,10] These analyses would

ultimately allow for the correlation between tendon composition, structure, and mechanics across multiple length scales.

Previous work with the neonatal mouse injury model discovered that the regenerative tendon healing response was present at P7 (early neonate) but was not at P21 (late neonate). Throughout development changes occur rapidly, and many variables need to be taken into consideration when attempting to find what causes the shift from regenerative to fibrotic healing. One unique variable that emerges between the early and late neonate is the increase in mechanical loading due to ambulation. The role of mechanical loading in the neonatal healing response is unknown, and future work should modulate mechanical loading after injury in the neonate to determine the role of ambulation in neonatal tendon healing. Additionally, functional measures should also be added to future developmental injury studies when possible. While the recovery of structural and mechanical tendon properties is accelerated in the early neonate post-injury it is unknown if this is true for function. For studies that occur early in development obtaining measures on whether ambulation is delayed or negatively impacted by measuring ground reaction forces over time would be important when comparing post-injury outcomes with adult models. Changes to mechanical loading could also be used as a variable in future neonatal studies by measuring the healing response after higher or lower levels of activity after injury has occurred.

This work has demonstrated that *Dcn* and *Bgn* play vital roles during tendon development and the maintenance of tendon structure and mechanics throughout aging. The knockdown of *Dcn* and *Bgn* also disrupted the recovery of tendon structure and mechanics after injury in the neonatal mouse model. Given the impact of decorin and biglycan on parameters vital to tendon function, their use as a therapeutic after injury in

adults should be explored. Previously, the use of decorin and biglycan as therapeutics was limited to the administration of exogenous proteins; however, recent developments and the widespread use of mRNA therapeutics presents an alternative method for delivering these molecules to injured tissues. The emergence of this technology combined with the previous suggestions for future studies regarding decorin and biglycan in tendon healing demonstrate the potential for these proteins to improve clinical outcomes after tendon injury.

6.7 Final Conclusions

This dissertation elucidated the regulatory roles of decorin and biglycan on tendon structure and mechanics during neonatal development and healing, in adults, and throughout the aging process. Throughout these studies, the importance of decorin and biglycan in the development and maintenance of tendon properties was better defined, demonstrating that their role in fibrillogenesis is often vital throughout the lifetime of the organism. The work looking at the roles of decorin and biglycan in neonatal tendon development and healing lays the groundwork to explore the mechanisms driving these processes. Ultimately, elucidation of these mechanisms will assist in creating therapeutics to improve health and quality of life.

6.8 References

1. Schaefer L, Babelova A, Kiss E, et al. 2005. The matrix component biglycan is proinflammatory and signals through Toll-like receptors 4 and 2 in macrophages. J. Clin. Invest. 115(8):2223–2233.

2. Merline R, Moreth K, Beckmann J, et al. 2011. Signaling by the matrix proteoglycan decorin controls inflammation and cancer through PDCD4 and microRNA-21. Sci. Signal. 4(199):1–15.

3. Inohara N, Chamaillard M, McDonald C, Nuñez G. 2005. NOD-LRR proteins: Role in host-microbial interactions and inflammatory disease. Annu. Rev. Biochem. 74:355–383.

4. Wu B, Huan T, Gong J, et al. [date unknown]. Domain combination of the vertebrate-like TLR gene family: implications for their origin and evolution. 401–408 p. Available from: http://pfam.sanger.ac.uk/search.

5. Moreth K, Iozzo R V., Schaefer L. 2012. Small leucine-rich proteoglycans orchestrate receptor crosstalk during inflammation. Cell Cycle 11(11):2084–2091.

6. Mescher AL, Neff AW, King MW. 2013. Changes in the inflammatory response to injury and its resolution during the loss of regenerative capacity in developing Xenopus limbs. PLoS One 8(11):1–11.

7. Aurora AB, Olson EN. 2014. Immune modulation of stem cells and regeneration. Cell Stem Cell 15(1):14–25 [cited 2017 Jun 22] Available from: http://www.ncbi.nlm.nih.gov/pubmed/24996166.

8. Lehner C, Spitzer G, Gehwolf R, et al. 2019. Tenophages: A novel macrophage-

like tendon cell population expressing CX3CL1 and CX3CR1. DMM Dis. Model. Mech. 12(12).

9. Notari M, Ventura-Rubio A, Bedford-Guaus SJ, et al. 2018. The local microenvironment limits the regenerative potential of the mouse neonatal heart. Sci. Adv. 4(5) Available from: https://www.science.org/doi/10.1126/sciadv.aao5553.

10. Segel M, Neumann B, Hill MFE, et al. 2019. Niche stiffness underlies the ageing of central nervous system progenitor cells. Nature 573(7772):130–134 Available from: http://www.nature.com/articles/s41586-019-1484-9.

APPENDICES: EXPERIMENTAL PROTOCOLS

Appendix A: Neonatal Mouse Tamoxifen Injections

Materials:

- Tamoxifen powder
- Digital scale
- Wax paper
- Oven
- Mini shaker table
- Corn oil
- Aluminum foil
- 15 mL conical centrifuge tube
- Drummond Portable Pipet-Aid XP Pipette Controller
- 10 mL disposable serological pipet
- 1 mL disposable syringe
- 20G needle
- 3/10 mL insulin syringe w/ needle

P7 Neonate Formulation & Dosing:

- 1 injection at P0, sacrifice at P7
- Batch formulation:
    - 80 mg tamoxifen (TM) / 10 mL corn oil
- TM Dose:
    - 0.16 mg TM per mouse
    - 20 µL injection

P17 Neonate Formulation & Dosing:

- 1 injection at P7, sacrifice at P17
- Batch formulation:
    - 100 mg TM / 10 mL corn oil
- TM Dose:
    - 0.40 mg TM per mouse
    - 40 µL injection

Procedure:

1. **Make batch of tamoxifen suspended in corn oil**

a. Use Drummond portable pipet-aid XP pipette controller with a 10 mL disposable serological pipet to transfer 10 mL of corn oil to fresh 15 mL conical centrifuge tube

b. Measure 80 mg (injection @ P0) or 100 mg (injection @ P7) of tamoxifen using digital scale on a piece of wax paper

c. Carefully pour the tamoxifen into the conical centrifuge tube containing 10 mL corn oil

d. Seal centrifuge tube containing TM + corn oil, then shake vigorously by hand for approximately 15 seconds to begin dissolving the tamoxifen
    i. IMPORTANT – Make sure there is no tamoxifen trapped in the tip of the centrifuge tube. If there is, tap the tube on lab bench until the tamoxifen is no longer trapped

e. Wrap centrifuge tube in aluminum foil to protect solution from light

f. Place the centrifuge tube on mini shaker table that has been placed inside of oven set to 40°C. Turn shaker table on and let the solution mix for ~4 hours

g. Once all tamoxifen has been dissolved in the corn oil you can remove the solution from the oven

h. Place tamoxifen in refrigerator for storage. Make a fresh batch weekly.

2. Prepare Syringes for Injections

a. Remove tamoxifen from refrigerator, and place in oven at 40°C until warm
b. Fill 1 mL disposable syringe (20G needle) with tamoxifen
c. Remove plunger from desired number of 3/10 mL insulin syringes w/ needle
d. Inject tamoxifen solution into barrel of insulin syringes, insert plunger after solution has been injected
    i. For injections at P0, insert >20 µL into each syringe
    ii. For injections at P7, insert >40 µL into each syringe
e. Wrap syringes in aluminum foil, then place in oven at 40°C until ready for injection

3. Injecting Neonates

a. Before injecting neonates, ensure each syringe contains correct volume of tamoxifen solution. Eject any excess from the syringe.
b. Grasp neonate by nape of the neck, then turn mouse over and identify milk spot in the abdominal region
c. Carefully insert syringe into milk spot and inject tamoxifen solution into the neonate for an intragastric injection.

Appendix B: Neonatal Mouse Achilles Tendon Surgery (Injury)

Materials:

- Sterile drape
- Sterile surgical instrument pack:
    1. Ultra-fine forceps
    2. Dressing forceps
    3. Micro scissors
    4. Hemostat
    5. Blade handle
    6. Plastic-coated scalpel for backing biopsy punch
- No. 15 Feather surgical blade
- 0.3 mm biopsy punch
- 6-0 prolene suture
- Dissection microscope
- Water circulating warming blanket

Procedure:

1. Microscope Setup:
    a. Prior to surgical procedure, setup dissection microscope with warming blanket placed over the microscope stage.
    b. Place sterile drape over heating blanket.
    c. Setup nose cone from isoflurane onto microscope stage so that the mouse hindlimbs can be seen through the objective lens while in the nose cone in prone position.
2. Surgical Procedure:
    a. Prior to the surgical procedure, mice are anesthetized with a mixture of isoflurane (2-4%) and oxygen. The right hindlimb is cleaned with alcohol and betadine, then the animal is placed on sterile drape under the microscope in prone position.
    b. Maintain isoflurane around 2% throughout the procedure.
    c. Make a midline incision over the right Achilles tendon.
    d. Place plastic coated blade beneath Achilles tendon.
        i. Can use fine forceps to assist by running them beneath the tendon to create space for the plastic-coated blade.
    e. Using the plastic-coated blade as support, use a 0.3 mm diameter biopsy punch to create a full thickness partial width transection in the middle of the Achilles tendon
    f. Close the skin wound with a figure 8 suture (6-0 prolene)
    g. Allow the mouse to recover under a heat lamp in a cage with alpha-dri bedding
    h. Once the mice have recovered, rub them with bedding from their original cage before reintroduction to mom

Appendix C: Neonatal Achilles Tendon Dissection and Sample Prep

- **Dissection & Sample Prep Supplies:**
  - Fine Forceps (x2)
  - Microscissors
  - Scalpel Handle
  - No. 11 Blade
  - Sand Paper
  - Superglue
  - Ruler
  - Kim wipes
  - Dental Wax Sheet
  - Verhoeff Stain
    - 5% hematoxylin solution (0.4g Hematoxylin + 20 ml 95% EtOH)
    - 10% aqueous ferric chloride (2g Ferric chloride + 20 ml dH2O)
    - Weigert's iodine solution (2g potassium iodide + 1g iodine + 100 ml dH2O)
  - dH2O)
  - 200 uL Pipette w/ tips
  - Silk Thread for stain lines
  - Weigh Boats
  - 1x PBS
  - Stereomicroscope
  - Dissection Mat
  - GISMO
  - Neonatal Achilles Grip w/ Allen Wrench

- **Verhoeff Stain**
  - Make Verhoeff stain before starting dissection
    - Allow the stain to sit while you dissect for better quality stain lines
    - Freshly made stain doesn't adhere to the tissue as well
  - Add in order B to A (mix thoroughly), then add C (and mix thoroughly) in the following ratio of A:B:C = 2:1:1
    - Solution A: 5% hematoxylin solution (0.4g Hematoxylin + 20 ml 95% EtOH)
    - Solution B: 10% aqueous ferric chloride (2g Ferric chloride + 20 ml dH2O)
    - Solution C: Weigert's iodine solution (2g potassium iodide + 1g iodine + 100 ml dH2O)
  - Place small amount (~0.5 ml) of stain in angled weigh boat

- **Gross Dissection:**
  - Perform gross dissection and fine dissection under stereomicroscope

- Make an incision lateral to the tendon from the calcaneus parallel to the tibia
- Use fine forceps to peel back the skin and expose the Achilles tendon and muscle
- Use scalpel to cut through the mouse femur to remove the leg from the mouse body
- Place scalpel blade deep to the Achilles tendon and cut proximally along the tibia through the muscle at its most proximal position
- Grip foot with forceps, then use second pair of forceps to gently scrape the gastrocnemius off of the tendon
- Use microscissors to cut through the calcaneus, leaving enough calcaneus attached to the tendon to grip for mechanical testing

- **Fine Dissection:**
  - Make sure you're hydrating the tendon throughout the rest of the preparation up until you're ready to test
  - Grip calcaneus with fine forceps and use second pair of fine forceps to remove any remaining connective tissue, muscle, and other non-tendonous tissue from the Achilles

- **Stain Lines:**
  - Briefly dry tendon using a Kim wipe
  - Place tendon on dental wax/ruler under the microscope
  - Using fine silk string, apply stain line just proximal to the calcaneal insertion
  - Reorient the sample or the ruler to ensure that the calcaneal stain line is your zero point
  - Place additional stain lines 1 mm and 2 mm (for P7) proximal to the calcaneal stain line

- **Cross-Sectional Area (GISMO):**
  - Turn on laser light and allow it to warm up for 20 minutes before you measure tendon CSA
  - Lightly dry the tendon using a Kim wipe
  - Place sample on the GISMO stage with stain lines facing up
  - Position the laser next to your first stain line
  - Press "Run" and "Capture" on the GISMO interface
  - Zero the X, Y, and Z positions
  - Make passes across the tendon every 0.5 mm from the first stain line to the last stain line
  - Place tendon back in PBS
  - Save data
  - Turn off laser

- **Sandpaper:**
    - Apply sandpaper under microscope
    - Cut very small pieces of sandpaper that will fit between the screws on the neonatal Achilles grips (~4 mm x 4 mm)
    - Apply a small amount of superglue to the dental wax sheet and place the smooth side of the sandpaper (A) on the glue to hold in place
    - Remove tendon from PBS and briefly dry using a Kim wipe
    - Place tendon next to sandpaper A and ensure stain lines are visible
    - Place a very small amount of super glue on the two outer thirds of one piece of sandpaper (B)
        - This will leave the middle third of the sandpaper with no superglue
    - Place small layer of super glue on opposing piece of sandpaper B, leaving a small strip uncovered to grip with forceps
    - Place myotendinous end of tendon in the middle column of the piece of sandpaper A, leaving the proximal stainline exposed once sandpaper B is applied
    - Grip sandpaper B along the strip without super glue, and carefully place over the myotendinous end of the tendon that is on top of sandpaper A
        - Your forceps and the strip of sandpaper B without super glue should be on the same side as your proximal stain line
        - Be careful not to cover stain line when apply sandpaper B
    - Using the blunt end of your forceps, apply force to the sandpaper on the same side as the proximal stain line, then press down, running the blunt end of your forceps across the sandpaper to spread the superglue away from the sample
    - Place sample in PBS to rehydrate, then place next to two more square of sandpaper
    - Cover sandpaper C in a thin layer of superglue
    - Cover sandpaper D in a thin later of superglue, leaving a thin strip without superglue to grip with forceps
    - Place calcaneus on sandpaper C, leaving the distal stain line exposed
    - Pick up sandpaper D with forceps along strip without superglue, then place on top of sandpaper C
        - Ensure distal stain line is visible once sandpaper D has been placed on top of sandpaper C
    - Place the calcaneal end of the sample in neonatal Achilles grips, and make sure the distal stain line is not covered by the grip
    - Use Allen wrench to tighten grip around calcaneal end of the sample
    - Place grip + sample in PBS
    - Place proximal end of tendon into the other grip, then tighten with Allen wrench.
    - Use bridge to connect each of the grips and protect sample while loading into Instron

Appendix D: Neonatal Achilles Tendon Mechanical Testing Protocol

Materials:

- Instron 5848
- Instron Computer
- Imaging Computer
- Camera & Accessories
- Cross Polarizer & Accessories
- 10N Load Cell
- Tank & Accessories
- Neonatal mechanical testing fixutres
- Hex Key

Procedure:

1. **Instron & Tank Setup:**
    - **a.** Screw 10N load cell into crosshead and plug into Instron.
    - **b.** Screw stage into Instron base with hex keys.
    - **c.** Place tank on stage and secure using vise grip.
    - **d.** Attach neonatal mechanical testing fixtures to tank.


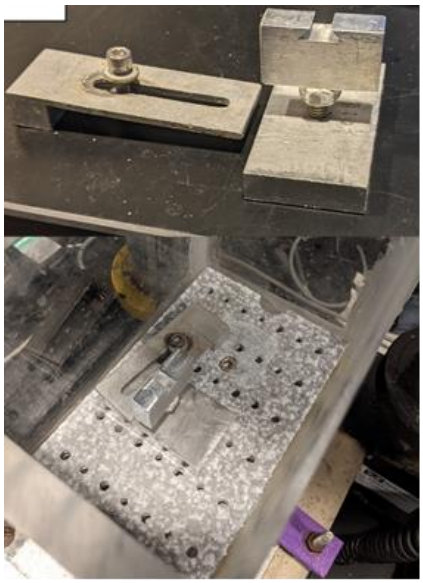

    - **e.** Plug in sous vide and place in tank.
    - **f.** Fill tank with PBS until “min” line on sous vide is submerged (approx. 1800 mL).
2. **Turn on Instron, login to Instron computer.**
    - **a.** Start Console software.
    - **b.** Open Wavemaker Runtime, then open Wavemaker Editor.

c. Calibrate load cell, then check accuracy with a calibrated weight.
d. In Wavemaker Editor select mechanical testing protocol
e. Select “Data Storage” tab at bottom of Editor, click box below “Output Filename”, and create folder to store mechanical testing data.
f. Select “Apply Current Blow to All Blocks” and make sure that output filename is consistent across all blocks in the protocol.
g. Save & Select Run.

3. **Login to imaging computer.**
   - **a.** Plug data acquisition device (DAQ) input into Instron.
   - **b.** Plug DAQ output into USB port on imaging computer.
   - **c.** Open Measurement and Automation Explorer (NI MAX)
   - **d.** In NI MAX, expand ‘Devices and Interfaces’ folder, select Camera.
   - **e.** Open CIMM Ware in Labview. Set trigger threshold to 1V.
4. **Load Sample**
   - **a.** Center load cell over testing fixtures in tank, connect dovetail jig to load cell with pin.
   - **b.** Lower load cell position until upper and lower dovetail fixtures are aligned and approximately as far apart as the clamp and fixtures that are securing the tendon.
   - **c.** Slide sample into dovetail fixtures, distal end of the tendon down. Adjust x, y, and z positions of fixtures via the Instron control and stage as needed to get proper alignment.
   - **d.** Remove protective bridge from the tendon grips once fixtures are secured in the tank.

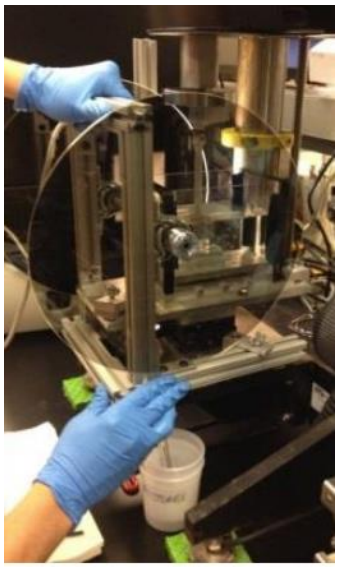

5. **Cross Polarizer & Camera Setup**
   - **a.** Put polarizer on Instron base, around the tank, and clamp into place. Make sure axle is not touching tank.
   - **b.** Plug in cord from toolbox to motor on left side of polarizer.
   - **c.** Position divot in polarizer wheel at top of the wheel.
   - **d.** Position light on the side opposite of the camera & perpendicular to the cross polarizer.
   - **e.** Turn light on.
   - **f.** Adjust camera height, position, and focus to view tendon.
   - **g.** Balance load cell while tendon is unloaded.
   - **h.** Adjust stage to ensure that the tendon is aligned.
   - **i.** Load tendon to 0.01N, reset displacement
   - **j.** Take pre-test image. Save in appropriate folder.

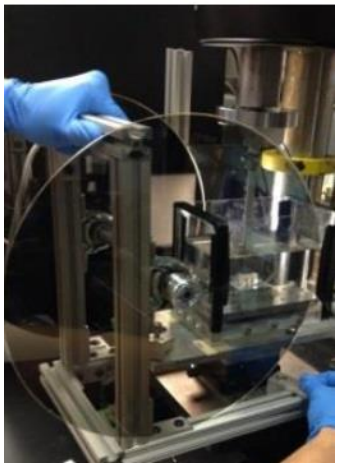

k. Click out of “Camera” in NI MAX

6. **Begin Test**
    - **a.** Ensure CIMM Ware is set to save images in correct location.
    - **b.** Run CIMM Ware
    - **c.** In CIMM Ware click “Zero Angle” and “Motor Start”.
    - **d.** Run Test.
        - **i.** Click “Yes” at the same time as clicking “Zero Time” on imaging computer.
7. **Collect Scale Image**
    - **a.** After test, jog Instron up to move upper fixture away.
    - **b.** Reopen camera in NI MAX.
    - **c.** Take image of ruler.
        - **i.** Ensure ruler is in same plane as failed tendon.
        - **ii.** Save in appropriate folder.

Appendix E: Hindlimb Fixation (Histology)

Materials

- PBS (store at RT)
- 10% neutral buffered formalin (store at RT)
- 30% (w/v) sucrose (Sigma S8501) dissolved in PBS (store solution at 4˚C)
- OCT (Fischer Scientific 23-730-571; store at RT)
- 2-methylbutane (Thermo Fischer Scientific O3551-4; store at -20˚C)
- Dry ice
- 50-ml tubes
- Plastic molds, 24mm x 24mm (Fischer Scientific 41-742)

Procedure

Fixation

1. Prepare 50-ml tubes with 25 ml/tube 10% formalin (1 tube per animal).
2. Cut limbs and drop into formalin.
3. Fix in formalin at 4˚C for at least 2 days and at most 4 days. Fluorescent background increases and fluorescent protein signal and antigen preservation decrease with more time in formalin.
4. Cryopreserve in sucrose at 4˚C for no more than 24 hours (minimum time = however long it takes for tissue to sink to bottom of tube; depends on age).

Embed

5. Place a plastic cup in the middle of an ice bucket and fill about 1/3 full with dry ice.
6. In the fume hood, pour 2-methylbutane into plastic cup (in ice bucket) until it's about ~1/2 full. Cover ice bucket and allow solution to cool. 2-methylbutane is cool enough when a CO_2 brick dropped into the solution produces no bubbles).
7. Fill plastic molds ~75% full with OCT. You will need 2/animal (one for left limbs, one for right limbs)
8. Trim and arrange tissue to be embedded in plastic mold. Be consistent and embed medial side down. Pour enough OCT to cover the tissue.
9. Using long forceps, carefully drop the plastic mold into the cup with cooled 2-methylbutane. Can freeze a few molds in the cup at the same time; wait until each block is frozen before adding another one. The block is fully frozen when the OCT is opaque white and the 2-methylbutane is no longer bubbling.
10. Immediately store the blocks wrapped in plastic wrap and/or in plastic bags in the freezer. Store blocks at -20˚C for up to 2 weeks. Store blocks at -80˚C for long-term storage.

Appendix F: Hindlimb Achilles Tendon Cryosectioning

Materials:
- Cryostat + chuck
- Blades (Sturkey #D554X50 and #D554D50)
- Cryostat roller
- Brush
- CryoJane tape (via Histology Core)
- Fine forceps - OCT embedding media
- Plastic slides
- Kimwipes
- Microscope (4x objective)

Procedure:

1. Precool blades, roller, brush, forceps, cryotape, and samples
    a. Turn on cryostat to -20ºC and cool supplies in hood for 20min
    b. While supplies are cooling, cut cryotape for cryosection
2. Trim sample block with blade to minimize excess OCT
3. Embed sample on chuck
    a. Turn on cryobar and place chuck on cryobar
    b. Embed sample in OCT on block
4. Mount sample and section through lateral hindlimb (Extremus blades, 30µm→20µm)
    a. Periodically check alignment by collecting on plastic slide and viewing with 4x objective microscope
    b. Adjust as needed based on embedded sample alignment
    c. When nearing Achilles tendon, reduce section thickness to avoid wasting sample
5. Collect sample sections (Diamond blades, 10 µm)
    a. Cleanest, most uniform sections are achieved when tibia is near parallel to cut surface
    b. When Achilles tendon is reached, place tape on sample surface, with long axis in same direction as the tibia, spanning the calcaneus through at least the midfoot
    c. Roll on tape with cryoroller to ensure adherence of tape to sample
    d. While gripping gold tape with forceps, section through tissue. Sample will glide onto blade stage, stuck to cryotape
    e. Swipe cryosection onto plastic slide just outside the cryohood. The OCT will melt and stick the section to the slide
    f. Repeat until Achilles tendon has been fully collected
6. Transfer slides on ice to -20ºC freezer for gluing and staining

Appendix G: Chitosan High Molecular Weight Film Adhesive

1. Prepare acetic acid solution: dissolve 0.25ml acetic acid (Sigma Aldrich 695092) in 100ml DI water, 0.25%, v/v

2. Prepare chitosan (HMW, >75% deacetylation, Sigma 419419-50G) solution in 0.25%, v/v acetic acid solution: put 0.75g in 100ml acetic acid solution and stir the solution overnight or until all the chitosan powder is dissolved.

3. Put the chitosan solution at room temperature for convenient use (low temperature would make the solution more viscous).

Appendix H: Chitosan Section Gluing

- Thaw slides
- Peel off sections and place in a safe place (weigh boat). Clean slide with 70% EtoH and kimwipe.
- Place a drop of chitosan that is approximately the size of the tape section onto the glass (~6 ul).
- Pick up a section with forceps with the gold tab facing up. Cut off the tab from the tape and place the tape tissue-side up on the glass
- Drag some of the chitosan towards the edge of the glass slide and place the slide in a slide box with a kimwipe underneath it such that excess chitosan wicks down onto the kimwipe. The wicking is important in getting a flat surface.
    - If the chitosan doesn't wick down, it tends to clump underneath the tape. This will lead to an uneven surface that makes it difficult to focus during imaging.
- Allow the chitosan to dry in a slide box for 48 hours at 4°C (Prop the slide box open to improve air flow and speed up drying time).
- After 48 hours, hydrate the slides in 1X PBS and proceed with staining, imaging, etc.

Appendix I: Hematoxylin and Eosin Staining

Reagents
Immunocal: StatLabs from FisherSci NC9044643
Harris Hematoxylin: Thermo Scientific 6765001
0.5% Aqueous Eosin Y: Millipore from FisherSci M1098442500
D-(−)-Fructose: Sigma-Aldrich F0127

1. Rehydrate section in PBS for 10 min.
2. Rinse slide in tap water
3. Stain slide in Harris Hematoxylin solution for 2 minutes.
4. Wash 3x in tap water for 10 min each.
5. Stain in 0.5% Aqueous Eosin Y for 3 min.
6. Rinse 2x in tap water for 30 Sec each.
7. Mount slide with 30% fructose in distilled water.
8. Image on same day or within few days of staining.

Appendix J: Toluidine Blue Staining

Preparation of Toluidine Blue O

- Toluidine Blue O: Sigma Aldrich T3260-5G
- Prepare 1% stock solution of T Blue in dH2O
- Dilute stock solution 1:40 in dH2O to make 0.025% solution.

Note: 0.025% can be used multiple times but should be replaced once dye doesn't stain as well (usually 3-6 months). Pour solution down sink to dispose of it.

Staining Slides

- If slides were previously in PBS or mounted with glycerol/PBS, wash the slides in dH2O 3X for 10 minutes each.

Note: It's important to remove as much PBS and glycerol as possible.

- Put the slides in 0.025% T Blue solution for 2 minutes.
- Wash in dH2O 3X for 5 minutes each.
- Mount slides with fructose mounting medium (see below).

Preparation of 30% Fructose Solution

- D-(-)-Fructose: Sigma Aldrich F0127
- Add 30g of Fructose to 50ml tube
- Add 100ml of dH2O to 50ml tube
- Mix until fructose dissolves
- Label tube with expiration date of 3 months

Appendix K: Cellularity and Nuclear Shape Analysis

Load image into ImageJ

1. Select Edit -> Options -> Colors -> Background: White
2. Select Analyze -> Set Measurements -> Select Area and Shape Descriptors -> OK

If you need to crop areas out of your image that are stained poorly, folded, etc., do steps 3-8, 18:

3. Load image into ImageJ (Drag from folder onto ImageJ toolbar)
4. Crop out any parts you wish to exclude from analysis: Select “Freehand selections” (fourth box over) and draw the part you wish to include/exclude, Select Edit -> Clear Inside/Outside
5. Select Image -> Adjust -> Color Threshold
6. Select a brightness range that captures all tissue not cropped out (0-254)
7. While tissue is highlighted in red, select Analyze -> Analyze Particles -> Check Display Results and Summarize-> OK (Don’t change other defaults)
8. Save %Area value for scaling cell count based on amount of tissue.
9. Save cropped image.

Resume measuring cell count and nuclear shape:

10. Select Image -> Adjust -> Color Threshold
11. Select a brightness range that captures only stained nuclei (~120-254)
12. Select Process -> Binary -> Make Binary

If you need to make manual adjustments to the thresholded particles:

13. Select Edit -> Options -> Colors -> Background: Black
14. Crop to make any manual adjustments: Select “Freehand selections” (fourth box over) and outline the particles the part you wish to exclude, Select Edit -> Clear Inside (or press Backspace)
15. If cells are connected/overlapping, try Process -> Binary -> Watershed

Resume measuring cell count and nuclear shape:

16. Select Image -> Adjust -> Threshold
17. Select a range that captures only stained nuclei (254-255)
18. While particles are highlighted in red, select Analyze -> Analyze Particles -> Check Display Results and Summarize-> OK (Don’t change other defaults)
19. Copy and save output. Count is cell count and Circ. is circularity.
20. If original image was cropped, scale cell count by dividing by %Area from Step 9.

Appendix L: RNA Extraction

Materials: Nuclease-free Eppendorf Tube, 95-100% Ethanol, RNA*later* (ThermoFisher, AM7020), TRIzol (ThermoFisher, 15596018), RNase-free Pestles (Fisherbrand, 12-141-368), and Direct-zol RNA Microprep Kit (Zymo, R2062)

1. At time of sacrifice, dissect Achilles tendon (AT) by cutting through the calcaneous and above the AT through the triceps surae muscles. Immediately place the AT complex in 1.5 mL nuclease-free Eppendorf tube with 500 µL RNA*later*.
2. Freeze tissue in RNA*later* at -80°C.
3. At time of RNA isolation, let tissue in RNA*later* thaw. Wipe excess RNA*later* off of tissue and place in nuclease-free Eppendorf tube with 200 µL TRIzol (should be ice cold).
    a. All steps with Trizol should be done in hood.
4. Using the RNase-free pestle, mash tissue in Eppendorf tube for ~60 seconds. Close tube and vortex for 2 min.
5. Let samples sit at room temperature for 5 min.
    a. This step is a potential stopping point if needed; store at -80°C.
6. While the tissue sits in TRIzol, mix 5 µL DNase I and 35 µL DNA Digestion Buffer in nuclease-free Eppendorf tube.
7. Transfer supernatant (no tissue) to new Eppendorf tube. Add 200 µL 95-100% ethanol, and mix well by vortexing.
8. Transfer sample to Zymo-Spin IC Column in a collection tube and centrifuge for 15 seconds at max speed (15-16k g). Discard the flow through.
9. Add 400 µL RNA Wash Buffer to the column. Centrifuge for 15 sec at max speed. Discard the flow through.
10. Add DNase Digestion Buffer mix directly to column matrix. Let incubate at RT for 15 min.
11. Add 400 µL Direct-zol RNA PreWash to column. Centrifuge for 15 sec at max speed. Discard the flow through and repeat this step.
12. Add 700 µL RNA Wash Buffer to column. Centrifuge for 2 min at full speed.
13. Carefully transfer column to nuclease-free Eppendorf tube. Add 15 µL of DNase/RNase-free water directly to column matrix. Let incubate at RT for 5 min. Centrifuge for 1 min at full speed to elute RNA.
14. If using Bioanalyzer to check RNA quality, put 3 µL into a separate nuclease-free Eppendorf tube.
15. Check RNA concentration and purity with NanoDrop (need 1.5 µL). Freeze rest of RNA at -80ºC.

Appendix M: cDNA Synthesis & Preamplification

Materials:
- Pipettes (1000µL, 200 µL, 20 µL, 2µL) and associated tips
- High-Capacity cDNA Reverse Transcription kit (Thermo, #4368814)
- RNase/DNase free water
- 96 well plates
- Plastic plate sealers
- Thermal cycler
- Preamp master mix (Fluidigm, #100-5580)
- Taqman probes for target genes
- Dilution reagent (Fluidigm, #100-8726)
- Ice

Procedure:
1. Thaw cDNA RT kit reagents on ice
2. Prepare cDNA RT master mix (MM, per sample):
    a. 2µL 10X RT Buffer
    b. 0.8µL 25X dNTP Mix
    c. 2µL 10X Random Primers
    d. 1µL Reverse Transcriptase (not included in NoRT MM)
    e. 4.2µL Nuclease-free water (for NoRT MM, becomes 5.2µL)
    f. 1.1x offset for pipetting error
3. Pipette 10µL of MM into each plate well allocated for samples
    a. Thaw RNA samples on ice during this step
4. Pipette 10µL of RNA sample into corresponding plate well
    a. Pipette up and down to ensure well-mixed
    b. If diluting RNA sample, add nuclease-free water to achieve 10µL (20µL total)
5. Seal plate, and centrifuge if air bubbles are present
6. Perform cDNA synthesis via thermal cycler with following protocol:
    a. 25ºC for 10min
    b. 37ºC for 120min
    c. 85ºC for 5min
    d. 4ºC indefinitely
7. POTENTIAL STOP: Plate can be stored at -20ºC indefinitely
8. Thaw preamp master mix and associated Taqman probes on ice
9. Prepare pooled assay mix:
    a. Determine volume needed i. 100µL minimum, or 1.25 x (# samples) x 1.1 (offset for pipetting error)
    b. Volume per Taqman probe: Total volume/100
    c. Volume of dilution reagent: Total volume – volume of Taqman probes
10. Prepare preamp master mix (MM, per sample):
    a. 1µL Preamp master mix
    b. 1.25µL pooled assay mix

    c. 1.5µL nuclease-free water
11. Pipette 3.75µL of MM into each plate well allocated for samples
12. Pipette 1.25µL of cDNA sample into corresponding plate well a. Pipette up and down to ensure well-mixed
13. Seal plate, and centrifuge if air bubbles are present
14. Perform preamplification via thermal cycler with following protocol:
    a. 95ºC for 2min
    b. 95ºC for 15sec
    c. 60ºC for 4min
    d. Repeat b + c until appropriate number of cycles are reached
    e. 4ºC indefinitely
15. Add 20µL dilution reagent to each sample well
16. Reseal and store at -20ºC

Appendix N: Transmission Electron Microscopy Processing & Embedding

Day 1:

SACRIFICE/ FIXATION (Steph)

Karnovsky's Fixative- 2-4 hours on ice on shaker (can sit in buffer for up to 1 day)

RINSE

0.1M Na Cacodylate buffer (pH = 7.4) [1:1 dH_2O + stock] - **5 min on ice**

Trim samples, remove all extra tissue, split injury ¾ way through, make two patellar cuts, remove tibia (this is harder to do later)

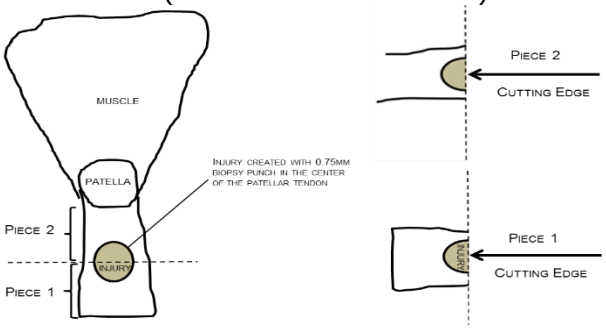

POST-FIXATION

1% OsO4 *(highly toxic)* in 0.1M Na **1 hr on ice** (can stay in longer (15 min), but not shorter)

Cacodylate buffer (pH=7.4) dilute from 2% OsO4 (suck dry)

While waiting, mix Epon

Epon Recipe (ml) by volume		**Epon Recipe (g) by weight**	
EPON (812)	15.6ml	EPON (812)	18.1g
DDSA (softener)	5.4ml	DDSA (softener)	5.5g
NMA (hardener)	9.3ml	NMA (hardener)	10.9g
*DMP-30 (catalyst)	0.6ml	*DMP-30 (catalyst)	0.6ml
	30.9ml		30.9ml

Method:

• Measure out the appropriate amount of each ingredient using a disposable syringe (30mL).

• Mix after measuring first three ingredients, i.e. measure Epon, measure/add DDSA, then measure/add NMA then mix thoroughly by gently rocking for **15 min**. Then add the DMP and mix again thoroughly. (on rocker at room temp for approx **45 minutes**)

• Store the final Epon mixture in 5ml, 10ml, 20ml (as is convenient) syringes tightly covered with parafilm. Recommend dating syringes.

• Place syringes in ziplock bags. Keep syringes containing Epon mixture in the freezer in an airtight container.

-Can use 70% ETOH to clean sticky bottles

Put some epon in mold with label and test overnight to make sure the recipe is correct

RINSE

0.1M Na Cacodylate buffer (pH = 7.4)- **5 min on ice**

DEHYDRATION (use EM grade ETOH) Samples should ALWAYS be wet

Dilute ETOH with dH2O

50% alc	**10 min on ice**
70% alc	**10 min on ice**
85% alc	**10 min on ice**
95% alc	**10 min start with cold alc and let it come to room temp**
100% alc	**10 min 3X's room temp**
Remove about half 100% alcohol and replace with prop oxide. approx. (1:1)	**10 min room temp**
Pure prop oxide	**10 min 2X'S room temp** (one extra untimed rinse)

***always under liquid once dehydrated, no air on tissue*

INFILTRATION

Prop oxide:epon 2:1 **2hrs or over night** [can do 2:1 for 2 hrs and then 1:1 overnight]

Day 2:

Take Epon out of the freezer 20-30 minutes before using and place into desiccated container to allow it to thaw and come to room temperature.

INFILTRATION

Prop oxide:epon	1:3	**next day on rotator (am)**
Pure epon		**overnight on rotator (pm)- 12-20 hours**

Print sample labels for blocks

Day 3:

EMBEDDING

Mix fresh epon

Let epon bubbles rise to top of syringe **15-20 min**

Place labels in mold

Finish cuts in tissue under microscope (keep samples wet in a drop of epon)

Embed with fresh epon **overnight in oven (60ºC) ~24 hours**

Post Embedding:

Check blocks with blade to make sure consistency is right

Break and nail polish glass knives

- Score with larger line first, break
- Position glass square in the holder
- Score with small line, break

Gross Trimming: Dremel rough surface and cut block face with razor blade to smooth
- Larger tissue- less border
- Smaller tissue- more border for structural support

Fine Trimming: Glass knife- 200-500 nm
- Thick sections: create even block face using microtome, important that the collagen fibers are perpendicular to block face
- Use fast stain to check progress/injury site
    - Put water on knife, use wooden spear to collect, put water on slide and then dry on slide warmer before quick stain

Sectioning: Diamond knife, 70-100 nm
- Thin sections: 80-100nm
- 1mm x 1mm square face (can be longer but no wider)
- Rinse grids, line up 3
- Use diamond knife with dH2O in 'boat'. Boat full evenly looks silver (use syringe to get correct level)
    - Clean knife by rubbing Styrofoam over knife face
    - Knife parallel to block face
    - Use air gently on the knife, not a brush
- Collect 80, 90, 100 nm sections; can tell by reflection how thick
    - 20 good sections
    - Set up at 70nm then increase to 80, 90, 100 nm
- Use eyelash tool to group different thickness sections together using color reflection chart
- Collect ~4 sections on each of 5 grids, multiple thickness sections on each grid, collect on dull side of grid, use lens paper to get rid of extra water
- Chloroform helps flatten the sections, hold above them in the boat, don't touch the water
- Store in the grid box
- Scoops up the extras on a slide, save the thickest for injury location determination

Staining: Stain the best 3 sections, let dry overnight
- 2% Uranyl Acetate - 20 minutes
    - Make and store isolated, refrigerated in brown bottle for months- hazardous

    - Fill up 1.5 mL tube of UA, spin 30s to get rid of particulate (don't suck up the particulate)
    - Filter it over the vertical grid
    - 20 minutes stain n in dark, collect waste and filters, nothing down the drain
- Suck up puddle, don't expose to air
    - put in rinsing well upside down
    - 'sloosh' across grid after build up of puddle
    - Use filter paper, gently touch edge of grid to get rid of H2O
- Phosphotungstic Acid (PTA) - 4+ minutes
    - 3.2 pH: pH matters!
        - Add NaOH if too low
    - Dropper onto grids
    - Don't trust expired buffer (Na Cacodylate)
    - 5-10 minute stain
    - Pour off, fresh rinsing well
    - Rinse off, wick off extra dH2O gently
    - Cover to protect and let dry overnight. Can image immediately once extra water is gone
    - Store in grid holder if not imaging immediately

<u>Imaging:</u>

- Image grid with 80-100 nm sections
- Avoid cracks, cells, grid, edges, dirt
- Good cross sections
    - Goal is 3 ROIs per image
    - 1 sample takes 1hr to image
    - 15-20 images per sample